VALVE-LESS RECTIFICATION MICROPUMPS BASED ON BIFURCATION STRUCTURES

Von der
Fakultät Architektur, Bauingenieurwesen und Umweltwissenschaften
der Technischen Universität Carolo-Wilhelmina
zu Braunschweig

zur Erlangung des Grades eines
Doktoringenieurs (Dr.-Ing.)
genehmigte

Dissertation

von
Ahmed Fadl
geboren am 10/02/1976
aus Alexandria

Eingereicht am	03. Juni 2010
Disputation am	29. Juni 2010
Berichterstatter/in	Prof. Dr.-Ing. habil. Manfred Krafczyk
	Prof. Dr. rer. nat. S. Büttgenbach

2010

ABSTRACT

Micropumps are key components in many Microsystems such as Lab-On-a-Chip (LOC) and Micro Total Analysis Systems (μTAS). An efficient, bidirectional, and multifunctional micropump is important to enhance the overall efficiency of any microsystem with fluid flow. Developing a bidirectional micropump with pumping and mixing capabilities will advance microsysetems technology and aid in fabricating more compact microsystems.

In this work, a valve-less rectification micropump based on bifurcation geometry is designed, fabricated, and tested. Three different designs were experimentally investigated. Numerical investigation based on Lattice Boltzmann Method (LBM) was employed prior to the experimental work to numerically measure the microfluidic diodicity in conventional and non-conventional geometries at low Reynolds numbers. Softlithography and optical lithography were used to fabricate the micropumps. The working fluid and actuator were chosen to be ethanol and PZT, respectively. Moreover, the effect of the fabrication material on the micropump efficiency was investigated where two micropumps were fabricated from two different materials, PDMS and SU-8, and the testing results were compared.

Additionally, the concept of valve-less rectification micropump based on a dynamic rectifying geometry was tested and verified. The results confirm the feasibility of the valve-less rectification micropump based on bifurcation geometry. Since streaming flow occurs in bifurcation structures when oscillatory flow in presence, the results of this work will lay the foundations for a micrcofluidic device that can perform two functions (bidirectional pumping and Mixing), generate

streaming flow at zero-mean velocity, reliable, easy to fabricate, cost effective, compatible with wide range of working fluids and materials, capable of delivering particles-laden fluids, and self priming.

ZUSAMMENFASSUNG

Mikropumpen sind Schlüsselkomponenten in vielen Mikrosystemen wie Lab-on-a-Chip und Micro Total Analysis Systemen (µTAS). Eine effiziente, bidirektionale und multifunktionale Mikropumpe ist wichtig, um die allgemeine Effizienz von Mikrosystemen mit Fluidströmungen zu verbessern. Die Entwicklung bidirektionaler Mikropumpen, die Pumpen und Mischen können, erweitert die Möglichkeiten der Mikrosystemtechnik und ermöglicht die Herstellung noch kompakterer Mikrosysteme. In dieser Arbeit wurde eine ventilfreie Gleichrichtermikropumpe basierend auf geometrischen Verzweigungen entworfen, hergestellt und getestet. Dabei wurden drei verschiedene Designs experimentell untersucht. Vor der eigentlichen Konstruktion wurden numerische Simulationen basierend auf der Lattice Boltzmann Methode durchgeführt, um die mikrofluidische Diodizität in konventionellen und nicht konventionellen Geometrien bei niedrigen Reynoldszahlen zu messen. Zur Herstellung der Mikropumpen wurden Softlithographie sowie optische Lithographie genutzt. Als Arbeitsfluid kam Ethanol und als Aktuator PZT zum Einsatz. Der Effekt des Konstruktionsmaterials auf die Mikropumpeneffizienz wurde untersucht indem zwei Mikropumpen aus zwei verschiedenen Materialien (PDMS und SU-8) hergestellt und die Testergebnisse miteinander verglichen wurden.

Zusätzlich wurde das Konzept einer ventilfreien Gleichrichtermikropumpe basierend auf einer sich selbst korrigierenden Geometrie getestet und validiert. Die Ergebnisse bestätigen die Machbarkeit einer ventilfreien Gleichrichterpumpe und bilden die Grundlage für ein mikrofluidisches Gerät, dass zwei Funktionen ausführen kann (bidirektionales Pumpen und Mischen), zudem einen Fluss bei einer Null-

Durchschnittsgeschwindigkeit erzeugt, zuverlässig und einfach zu fabrizieren ist und dabei kosteneffizient und kompatibel mit einer Vielzahl von Arbeitsfluiden und Materialien ist. Die Pumpe ist selbstbefüllend und es können mit ihr partikelbeladene Flüssigkeiten gepumpt werden.

ACKNOWLEDGMENTS

I would like to express my sincere appreciations to all persons whom walked me through all different stages and parts of my doctoral research. The professional supports from my advisors, Professor Zongqin Zhang and Prof. Dr.-Ing. habil. Manfred Krafczyk, were essential to the completion of the dissertation. Their guidance, mentoring, supervision, and encouragements are greatly valued and appreciated. I am also thankful for giving me the academic freedom to test and apply new ideas in my research. Very special thanks are due to Prof. Dr. rer. nat. Stephanus Büttgenbach who kindly accepted to be the second examiner of my thesis as well as giving me the opportunity to work in his institute where I conducted most of my experimental studies. I also would like to thank him for his support and advices.

I would like to thank all of my colleagues at the Institute of Computational Modeling in Civil Engineering (iRMB, TU-BS); the Institute of Microtechnology (imt, TU-BS); and the Department of Mechanical, Industrial and Systems Engineering (URI) especially Dr.-Ing. habil. Jonas Tölke, Dr.-Ing. Sebastian Geller, Dipl.-Ing. Stefanie Demming, Dipl.-Ing. Björn Hoxhold, and Dipl.-Ing. Andrew Marchesseault for their help, time, and valuable discussions.

Moreover, I would like to thank my parents for their unconditional love, care, and unlimited support. Finally, I would like to express my gratitude to my wonderful wife for her patience, devotion, and encouragement. At the end, I would like to thank my five months old baby girl for giving a new meaning, colors, and spirit to my life.

DEDICATION

To the soul of my mother who passed away on February 14th, 2010.

TABLE OF CONTENTS

LIST OF TABLES

LIST OF FIGURES

CHAPTER 1

1 Introduction

"A fact is a simple statement that everyone believes. It is innocent, unless found guilty. A hypothesis is a novel suggestion that no one wants to believe. It is guilty, until found effective."

Edward Teller

1.1 Abstract

Pumps are well recognized machinery for delivering fluids (liquids or slurries) between different locations. Despite the popularity of pumps at the macroscale, pumps at microscale (micropumps) are relatively new and have much more pumping mechanism than those at the macro scale. With the advancements in Microsystems technologies, micropumps became key parts in many Microsystems involving fluids flow such as Micro Total Analysis System (μTAS) or Lab-On-a-Chip (LOC). Micropumps were first introduced in the mid 1970s, and since then steadily flows of micropumps were continuously running to deliver micropumps with a wide diversity of operating principles, applications, technical concepts, fabrications techniques, and actuators.

Micropumps are categorized with respect to their working principles to mechanical and non-mechanical micropumps. While most mechanical micropumps are direct results of miniaturizing macropumps, non-mechanical micropumps used physical phenomenon that became only feasible at the microscale. As MicroElectroMechanical Systems (MEMS) have stimulated micropumps research and development in the past, they are expected to continuously do so in the future.

1.2 Micropumps

Micropumps are one of the most important parts in microfluidics, an emerged field from MEMS-technology. In the last three decades, many micropumps have been developed from various pumping principles (Nguyen, et al., 2006). As a result, micropumps have typically been categorized with respect to their pumping principles to mechanical and non-mechanical micropumps. Mechanical micropumps usually use

mechanical parts to deliver constant fluid volume. Most of the mechanical parts are driven by electromechanically actuators. Mechanical micropumps can be further categorized with respect to the form of applying mechanical energy to fluids. Under this classification, mechanical micropumps are divided into displacement and dynamic micropumps. In displacement micropumps, mechanical energy is periodically added by one or more movable boundaries of any number of fluid-containing volumes resulting in a pressure increase sufficient to deliver fluids through check valves or ports. Typical examples of displacement micropumps are check-valve, valve-less rectification, peristaltic, and rotary micropumps. On the other hand, dynamic micropumps principles are based on adding mechanical energy continuously to increase the fluid velocities within the micropump. As a result, the higher fluid velocities increase the pressure enough to move the fluids through channels. Centrifugal micropumps and ultrasound micropumps are typical examples of dynamic micropumps.

In contrast, non-mechanical micropumps add momentum to a fluid by converting a non-mechanical energy to kinetic energy. While mechanical pumping is mostly used in macroscale pumps and micropumps with a relatively large size and high flow rates, advantages of non-mechanical micropumps are noticeable in the microscale. Many pumping principles are employed in the non-mechanical micropumps including concentration gradient, electrical potential gradient, and magnetic potential. Electrohydrodynamic (EHD), electrokinetic, interfacial, acoustic streaming, electrochemical, and magnetohydrodynamic effects are typically used in non-mechanical micropumps.

1.2.1 Mechanical Micropumps

Mechanical micropumps are the first choice for high flow rates and maximum back pressure applications. They deliver higher flow rates than other non-mechanical micropumps (Nguyen, et al., 2002). Mechanical micropumps require mechanical actuators, which are generally electromechanical actuators.

The check-valve micropump is the most common type in displacement mechanical micropumps. In fact, the first realization of a micropump was the miniaturization of check-valve pumps. The check-valve micropump consists of a pump chamber, an actuator, and two check-valves. The actuator generates oscillatory pressure inside the chamber by expanding (negative pressure) and compressing (positive pressure) inside/into the pump chamber. At each oscillating pressure cycle, depending on the pressure, one check-valve opens and the second closes inducing a one way flow. Figure 1.1 shows the operating principles of check-valve micropumps.

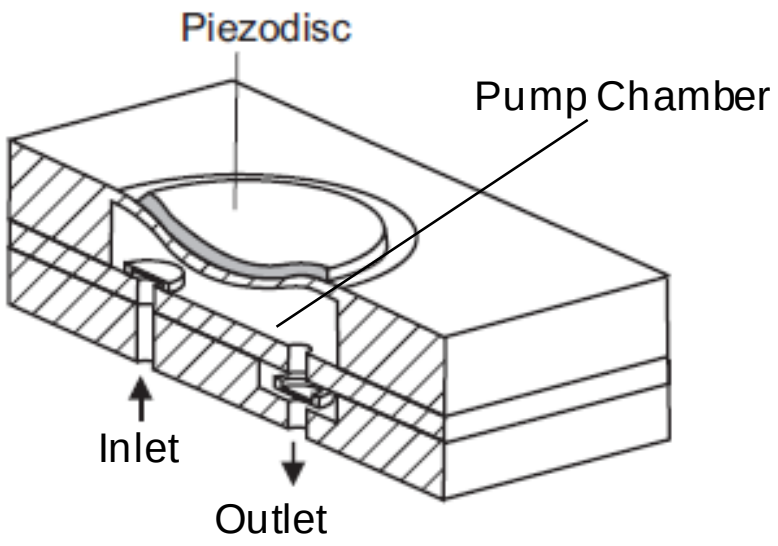

Figure 1.1: General assembly of the check-valve micropump (Nguyen, et al., 2006)

Different types of actuators have been employed with check-valves micropumps including piezoelectric (van Lintel, et al., 1988; Linneman, et al., 1998; Li, et al., 2000), thermopenumatic (van den Pol, et al., 1990; Lammerink, et al., 1993), penumatic (Schomburg, et al., 1993; Meng, et al., 2000), electromagnetic ((Dario, et al., 1996), electrostatic (Zengerle, et al., 1992; Zengerle, et al., 1995), and shape-memory alloy (Benard, et al., 1998). Check-valves have been reported to be fabricated from different materials including silicon (van Lintel, et al., 1988), polysilicon (Shoji, et al., 1990), polyimide (Schomburg, et al., 1993; Rapp, et al., 1994), polyester (Boehm, et al., 1999), and parylene (Meng, et al., 2000). Check-valves also have taken different shapes such as disk (van Lintel, et al., 1988) and cantilever (Zengerle, et al., 1992; Zengerle, et al., 1995). Additionally, improved designs were reported such as gas pumping and self-priming (Linneman, et al., 1998; Richter, et al., 1998). The literature shows that the development trend was in the

direction of favoring smaller pump chambers (high compression ratio), flexible membranes , and piezoelectric actuators. The reported maximum flow rates were between 4 µl/min and 13 ml/min (Nguyen, et al., 2006).

The peristaltic micropump is the second type of the mechanical displacement micropumps. No valves for flow rectification are required as it is the case for check-valves micropumps and valve-less rectification micropumps. Peristaltic micropumps usually have at least three pump chambers with three actuators that squeeze the flow in the desired direction with respect to their order of actuation. Figure 1.2 illustate the operation principles of peristaltic micropumps.

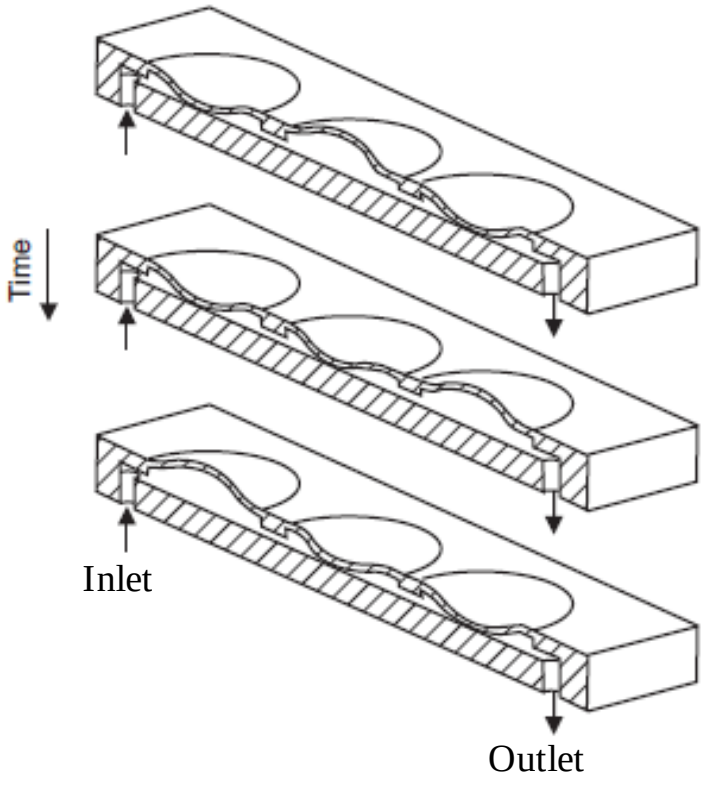

Figure 1.2: Peristaltic micropump with three pump chambers

Since peristaltic micropumps do not require high chamber pressure, the most critical optimization factors are the large stroke volume and the large compression ratio (Nguyen, et al., 2002). Persitaltic micropumps utilize different types of actuators such as piezoelectric (Smits, 1988; Shinohara, et al., 2000), thermopeneumatic (Folta, et al., 1992; Mizoguchi, et al., 1992; Grosjean, et al., 1999), and electrostatic actuators (Judy, et al., 1991; Cabuz, et al., 1999). Different technoloiges have been used to fabricate peristaltic micropumps including bulk micromaching (Smits, 1988; Mizoguchi, et al., 1992), surface micromachining (Judy, et al., 1991), precision engineering (Grosjean, et al., 1999), and plastic molding (Cabuz, et al., 1999). The reported flow rates were between 3 µl/min and 8 ml/min (Nguyen, et al., 2002).

Valve-less rectification micropumps are the third type of mechanical displacement micropumps. Their operation principles depend on rectifying oscillatory flows by using rectifying structures such as nozzle/diffuser and Tesla structures. This micropump will be discussed in more details later in this chapter.

Rotary micropumps are another example of mechanical displacement micropumps and have been realized with micromachining techniques. The operation principle of this micropump relies on adding momentum to the fluid through rotational mechanical parts such as gears and rotors (See Figure 1.3). One of most significant advantages of this micropump is its ability to pump high viscosity fluids. Two different kinds of motors were utilized in the literature: external motors (Ahn, et al., 1995) and internal motors (Doepper, et al., 1997). This micropump can be realized in mass production through injection molding. The reported flow rates were around tens of micro liters per minute.

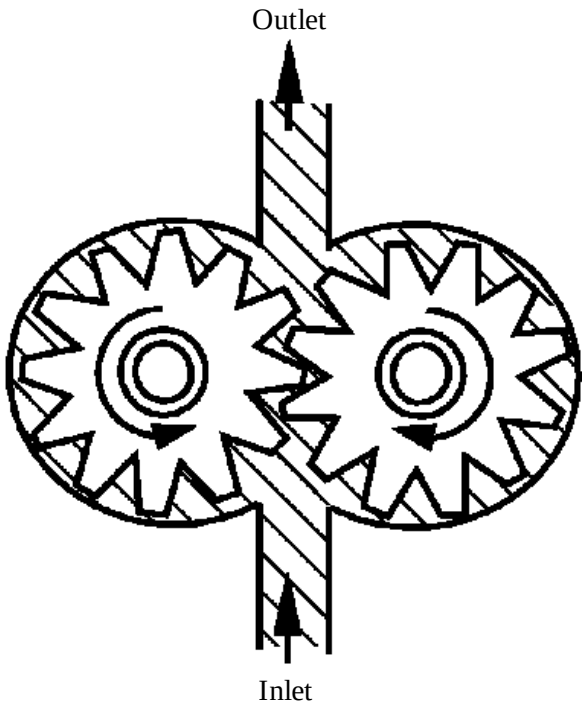

Figure 1.3: Example of the rotary micropump (Nguyen, et al., 2002)

The first mechanical dynamic micropump is the centrifugal micropump. The pumping principle of this type of micropump depends on adding momentum to the fluid by means of fast moving blades. The rotor, stator, and coils are fabricated using electroplating of iron-nickel alloy. To fabricate high aspect ratio structures at low cost, conventional photolithography of polyimide was employed. Two types of actuators were used to activate the centrifugal micropumps, internal and external actuators. Because of the high viscosity and the small radius of the rotor, centrifugal pumps with internal actuators do not have the sufficient power to drive liquids in microchannels. Therefore, an external spinning motor was used. The micropump has only channel structures in a compact disc (CD) platform. The flow velocity is controlled by the

angular velocity of the CD (Nguyen, et al., 2006; Ahn, et al., 1995; Madou, et al., 2001)

The second mechanical dynamic micropump is the ultrasonic micropumps. This gentle micropump has no-moving parts, and its operational principles depend on driving the flow by acoustic streaming induced by travelling sound waves. The mechanical waves can be a flexural plate (Moroney, et al., 1991; Nguyen, et al., 2000) or a surface acoustic wave (Miyazaki, et al., 1991; Kurosawa, et al., 1995). The mechanical waves are excited by interdigitated transeducers (IDT) placed on a thin membrane coated with piezoelectric film (Moroney, et al., 1991; Nguyen, et al., 2000) or on a piezoelectric bulk material (Miyazaki, et al., 1991; Kurosawa, et al., 1995).

1.2.2 Non-Mechanical Micropumps

The first type of non-mechanical micropumps is the electrohydrodynamic (EHD) micropump, and its pumping principle is based on electrostatic forces acting on dielectric fluids. EHD micropumps are further categorized into two main types: EHD induction and EHD injection micropumps (Laser, et al., 2004). The EHD induction micropump is based on the induced charge at the material interface. A traveling wave of electric field drags and pulls the induced charges along the wave direction. EHD induction can be categorized as:

- Micropumps with layered fluids;
- Micropumps with suspended particles;
- Micropumps with anisotropy of fluid properties.

On the other hand, the EHD injection micropump is based on injecting ions from one or both electrodes by means of electrochemical reaction. The coulomb force is responsible for moving the injected ions, and as a result, the pressure gradient builts up in the electric field causing the pumping effect (Nguyen, et al., 2002).

The EHD induction micropump can achieve a fluid velocity of several hundred micron per second. For a better pumping effect, an external heat source and heatsink were used to generate a temperature gradient and consequently a conductivity and permittivity gradient a cross the channel height. This leads to a lower charge relaxation time. As a result, a temperature gradient and a traveling charge wave on the channel wall lead to a gradient of charge relaxation time in the fluid, which in turn causes a better pumping effect. The heat sink is actively cooled by Peltier element (Bart, et al., 1990; Fuhr, et al., 1992; Fuhr, 1997; Fuhr, et al., 1992; Fuhr, et al., 1994)

In contrast, the EHD injection micropump can deliver 0.12 ml/min with a driving voltage of 200 V. Most of these micropumps are bulk machnied and the electrodes are made of silicon (Ahn, et al., 1998; Richter, et al., 1990; Richter, et al., 1991; Furuya, et al., 1996)

The second type of non-mechanical micropumps is the electrokinetic micropump. This type uses the electrical fiels for pumping conductive fluids. The electrokinetic phenomenon can be divided into electrophoresis and electro-osmosis.

In the electrophoresis phenomena, charged species in a fluid are moved by an electrical field relative to the fluid molecules. The electric field accelerates charged species until the electric force is equal to the frictional force. The acceleration process after applying the electrical field is on the order of a few picoseconds. Thus, the

velocity of the charged species is proportional to the field strength. Electrophoresis is used for separation of molecules like DNA-molecules. In contrast, electro-osmosis is the effect where fluids move in the channels under the application of an electrical field. Above pH 2, a negative surface charge characterized by the zeta potential exists at the plane of shear between the stationary and mobile layers of the electric double layer. The zeta potential is typically on the order of -20 mV to -150 mV. The surface charge comes either from the wall property or the absorption of charged species in the fluid. In the presence of an electrolyte solution, the surface charge induces the formation of a double layer on the wall by attracting oppositely charged ions from the solution. This layer has atypical thickness on the order of nanometers. An external electrical field forces the double layer to move. Due to the viscous force of the fluid, the whole fluid in the channel moves until the velocity gradient approaches zero across the microchannel. This effect results in a flat velocity profile (plug flow). The momentum transfer process after applying the electrical field is on a time scale between 100 µm and 1 ms. (Nguyen, et al., 2000).

The most common applications of electrokinetic micropumps are delivering buffer solution and separating large molecules such as DNA and proteins. A fluid velocity of 100 µl/s with a field strength of 150 V/cm was reported in the literature as well as using the gel electrophoresis for separating DNA-molecules in microchannels with rtelatively low field strength of 5 to 10 V/cm (Harrison, et al., 1991; Harrison, et al., 1992; Webster, et al., 1996; Webster, et al., 2000).

The third type of non-mechanical micropumps is phase transfer micropump. The principle of this micropump relyies on generating a pressure gradient by changing the

fluid pahse from liquid to vapor in order to overcome the high fluidic impedance caused by viscouse forces. The realization of this pump is much easier and simpler than other micropumps. The micropump contains only a microchannel with integrated microheaters. This micropump was reported to be realized with stainless steel and polysilicon, and the reported flow rates are less than 1 nl/min (Takagi, et al., 1994; Ozaki, 1995; Jun, et al., 1996; Jun, et al., 1998)

The electro wetting micropump is the fourth type on the list of non-mechanical micropumps. Its principle is based on the dependence of the tension between soild/liquid interface on the charge of the surface. A microactuator based on electro-wetting of mercury drop was proposed for driving a check-valve mechanical micropump. However, no example was reported in the literature (Matsumoto, et al., 1990; Lee, et al., 1998)

The electrochemical micropump is the fifth type, and its operational principle is based on using the pressure of gas bubbles generated by electrolysis of water. Bidirectional pumping can be achieved by reserving the actuating current, which makes the hydrogen and oxygen bubbles reacting back to water (Boehm, et al., 2000).

The last type of the non-mechanical micropumps is magnetohydrodynamic micropump (MHD). As the name applies, the pumping effect of this micropump is based on the Lorentz force acting on a conducting fluid. This micropump was realized in silicon and was able to generate a non-pulsatile flow similar to EHD and electrokinetic micropumps. The velocity profile was observed to be paraboloic and the maximum reported flow velocity was 1.5 mm/s (Lemoff, et al., 1999; Lemoff, et al., 2000).

1.3 Valve-less Rectification Micropumps

A valve-less rectification micropump (see Figure 1.4) is also known as a non-moving-parts rectification micropump, and it has gained increased attentions in recent years. In comparison to other mechanical and non-mechanical micropumps, valve-less rectification micropumps enjoy many advantages such as reliability (no-moving-parts), easy fabrication, combatibility with biological application, capability of pumping particles laden fluids and living cells, combatibility with wide range of materials and working fluids, cost effective, the ability of delivering favorable flow rates as well as maximum back pressures, and offering self-priming capabilitiy. It is realized with bulk micomachining and softlithography. In contrast to check-valves micropumps, valve-less rectification micropump utilizes rectifying structures for flow rectification instead of check-valves (Stemme, et al., 1993; Olsson, et al., 2000; Yamahata, et al., 2005).

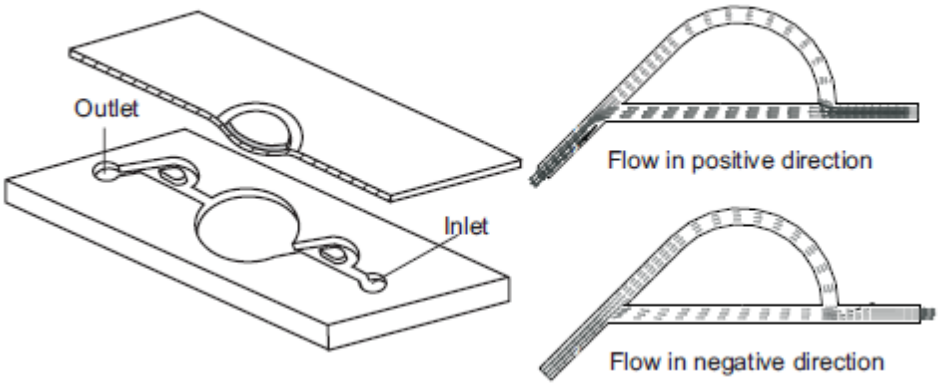

Figure 1.4: Example of a valve-less rectification micropump based on Tesla rectification structure (Nguyen, et al., 2006)

The idea of using direction-dependent flow resistances(rectifying structures) in micropump design was first introduced three decades ago (Van de Pol 1989). Since then much progress has been made in understanding, modeling, and characterizing valve-less rectification micropumps. Based on the literature review, several statements can be drawn: first, there is a lack of a unified expression for the rectifying efficiency. While some use the microfluidic diodicity (Foster, et al., 1995; Gamboa, et al., 2005; Bardell, et al., 1997), at constant flow rate or total pressure difference, others use the ratio of pressure drop coefficients to calculate the rectifying efficiency (Olsson, et al., 2000; Stemme, et al., 1993; Yang, et al., 2004; Wang, et al., 2009)

Second, there is a lack of a general expression for the pressure drop characteristics in the low Reynolds number (a dimensionless number that gives a measure of the ratio of inertial forces to viscous forces and consequently quantifies the relative importance of these two types of forces for given flow conditions) region in the case of the nozzle/diffuser structure. In fact, the equations which were used in the pressure loss analysis were based mainly on experimental results at Reynolds numbers greater than 30,000 (White, 1999; Runstadler, et al., 1975), while Reynolds numbers for most of the nozzle/diffuser micropumps are far less than 30,000 (Stemme, et al., 1993; Gravesen, et al., 1993; Olsson, et al., 1995; Nguyen, et al., 2002). The study by Jiang et al. (1998) showed that pressure loss coefficients and the rectifying efficiency for a diverging diffuser exhibits different trends in laminar and turbulent flows. Moreover, Rosa and Pinho (2006) showed that the often used expressions for the diffuser loss

coefficients in the literature are only valid for turbulent flows and significant errors will be introduced if the typical expressions are used for laminar flows.

Third, many contradictory results are found in the literature. For example, some studies suggested that flow rectification in a nozzle/diffuser element is not achievable in laminar flow (Gerlach, et al., 1995; Olsson, et al., 1996; Koch, et al., 1998), while (Singhal, et al., 2004a; Singhal, et al., 2004b) reported that flow rectification is achievable in a nozzle/diffuser element for laminar flow. (Olsson, et al., 1997a; Olsson, et al., 1997b) suggested that flow rectification in a nozzle/diffuser element significantly depends on the length of the nozzle/diffuser element, while Yang et al. (2004) reported that the dependence of the flow rectification on the nozzle/diffuser lengths is insignificant. Moreover, Olsson et al. (1997a, b, 2000) suggested that flow separation in the diffuser element increases losses dues to the ‘‘vena-contracta’’ effect. On the other hand, Wang et al. (2009) reported that flow separation plays a crucial role in reducing the losses in the diffuser due to the reduction of the wall shear stress.

Fourth, there are also many common grounds in the literature. For example, it is widely believed that flow rectification depends on Reynolds number, particularly in the laminar region, as well as the converging/diverging angle in the case of the nozzle/diffuser structure (Olsson et al., 2000; Gamboa et al., 2005; Yang et al., 2004; Jiang et al., 1998; Wang et al., 2009; Singhal et al., 2004a, b; Chen, et al., 2008; Olsson et al., 1995). There is also an agreement on the capability of the diffuser element to direct the flow (Olsson et al., 2000; Jiang et al., 1998).

To conclude, more investigations are needed especially in the laminar flow region. Only two rectification structures are employed in the literatre, nozzle/diffuser and

Tesla structure (see Figure 1.4 and 1.5). The rectification structures that reported in the literature are passive, and to the best of our knowledge no dynamic structures have been reported in the literature. Finally, with the contradiction results in th literature which was recently pointed out by Nabavi (2009), more works are definitly needed to better understand this type of micropump.

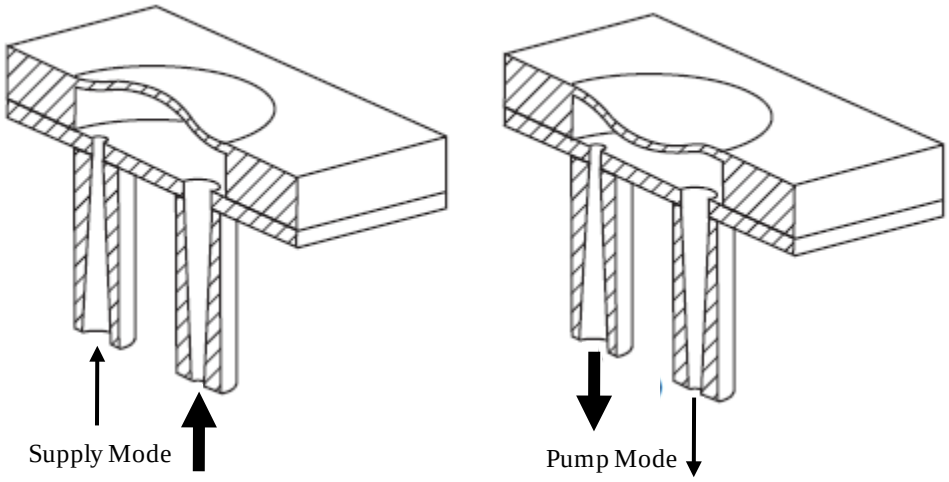

Figure 1.5: Nozzle/diffuser valve-less rectification micropumps (Nguyen, et al., 2006).

1.3.1 Pumping Principles

The pumping principles of the valve-less rectification micropumps depend on rectifying oscillatory flows through rectifying structures. The nozzle/diffuser micropump is used here to illustrate the pumping principles, see Figure 5. The Piezoelectric Transducer (PZT) generates oscillatory flows by bending upward and downward. When the PZT bends upwards, a negative pressure is generated in the pump chamber. As a result, the fluid enters the chamber from the right and left. The

fluid entering from the left confronts higher resistance than the one entering from the right (nozzle action at the left entrance compared to diffuser action at the right entrance). As a result, more fluid enters from the right compared to the left (supply mode).

On the other hand, a positive pressure is generated when the PZT bends downward resulting in fluid discharging from the pump chamber. More fluid discharges from the left compared to the right due to higher resistance in the right (nozzle action at the right entrance compared to diffuser action at the left). Hence, more fluid discharge from the left compared to the right (pump mode). Repeating the supply and pump modes result in net flow rate entering from the right and exiting at the left, please see Figure 1.6 for more details.

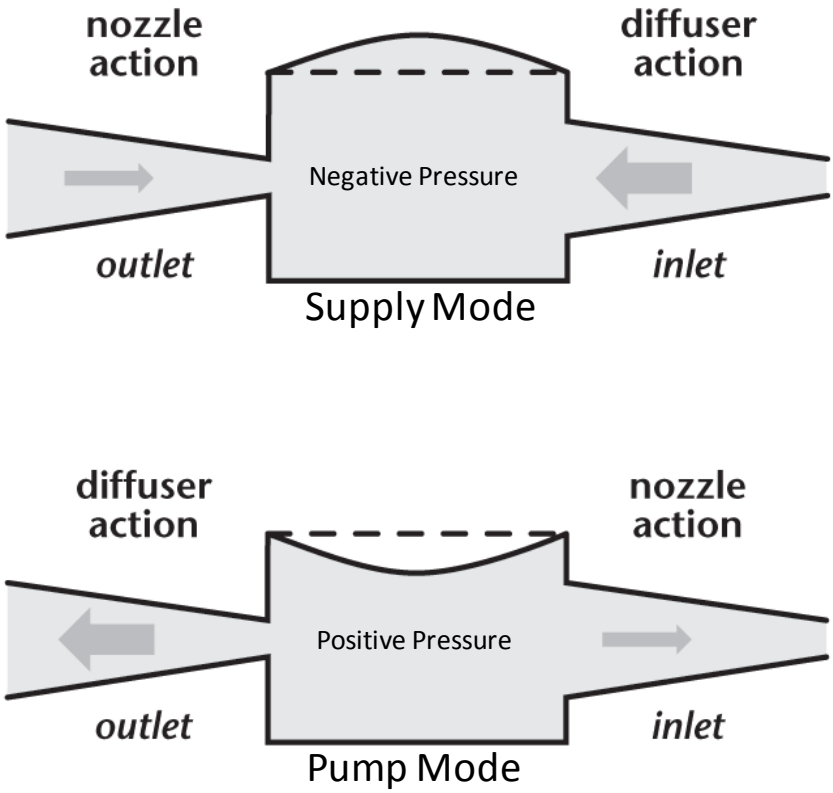

Figure 1.6: Pumping principles of nozzle/diffuser valve-less rectification micropumps.

The principles described above are valid for other types of valve-less rectification micropump with different rectifying structures, geometries with directional flow resistance. All the rectifying structures that are used in these types of micropumps have high and low flow resistances depending on the flow direction. The fluid flow in the direction where it faces higher flow resistance is called backward flow. Reversibly, the fluid flow in the direction where it faces lower flow resistance is called forward flow.

1.3.1.1 Microfluidic Diodicity

Microfluidic diodicity is a term that is used to evaluate rectifying structures as well as their rectification efficiency. Any structure with a microfluidic diodicity not equal

to one is considered a rectifying structure. The absolute value of the microfluidic diodicity is an indication of the efficiency of the rectifying structures.

In general, the microfluidic diodicity is defined as the ratio of the pressure drop in the backward direction to the forward direction (Foster, et al., 1995; Bardell, et al., 1997). To measure the microfluidic diodicity, the pressure drop is measured in the forward and backward directions at a constant flow rate, and the microfluidic diodicity is evaluated by dividing the pressure drop in the backward direction over the pressure drop in the forward direction (see equation 1.1).

$$D = \frac{\nabla P_b}{\nabla P_f} \tag{1.1}$$

Where D, ∇P_b, ∇P_f are the microfluidic diodicity, pressure drop in the backward direction, and pressure drop in the forward direction, respectively.

The microfluidic diodicity can be also measured by dividing the flow rate in the forward direction over the flow rate in the backward direction in the case of constant pressure drop over the rectifying structures (see equation 1.2).

$$D = \frac{Q_f}{Q_b} \tag{1.2}$$

Where Q_f and Q_b are the flow rates in the forward and backward directions, respectively.

Finally, the microfluidic diodicity can also be evaluated by using the pressure loss coefficient (the method of choice for nozzle/diffuser valve-less rectification micropumps). The pressure loss coefficient is defined in the following equation:

$$K = \frac{\nabla P}{\rho V^2/2} \tag{1.3}$$

Where K, ∇P, ρ, and V are pressure loss coefficient, pressure drop, fluid density, and mean flow velocity, respectively. Therefore, the microfluidic diodicity can be calculated as follow:

$$D = \frac{K_b}{K_f} \tag{1.4}$$

Where K_b and K_f are the pressure less coefficients in the backward and forward directions, respectively. In the case of the nozzle/diffuser micropump, the backward direction is the nozzle direction and the forward direction is diffuser direction. Additionally, when D >1 the pumping action takes the diffuser direction; while when D<1 the pumping action takes the nozzle direction. Finally, D=1 means equal pressure drop in both the backward and forward directions (the nozzle and the diffuser directions), leading to no flow rectification and, therefore, zero flow rate (Singhal, et al., 2004b).

1.3.2 Rectifying Structures

Rectifying structures are structures with directional flow resistance (pressure drop in backward and forward directions differ). In the literature, only two rectification structures have dominated the reported works, nozzle/diffuser and Tesla structures (Stemme, et al., 1993; Olsson, et al., 1995, Olsson, et al., 1996; Olsson, et al., 1997a; Olsson, et al., 1997b; Olsson, et al., 2000; Gerlach, et al., 1995; Gerlach, 1997; Jiang, et al., 1998; Singhal et al., 2004; Chen et al., 2008; Shen, et al., 2008); Sun, et al., 2006; Cui, et al., 2007; Cui, et al., 2008; Forster et al., 1995; Bardell et al., 1997). Theses conventional structures are shown in Figure 1.7.

Rectifying structures are usually placed on the sides or under the micro pump chamber. The existence of Rectifying structures and generation of oscillatory flows are the two conditions that must be met in any valve-less rectification micropumps.

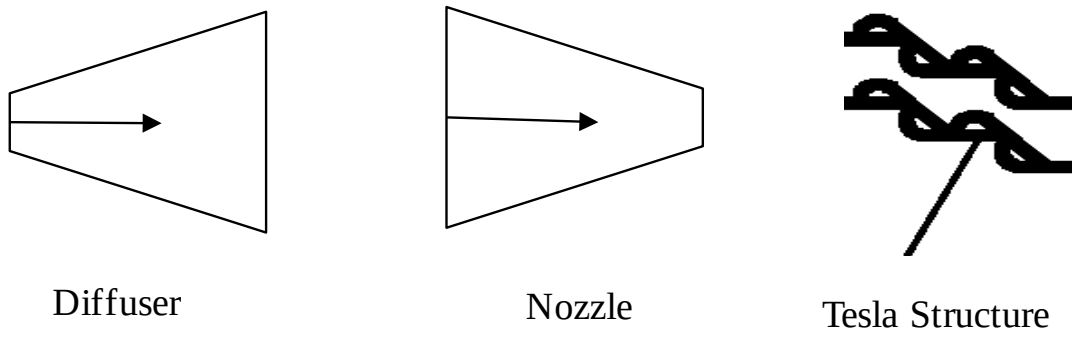

Figure 1.7: Conventional rectifying structures; nozzle, diffuser, and Tesla structures.

It is also noticed that all rectifying structures reported in the literature were passive and, according to our extensive literature search, no dynamic rectifying structures were reported in the literature.

1.4 Streaming Flow

Streaming flow is a phenomenon that occurs in asymmetrical channels when oscillatory flow is introduced. Due to the discrepancy of the velocity profiles, two flow streams occur in opposite directions while the total mean velocity is still zero. In other words, the flow rates of two flow streams are equal resulting in a zero net flow rate. One stream is located near the wall, while the second is located at the center of the channel. Streaming flow plays an important role in flow exchange, mixing, particle distribution dynamics, mass transfer, and heat transfer without a need to a net flow

convection. Figure 1.8 shows the velocity profiles of the streaming flow in a bifurcation channel during oscillatory flow. The streaming flow characteristics depend on the geometrical parameters, Reynolds number, and Womersley number (a dimensionless expression of the pulsatile flow frequency in relation to viscous effects) (Haselton, et al., 1982).

Many papers on steady streaming in macro-channel oscillatory flows have been published in the past few decades (Nyborg, 1953; Rosenblat, 1959; Rosenblat, 1960; Riley, 1965; Riley, 1967; Jones, et al., 1969; Lyne, 1970; Haselton, et al., 1982; Simon, et al., 1982; Tarbell, et al., 1982; Grotberg, 1984; Gaver, et al., 1986; Briant, et al., 1992; Goldberg, et al., 1999; Zhang, et al., 2008). Various geometry and flow arrangements were covered in the literature, including: streaming flow induced by a torsionally oscillated disk (Rosenblat, 1959; Rosenblat, 1960; Jones, et al., 1969), streaming adjacent to a cylinder oscillating along its diameter ((Riley, 1965; Riley, 1967), streaming in oscillating flow along a curved tube (Lyne, 1970), pressure-driven oscillatory flow within a tapered tube (Grotberg, 1984; Gaver, et al., 1986), oscillatory flow through bifurcations (Haselton, et al., 1982; Simon, et al., 1982; Zhang, et al., 2008), and streaming in the channel entrance region (Goldberg, et al., 1999).

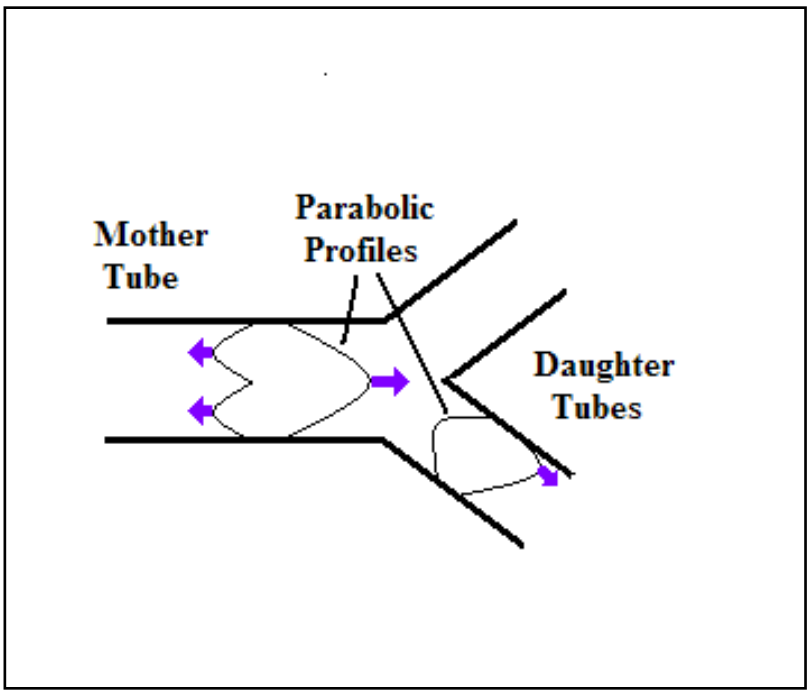

Figure 1.8: Streaming flows in the bifurcation channels

1.5 Bifurcation Geometry

Bifurcation Geometry is a natural shape that can be easily noticed in nature such as blood veins, tree branches, and bronchial airways. In fact, they can also be identified in technical systems such as pipe networks and roads. Bifurcation geometries are expected to have microfluidic diodicity not equal to one, which means they can be used to rectify the flow in valve-less rectification micropumps. Additionally, their natural shape can be used for mixing different fluids before pumping. Moreover, bifurcation is proven to promote streaming flow during oscillatory flow.

1.6 Mechanisms of Flow Streaming in Bifurcation

The mechanisms of flow streaming in a bifurcating channel are illustrated in Figure 1.8. It shows a qualitative picture of the axial velocity profiles of a Newtonian fluid in a macro-channel bifurcation tube based on the work of (Haselton, et al., 1982;

Zhang, et al., 2008). During the inflow (to the right), the parabolic velocity profile in the mother tube is split in half at the location of U_{max} when entering the daughter tubes, resulting in a nonsymmetrical profile with the maximum velocity skewed to the inner wall of the daughter tubes. During the backflow (to the left), two fully developed, parabolic flow profiles in the daughter tubes merge at the center of the bifurcation and result in an ε-shaped symmetrical profile in the mother tube with a zero velocity at the center. The discrepancy in velocity profiles between inflow and backflow causes fluid elements near the walls to drift toward the mother tube (negative drift) while fluids near the centerline drift to the daughter tubes (positive drift).

It is noted that the mechanisms of flow streaming in bifurcation is different from those of acoustic streaming. Acoustic flow streaming originates from attenuation of the acoustic field. The attenuation spatially reduces the vibrating amplitude of the acoustic wave and hence generates Reynolds stress distributions and drives the flow to form the acoustic streaming. Acoustic streaming occurs in most geometries when an acoustic field exists, while the streaming flows we study are induced by the pressure-driven asymmetrical oscillating flows. In addition, oscillating parameters are quite different. In most cases, the acoustic vibration has much higher frequency (>100 kHz vs. <0.1 kHz) and much smaller amplitude (< 0.1 mm vs. > 0.1 mm).

CHAPTER 2

2 Numerical Measurements of the Microfluidic Diodicity using Lattice Boltzmann Method (LBM)

"Science does not know its debt to imagination. "

Ralph Waldo Emerson

2.1 Abstract

The efficiency of the valve-less rectification micropump depends primarily on the microfluidic diodicity. In this chapter, different rectifying structures, including the conventional structures (nozzle/diffuser and Tesla structures), were investigated at very low Reynolds numbers (between 0.2 and 60). The rectifying structures were characterized with respect to their design, and a numerical approach was illustrated to calculate the diodicity for the rectifying structures. In this study, the microfluidic diodicity was evaluated numerically for different rectifying structures including half circle, semicircle, heart, triangle, bifurcation, nozzle/diffuser, and Tesla structures. The Lattice Boltzmann Method (LBM) was utilized as a numerical method to simulate the fluid flow in the microscale. The results suggest that at very low Reynolds number flow, rectification and multifunction micropumping may be achievable by using a number of the presented structures. The results for the conventional structures agree with the reported results.

2.2 Introduction

The micropump is a key component in many microsystems, such as the Micrototal Analysis System (μTAS) and the Microelectromechanical Systems (MEMS). Typical examples, where micropumps play a significant role, are microcoolers, micromixers, microreactors, microheat exchangers, and the Lab-On-a-Chip (LOC).

There are two different types of micropumps (Nguyen, et al., 2002; Laser et al., 2004), with respect to their pumping principle, mechanical micropumps, and non-mechanical micropumps. Mechanical micropumps usually use moving parts, such as check valves, oscillating diaphragms, turbines, and gears, to deliver a constant fluid

volume. Examples of mechanical micropumps are rotary, peristaltic, check valves, and valve-less rectification micropumps. In contrast, non-mechanical micropumps add momentum to the fluid by converting another energy form into kinetic energy. Examples of non-mechanical micropumps are electrokinetic, magnetohydrodynamic, and electrochemical micropumps. One of the mechanical micropumps is the valve-less rectification micropump which is categorized as a displacement micropump. It has several advantages over other micropumps, such as no moving parts, easy to fabricate, reliable, and cost effective. Additionally, it is capable of pumping particle-laden fluids, fluids with live cells (Olsson, et al., 2000), and a wide range of working fluids. Moreover, the micropump can be fabricated using a wide range of materials. Flow rectification is owed entirely to the diodicity of the rectifying structures. Increasing the diodicity will result in more efficient micropumps, which will result in high efficiency microsystems. There are two conventional rectifying structures in the literature: the first is the nozzle/diffuser (Stemme, et al., 1993), and the second is the Tesla structure (Foster, et al., 1995). While many studies have been devoted to experimentally and/or numerically test (Stemme, et al., 1993; Gerlach et al., 1995), optimize (Gamboa, et al., 2005), and characterize (Yang, et al. 2004) conventional valve-less rectification micropumps, less attention was paid to investigate the behavior of rectifying structures at very low Reynolds numbers, even though many microsystems, especially in biological applications, work in this region such as LOC (Geschke, et al., 2004) Moreover, according to our literature search, there are no studies which investigated the performance of a wide range of non-conventional rectification structures and compared them with the conventional structures, nozzle/diffuser and Tesla structures.

The absence of these studies is limiting the potential and options for microsystems design.

In this chapter, a study was conducted to evaluate the microfluidic diodicity for different rectifying structures at low Reynolds numbers. The flow field was simulated in a low Reynolds number region, between 0.2 and 60, which is within the typical operational range for many microbiological applications (Geschke, et al., 2004). Several rectifying structures have been presented and tested including the conventional structures.

2.3 Research Approaches

The rectifying structures were categorized with respect to their design method. The details of the categorization method have been fully illustrated in the present study. A numerical evaluation of the microfluidic diodicity was used and details and results were presented. The microfluidic diodicities were evaluated to only include the rectifying structure without external losses; all external losses were excluded in this study. Examples of the external losses are entrance and exit losses. The numerical model, which was used to simulate the flow in the microscale, is based on the Lattice Boltzmann Method, which is a distinctive approach to discretize the Navier–Stokes Equations (NSE). In this study, LBM was used for the first time to evaluate the microfluidic diodicity for different rectifying structures. In the literature, it is common to utilize numerical models which directly discretize the Navier–Stokes Equations to model the flow and then, evaluate the microfluidic diodicity or the pressure loss coefficients. Where in this study, the flow fields were numerically modeled using LBM and then, the microfluidic diodicity was numerically evaluated to investigate the

potential of rectifying the flow at very low Reynolds numbers, especially, in the non-conventional rectifying structures.

The objective of this numerical study is to provide a quick, simple, and easy tool to qualitatively compare and analyze the microfluidic diodicity for different structures. This qualitative assessment is a pre-step to the experimental investigation in order to choose which rectification structure should be considered for the experimental studies. In other words, which rectifying geometries have the highest microfluidic diodicity at the current low Reynolds numbers? The qualitative results will serve well our objectives and, therefore, 3-D simulations were not considered at this stage and the presented 2-D simulations are sufficient for the current work.

2.4 Rectifying Structures

In this study, the rectifying geometries were characterized with respect to their design approach. There are six different approaches which can be implemented to design the rectifying geometries. The following is a summary of the approaches:

(1) Introduce a rectifying structure inside the flow channel. For example, placing a half circle or semicircle inside a channel.

(2) Changing the shape, dimension, or cross section of the channel, while the inlet and outlet of the rectifying geometry are identical. An example would be triangle and heart shape geometries.

(3) Changing the shape, dimension, or cross section of the channel, while the inlet and outlet of the rectifying geometry are different. An example would be nozzle/diffuser geometry.

(4) Bifurcating the flow into two channels, or more, will result in flow rectification. A typical example is the bifurcation geometry.

(5) Dividing the flow into two different channels with different lengths or dimensions and merging both of them into a channel with the same exact dimension as the inlet channel. An example would be the Tesla structure.

(6) Superimposing two rectifying structures for the benefit of maximizing the microfluidic diodicity. This approach was not considered in this study. Figure 2.1 shows the rectifying geometries which have been characterized with respect to the above design approaches, and Table 2.1 shows the dimensions of each

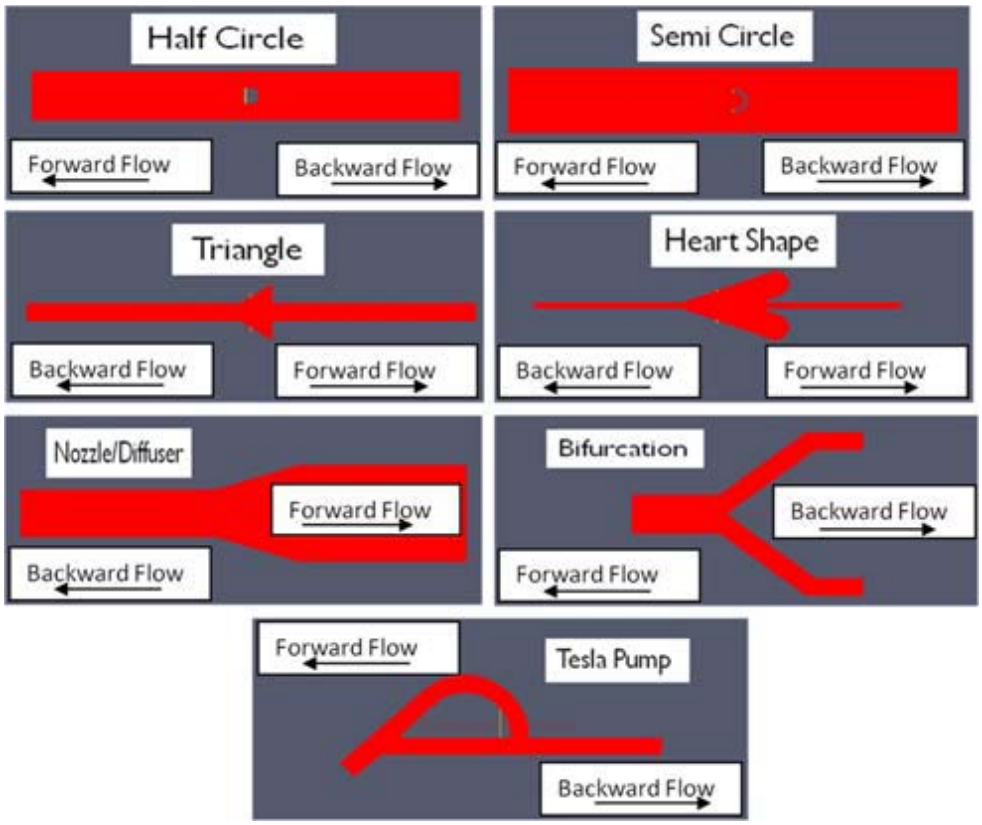

Figure 2.1: The rectifying geometries which have been employed in the present investigation

Geometry	Dimensions (all in μm)
Half circle	Channel (800 × 4,000), half circle (diameter = 250)
Semicircle	Channel (800 × 4,000), semicircle (inside and outside diameters = 218, 250)
Triangle	Channel width and length (200 × 4,000), triangle height and length (600 × 75)
Heart shape	Channel width = 100, heart half angle = 45°
Nozzle/diffuser	Max. width = 400 and min. width = 200, half angle = 18.4°
Tesla structure	Channel width = 100, and channel angle = 45°
Bifurcation	Mother and daughter channel (200, 100), bifurcation half angle = 45°

Table 2.1: The dimensions of the rectifying geometries (in microns)

2.5 The Numerical Model

2.5.1 Introduction to Lattice Boltzmann Method (LBM)

In the last 20 years, there has been rapid progress in developing the method of the Lattice Boltzmann Equation (LBE), which statically describes the particles interaction on the microscale, for solving a variety of fluid dynamic problems. The method of LBM is a kinetic-based approach for fluid flow simulation. LBM is a special finite difference discretization of the simplified Boltzmann equation with a collision model, such as Bhatnagar–Gross–Krook (BGK) (Benzi, et al., 1998; Chopard B, 1998; Succi, 2001), which describes the transport phenomena at the mesoscale level. This method is different from the traditional CFD methods, which obtain the velocity and pressure by solving the Navier–Stokes equations and computing the shear stress from gradients of the velocity fields. The LBM can be compared to a Navier–Stokes-based fluid solver, according to Pingen (2005) and Succi (2001), as follows: LBM is an explicit, fully local scheme with second order accuracy in space and time. LBM is unconditionally stable in the linear case and conditionally stable in the non-linear case. Moreover, it is accurate for low Mach numbers and does not require solving the Poisson pressure equation. LBM can be easily parallelized, uses regular mesh, and is able to present boundaries through a simple on/off nature of nodes. However, limitations exist in the case of grid refinement and higher order no-slip boundary conditions.

Lattice Boltzmann Method has been successfully applied to multi-phase and multi-component flows (Gunstensen, et al., 1991; Kehrwald, 2003; Tölke, 2001; Tölke, et al., 2007). The wide applications and fast advancements of this method during the past 20 years have proven its potential in computational physics, including microfluidics.

In the LBM, one solves the kinetic equation for the particle distribution function f(x, v, t), in which v is the particle's velocity vector, x is the spatial position vector, and t is time. The macroscopic quantities (such as mass density and momentum density) can be obtained by evaluating the hydrodynamic moments of the distribution function f. The Boltzmann equation is of the form:

$$\frac{\partial f}{\partial t} + \overline{v}\nabla f = \Omega. \tag{2.1}$$

And it can be extended to:

$$\partial_t f + v\partial_x f + F\partial_v f = \Omega, \tag{2.2}$$

where F is an external force and Ω is a collision operator. The LBM discretizes this equation by mapping the microscopic velocity space to a lattice spanned by a set of discrete microscopic velocity vectors $v_i e_i$. The discretized Lattice Boltzmann Equation (LBE) then reads:

$$\partial_t f_i + e_i\partial_x f_i + F\partial_{e_i} f_i = \Omega. \tag{2.3}$$

Then, by discretizing space and time by an explicit Euler Finite Difference scheme one can obtain the Lattice Boltzmann equation

$$f_i(x + e_i, t + 1) - f_i(x, t) = \Omega\ ;\ (\Delta t=1) \tag{2.4}$$

A popular kinetic model adopted in the literature is the single-relaxation-time (SRT) approximation, the so called BGK model (Bhatnagar, et al., 1954):

$$f_i(x + e_i, t + 1) - f_i(x, t) = -\frac{1}{\tau}(f_i - f_i^{(eq)}) \tag{2.5}$$

In the above equation, $f_i(x,t) \equiv f(x, e_i, t)$ is the distribution function associated with the ith discrete velocity $v_i e_i$ and $f_i^{(eq)}$ is the corresponding equilibrium distribution function in the discrete velocity space; and τ is a relaxation time. The nine-velocity square lattice model, which is often referred to as the 2-D 9-velocity (D2Q9) model (Qian, et al., 1992), has been widely and successfully used for simulating two dimensional (2-D) flows (Figure 2.2). In the D2Q9 model, which has been used in this study, e_i $v_i$denotes the discrete velocity set, namely,

$$e_i = \begin{cases} (0,0), & i = 0\ ; \\ (\pm 1,0)c, (0,\pm 1)c, & i = 1,2,3,4; \\ (\pm 1,\pm 1)c, & i = 5,6,7,8. \end{cases} \tag{2.6}$$

where $c = \delta x/\delta t$, δx and δt are the lattice constant and the time step size, respectively. The equilibrium distribution function for D2Q9 is of the form:

$$f_i^{eq} = \rho w_i[1 + \frac{3}{c^2} e_i * u + \frac{9}{2c^4}(e_i * u)^2 - \frac{3}{2c^2} u * u] \tag{2.7}$$

where *u* is the macroscopic fluid velocity, and w_i is the weighting factor given by

$$w_{i=} \begin{cases} 4/9, & i = 0; \\ 1/9 & i = 1,2,3,4; \\ 1/36 & i = 5,6,7,8. \end{cases} \tag{2.8}$$

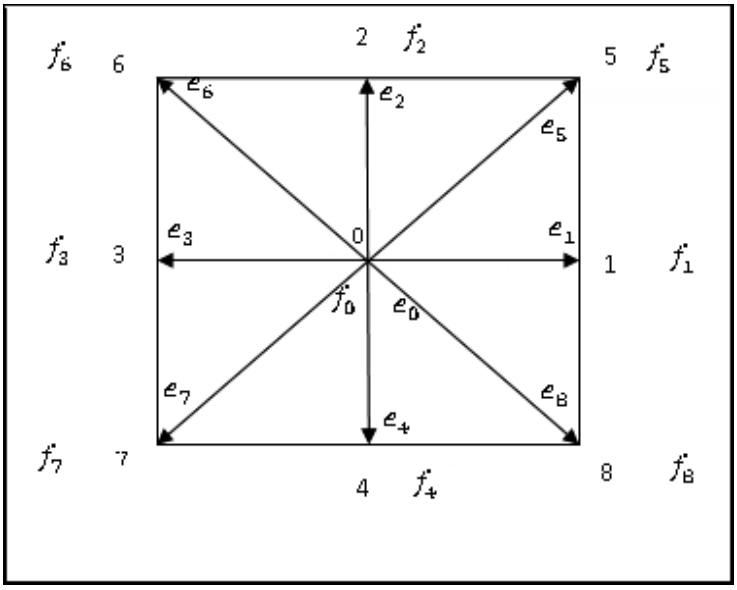

Figure 2.2: A 2-D 9-velocity lattice (D2Q9) model

In the discretized velocity space, the density and momentum fluxes can be evaluated as

$$\rho = \sum_{i=0}^{8} f_i = \sum_{i=0}^{8} f_i^{eq} \tag{2.9}$$

$$\rho u = \sum_{i=0}^{8} f_i \, e_i = \sum_{i=0}^{8} f_i^{eq} \, e_i \tag{2.10}$$

The speed of sound in this model is $c_s = c/\sqrt{3}$ $c_s = c/\sqrt{3}$ (Qian et al. 1992) and the equation of state is:

$$P = \rho c_s^2 \tag{2.11}$$

where P is the hydrodynamic pressure. The full discretization of equation (2.3), with ∂t $\partial x = e_i \, \partial t$ the time step ∂t and space step $\partial x = e_i \, \partial t$, is:

$$f_i(x + e_i \delta t \, , t + \delta t) - f_i(x, t) = -\frac{1}{\tau}[f_i(x, t) - f_i^{eq}(x, t)] \tag{2.12}$$

where $\tau\ \tau = \lambda/\delta t\ \tau = \lambda/\delta t$and xx are a relaxation time and a point in the discretized physical space, respectively. Equation (2.12) is usually solved in two steps. First, the collision step:

$$\widetilde{f_i}(x\ , t + \delta t) = f_i(x, t) - \frac{1}{\tau}\left[f_i(x, t) - f_i^{eq}(x, t)\right] \tag{2.13}$$

Second, streaming step:

$$f_i(x + e_i\delta t, t + \delta t) = \widetilde{f_i}(x\ , t + \delta t) \tag{2.14}$$

where $\widetilde{f_i}$ represents the particle distribution function for the post-collision state (Yu et al. 2003). In this study, the multiple-relaxation-time collision operator was implemented in the present model (d'Humieres, et al., 2002). For the no-slip wall boundary condition, the interpolated bounce back scheme was used to precisely locate the no-slip boundaries (Bouzidi, et al., 2001). The open boundaries for the simulation were velocity inlet and density outlet. In addition, the stress integration scheme described in (Mei, et al., 2002), for force evaluation, was used to calculate the drag and left in the validation step of numerical model. Moreover, uniform and non-uniform grids were implemented in the code (Freudiger 2009).

2.5.2 Model Validation

In order to validate the numerical model, the laminar flow field around a cylinder was solved and the drag and lift coefficients were calculated (Freudiger, 2009). The results were compared with (Schäfer and Turek 1996) whom benchmarked the computations of laminar flow around a cylinder. Table 2.2 shows a comparison between the present numerical model based on LBM and the published benchmarked results. Table 2.2 shows the agreement between both results.

	Benchmarked results	LBM numerical model
Drag coefficient	Lower bound: 6.05 Upper bound: 6.25	6.08
Lift coefficient	Lower bound: 0.008 Upper bound: 0.100	0.0082

Table 2.2: A comparison between the benchmarked results and LBM results

When Re<1, Stokes flow where simulated. All terms in the governor equation were used when Re>1 including convective and viscous terms. Mach number (the local flow-speed divided by the local speed of sound) was chosen to be 0.01 when Re<1 and 0.05 when Re>1.

Two levels grid resolutions were used in this study, level 6 and level 7. In level 6, a square with a side length equal to 100 microns will have 64 lattices. On the other side, the same square will have 256 lattices in the case of level 7 grid resolution. The choice of the grid resolution level were based on the fact that increasing the grid resolution to next level will only result in a relative change of the microfluidic diodicity value less than 1%. For example, if the microfluidic diodicity is 2.3 using level 6 grid resolution the next level will only be used if the microfluidic diodicity relatively changes more than 1%. Level 6 and 7 were sufficient in all simulations and there was no need to consider higher level of grid resolution in the selected low Reynolds number range.

2.6 Microfluidic Diodicity Evaluation

As the diodicity definition suggests, diodicity was calculated by dividing the total pressure drop in the backward direction over the total pressure drop in the forward direction. The backward direction is the direction where the flow is expected to confront the higher resistance, while the forward direction is the direction where the flow is expected to confront the lower resistance. This definition was applied under one condition: the flow rates in the forward and backward directions are equal. In general, microfluidic diodicity can be calculated by using the following equation:

$$D = \frac{\nabla P_{t,b}}{\nabla P_{t,f}} = \frac{(P_{t,i} - P_{t,o})_b}{(P_{t,i} - P_{t,o})_f}, \qquad Q_f = Q_b \tag{2.15}$$

where $D, \nabla P_{t,f}, \nabla P_{t,b}, P_{t,i}, P_{t,o}, Q_f,$ and Q_b are microfluidic diodicity, total pressure drop in the forward direction, total pressure drop in the backward direction, inlet total pressure, outlet total pressure, forward flow rate, and backward flow rate, respectively. The total inlet and outlet pressures were calculated just before and after the rectifying geometry. The total pressure (inlet or outlet) was calculated as follows:

$$P_t = \frac{1}{A}\int (P_S + {}^1\!/_2\,\rho V^2) dA \tag{2.16}$$

where P_S, V, and A are the static pressure, the fluid velocity, and cross sectional area, respectively. In other words, the total pressure is equal to the sum of the static and dynamic pressures. Total pressure can be evaluated numerically by using the following formula:

$$P_{t=} \frac{1}{N}\sum_{i=1}^{N}(P_i + 0.5\rho V_i^2) \tag{2.17}$$

where N is the total number of nodes where the pressures and the velocities were measured.

2.7 Results and Discussion

The microfluidic diodicity was calculated just before and after the rectifying geometries to eliminate external losses such as inlet and exit losses. Figure 2.3 shows the diodicity versus Reynolds number in the case of the Tesla and Triangle structures. The results suggest that flow rectification is not achievable for very low Reynolds numbers. In the case of the Tesla structures, the flow faces two different paths, long and short. Typically, the fluid flows in the path that has less resistance, which, in this case, is the short channel. In order to achieve rectification, the fluid should flow in the long path in the backward direction and in the short path in the forward direction. In this low region of Reynolds numbers, our result suggests that the inertia is not sufficient to drive the fluid in the long channel (in the backward direction). As a result, the fluid flows in the short channel and flow rectification is not achievable. In the case of the triangle structure, the majority of pressure drops are caused by the nozzle effect (in the backward direction) and stagnation lines effect (in the forward direction). In this very low Reynolds number region, the results suggest that the pressure drops in both directions are evenly balanced. As a result, flow rectification may not be achievable in this range. It may be worth noticing that microfluidic diodicity started to increase after Re = 25 in the case of the triangle geometry but not sufficient to achieve efficient rectification. The results of the present numerical model agree with results published by Gamboa et al. (2005). Their study was in the Reynolds numbers ranging between 0 and 2,000, and it shows no rectification when Re $\leq$ 60. Figure 2.4 and 2.5

show the flow fields in the forward and backward directions in the case of Tesla and triangle geometries at Reynolds number equal to 60.

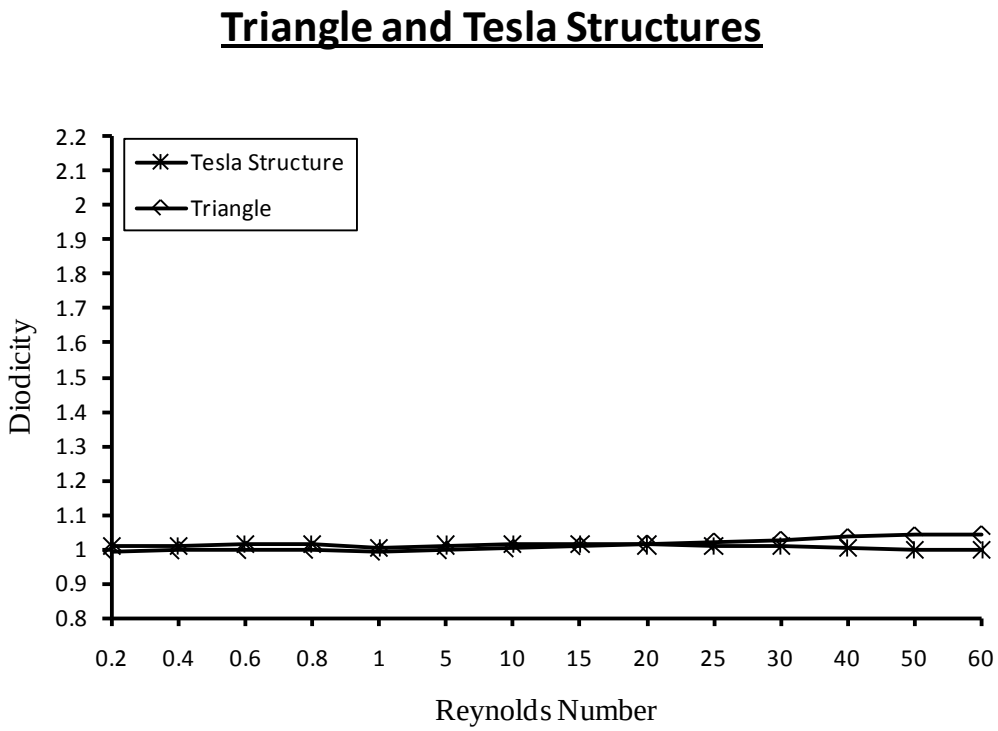

Figure 2.3: The diodicity versus Reynolds number in the case of triangle and Tesla structures

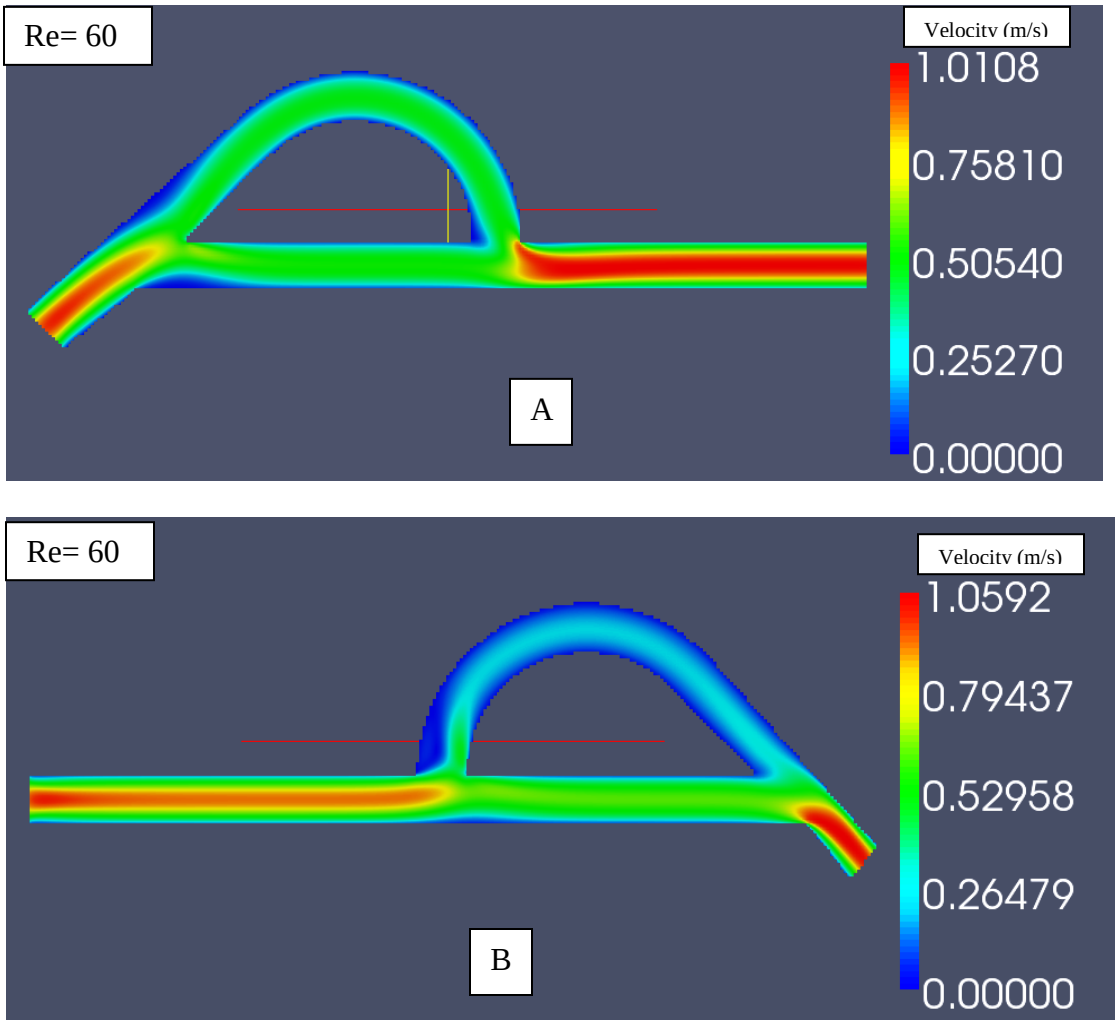

Figure 2.4: The flow field in the case of Tesla geometry at Re=60; A: Backward flow field; B: Forward flow field

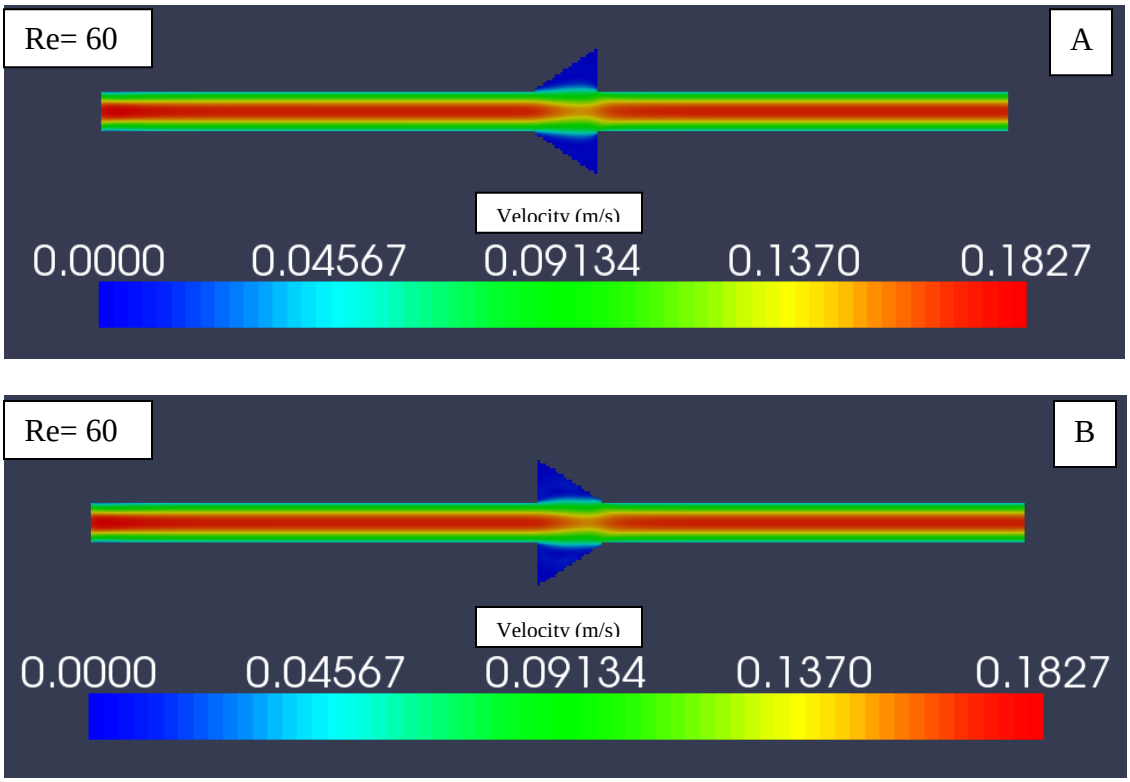

Figure 2.5: The flow field in the case of triangle geometry at Re=60; A: Forward flow field; B: Backward flow field

Figure 2.6 shows the microfluidic diodicity values in the case of the half and semicircles geometries. The results suggest that both structures have a comparable trend. From Re = 0.2 to 0.8, the diodicity is almost equal to one. As a result, flow rectification is not achievable in this range. From Re = 1 to 20, in the case of the semicircle, and Re = 1–25, in the case of the half circle, the microfluidic diodicity is less than one but not sufficient to efficiently rectify the flow in the backward direction. From Re = 20 to 60, in the case of the semicircle, and from Re = 25 to 60, in the case of the half circle, the microfluidic diodicity increases monotonically until it reaches its maximum at Re = 60. At Re = 60, both geometries can moderately rectify the flow, the value of the microfluidic diodicity is 1.22 and 1.33 in the case of the semi- and half

circles, respectively. The rectification is, as expected, in the forward direction. Figure 2.7 shows the flow fields in the forward and backwards directions at Reynolds number equal to 60 and 25, respectively, in the case of half circle geometry. On the other hand, Figure 2.8 shows the flow field in backward direction at 0.2 and 60 Reynolds numbers in the case of a semi circle geometry.

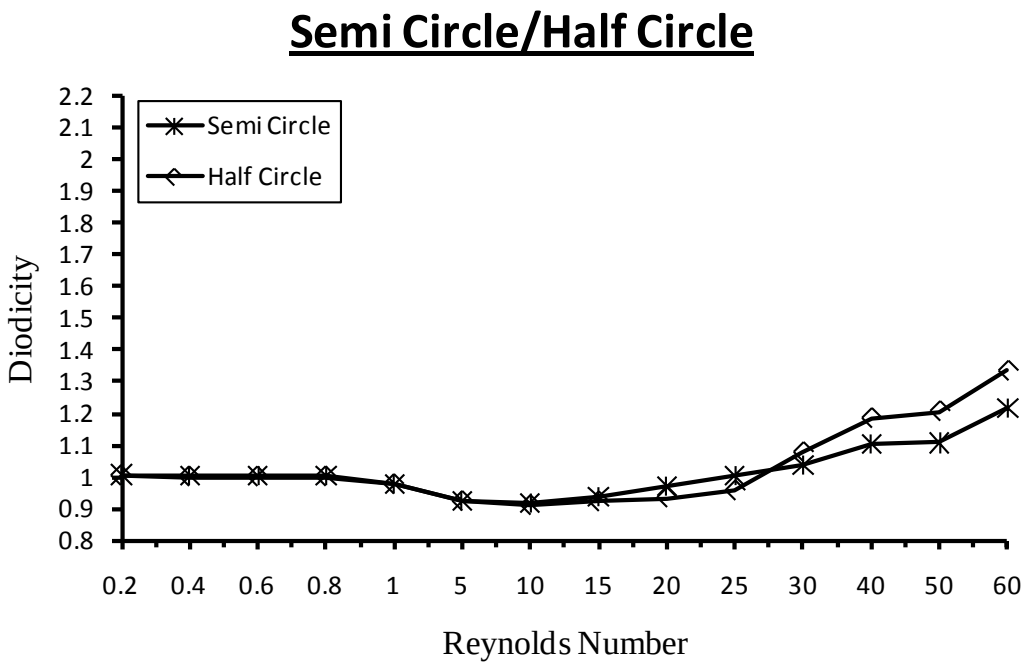

Figure 2.6: The diodicity versus Reynolds number in the case of semi and half circles

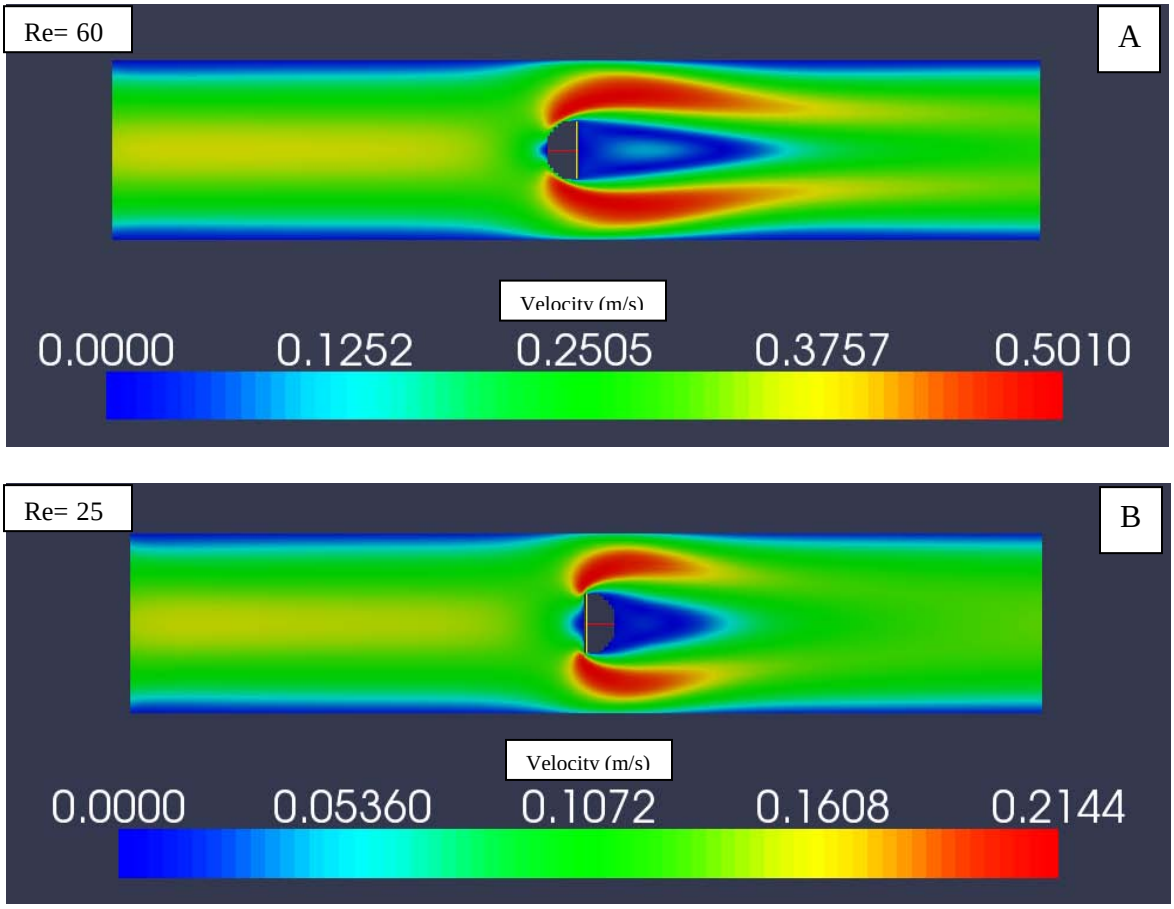

Figure 2.7: The flow field in the case of half circle geometry; A: Forward flow field (Re=60); B: Backward flow field (Re=25)

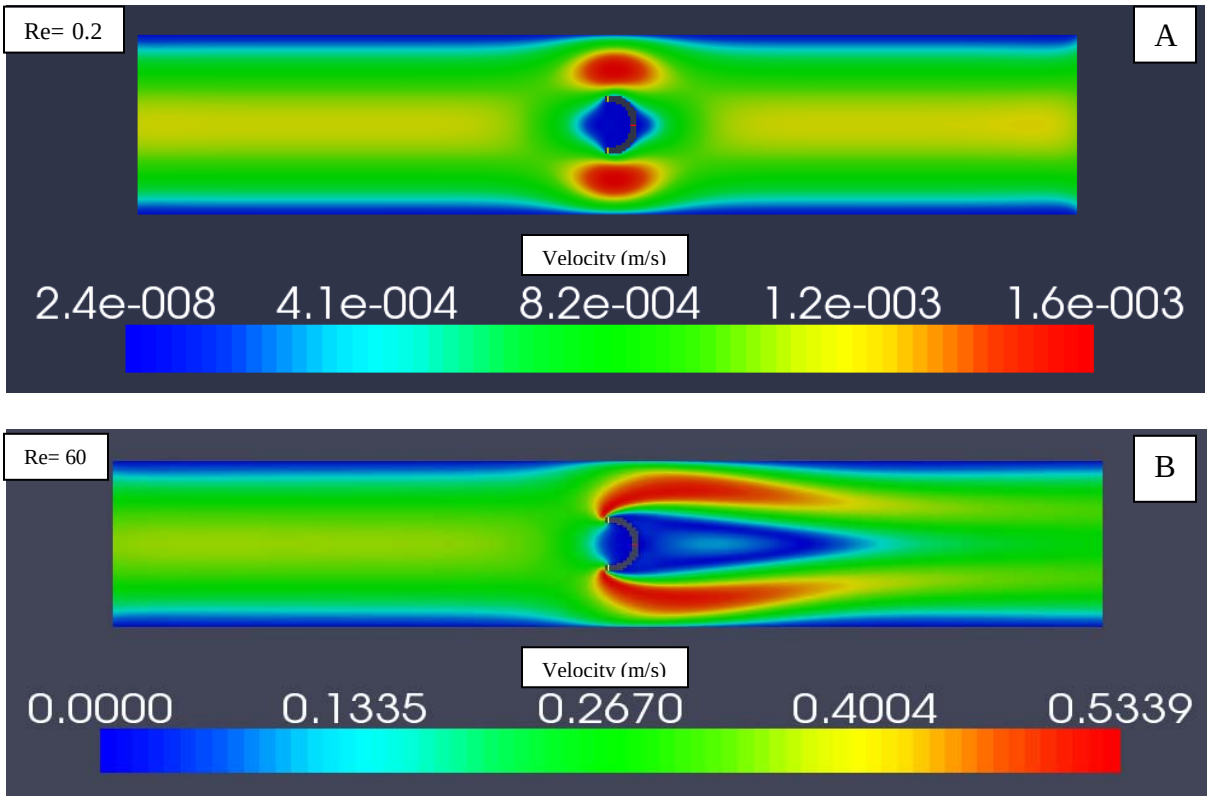

Figure 2.8: The backward flow field in the case of semi circle geometry; A: Re=0.2; B: Re=60

Figure 2.9 shows the results of the heart shape structure. The microfluidic diodicity is less than one in the Reynolds number range is between 0.2 and 10, which suggests that the rectification will not be efficient (the diodicity between 0.916 and 0.995), and the rectification will be in the backward direction. When the Reynolds number increases from 10 to 60, the diodicity also increases monotonically until it reaches the value of 1.35. As a result, the flow rectification is achievable with moderate diodicity, particularly when the Reynolds number range is between 30 and 60; the rectification is, as expected, in the forward direction. Figure 2.10 shows the flow fields in the forward and backward directions at Reynolds number equal to 60 in

the case of the heart shape geometry. Secondary flow is clearly observed in the backward flow direction as shown in Figure 2.11.

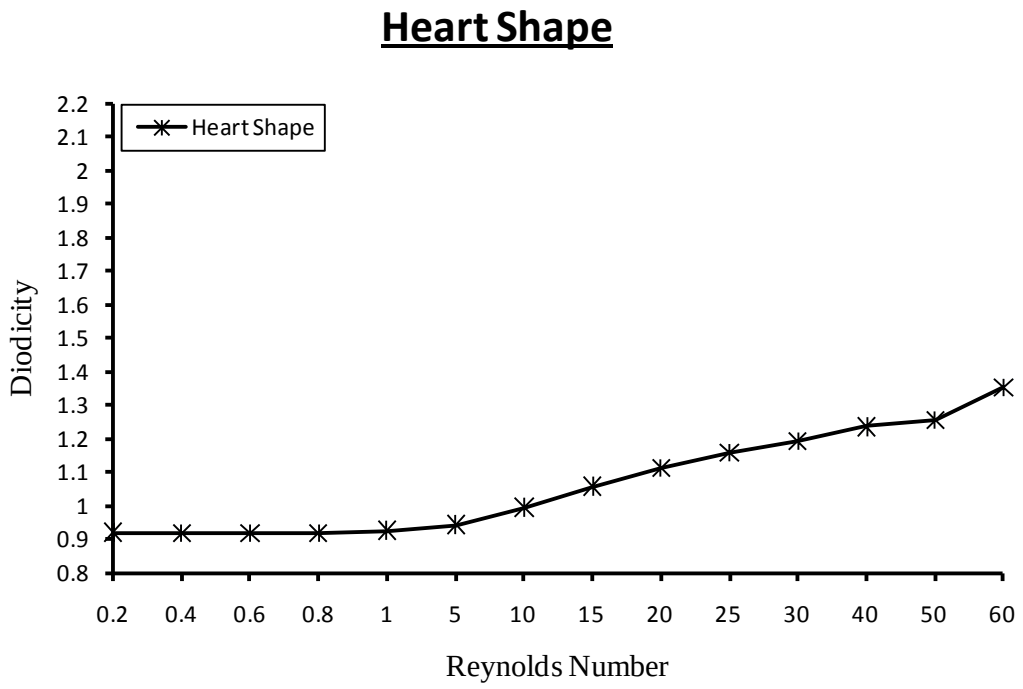

Figure 2.9: The diodicity versus Reynolds number in the case of the Heart shape structure

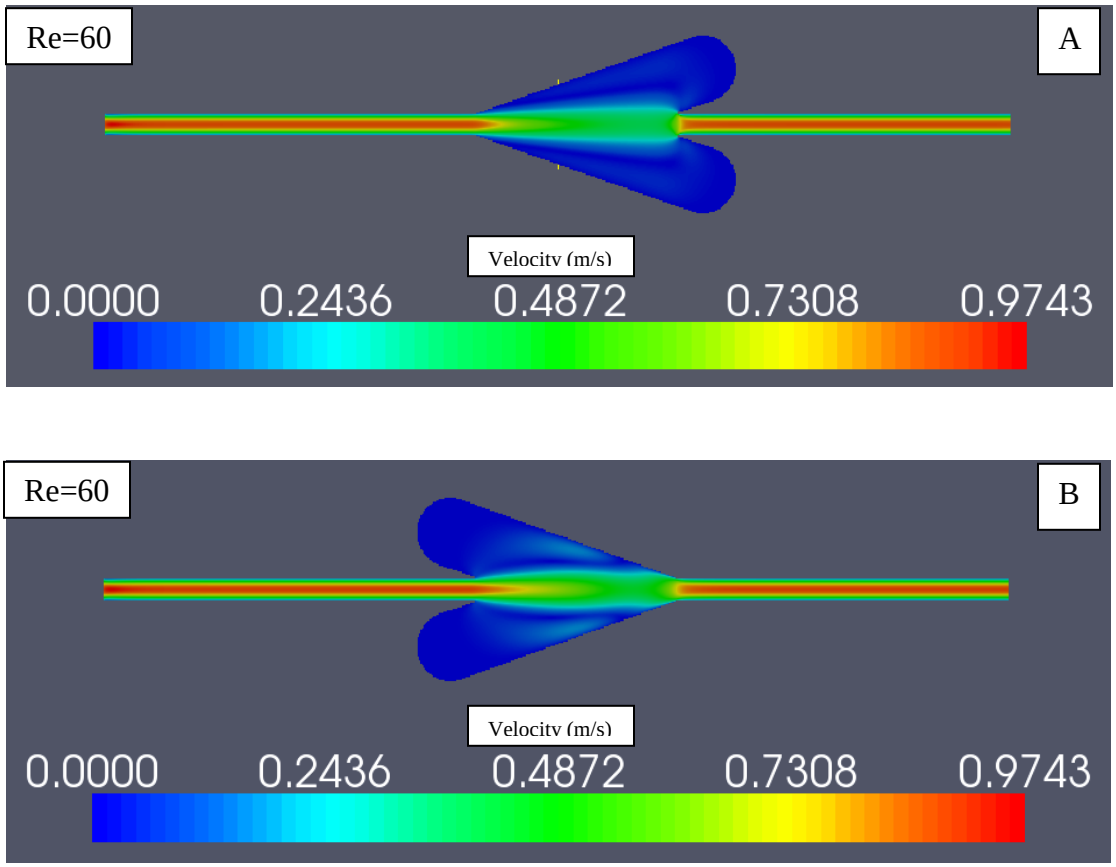

Figure 2.10: The flow field in the case of heart shape geometry at Re=60; A: Forward flow field; B: Backward flow field

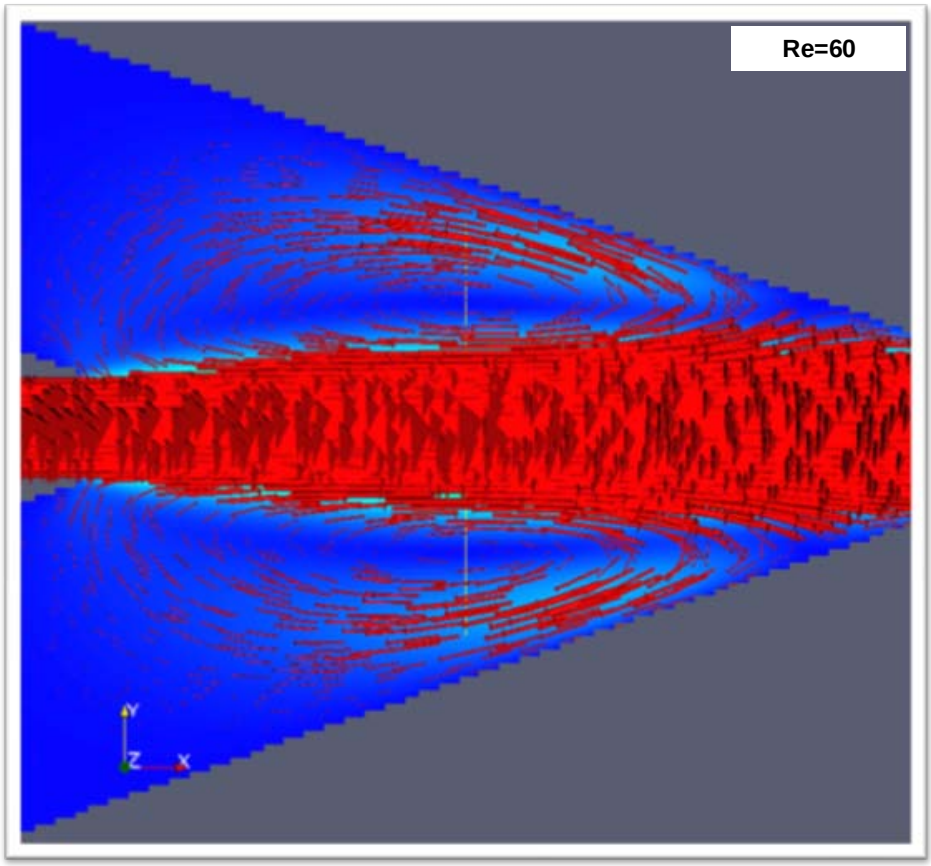

Figure 2.11: Secondary flow is observed in the backward direction at 60 Reynolds number

The results for the first conventional geometry, the nozzle/diffuser, are shown in Fig. 2.12. The microfluidic diodicity is approximately one in the Reynolds number range of 0.2–25, and increases monotonically until it reaches 2.075. However, the rectifying direction is not in the forward direction; instead it is in the backward direction (the nozzle direction). The results agree with the trend that suggests, when a nozzle/diffuser angle is more than 20º, the loss in the diffuser is larger than the loss in the nozzle. The flow simulation shows a flow separation occurring in the diffuser and increasing with the increase in Reynolds number. The function of the diffuser is to recover the pressure due to the diverging wall, but due to the ‘‘vena-contracta’’ effect

(Olsson, et al., 1997a,b) the diffuser will not recover the pressure and the losses in the diffuser will be larger than those of the nozzle, which agrees with the reported results (Olsson et al. 2000). As a result, the rectification direction will be in the nozzle direction. This result is angle-dependent, and the results will change if the diffuser/nozzle angle is not 36.8º (or a half angle equal to 18.4º). Figure 2.13 shows the flow stream lines in two cases: when Reynolds number is 0.2 and 60. The flow separation is apparent when Re = 60. As the results show, the rectification is expected to be in the backward direction. Examples of the flow fields in the forward direction are shown in Figure 2.14 at Reynolds numbers equal to 0.2 and 60.

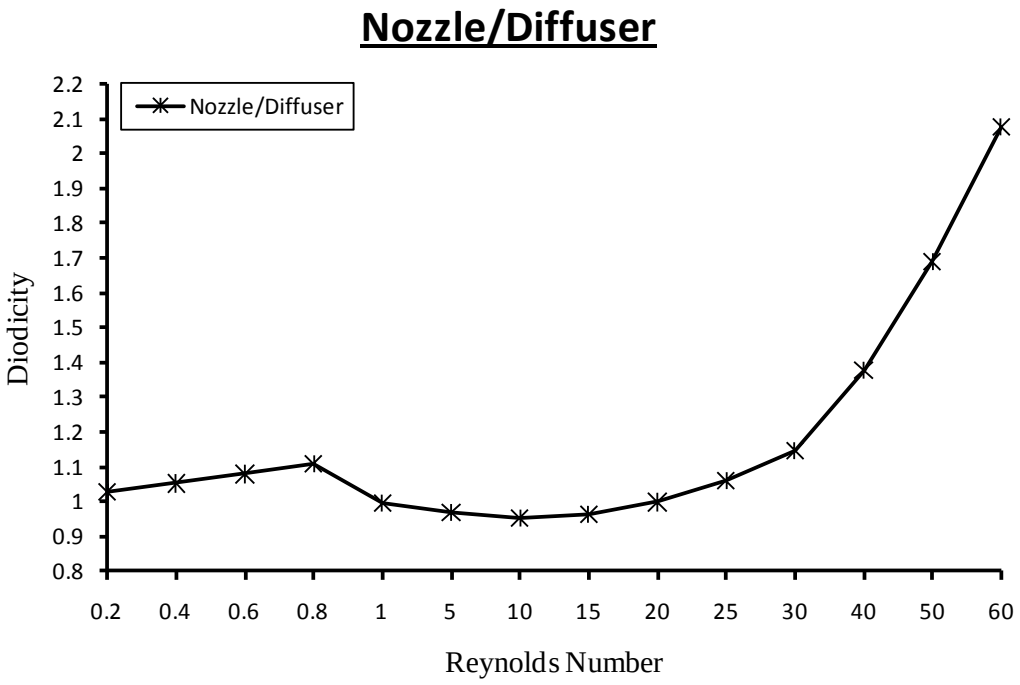

Figure 2.12: The diodicity versus Reynolds number in the case of the nozzle/diffuser structure

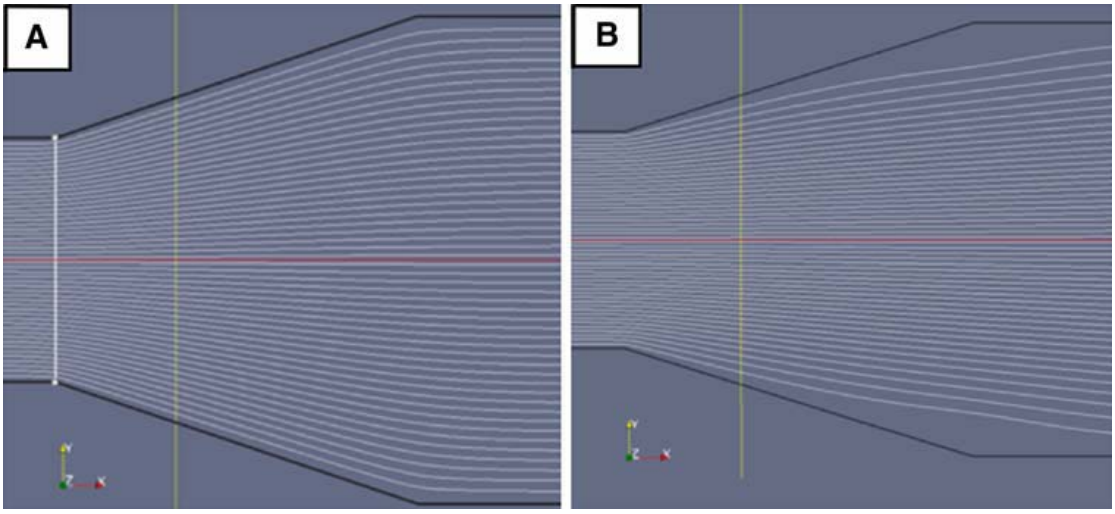

Figure 2.13: The steam line field in the case of the nozzle/diffuser when A: Re = 0.2 and B: Re = 60

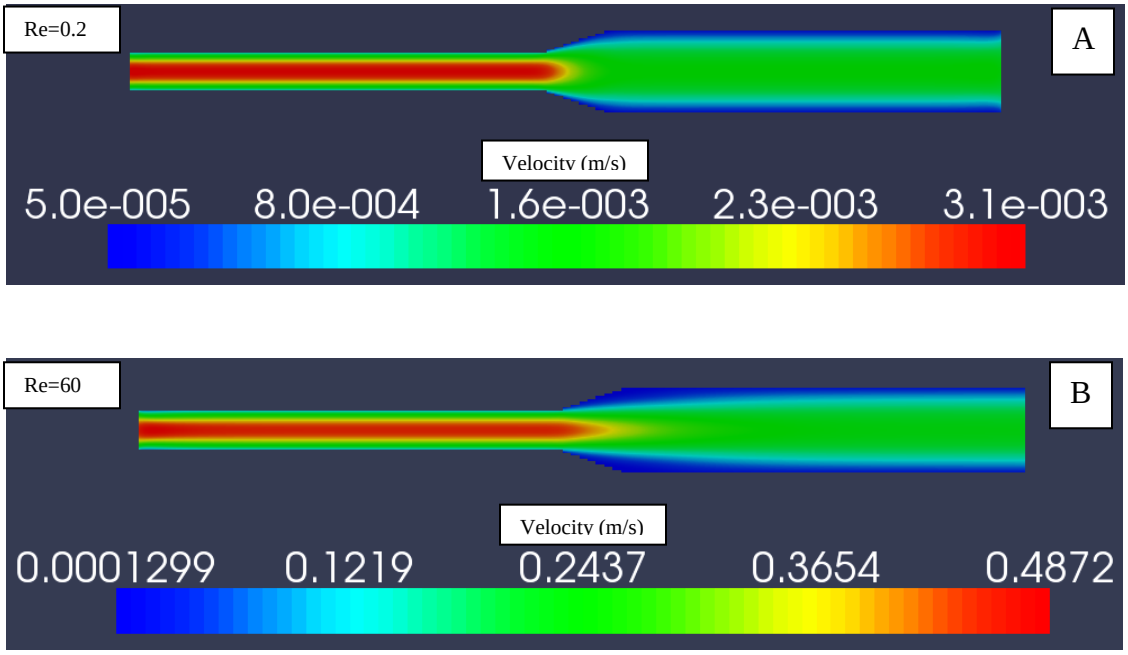

Figure 2.14: The forward flow fields in the case of nozzle/diffuser geometry; A: Re=0.2; B: Re=60

The last geometry which was tested in this study is the bifurcation structure, depicted in Fig. 2.15. The results suggest that rectification is not achievable for Reynolds numbers between 0.2 and 5 but diodicity increases monotonically afterward until it reaches 2.03 at Re = 60. This indicates that efficient rectification can be reached through the bifurcation structure at low Reynolds number (Re = 10–60) with a maximum diodicity at Re = 60. Moreover, the diodicity increases with the increase of the inertia and it suggests that the bifurcation structure diodicity is inertia-dependent. The diodicity mechanism depends on generating a higher pressure drop in the forward direction than in the backward direction. The flow in the forward direction (started at the mother tube) will split into two flows in the daughter tubes. As a result, the maximum velocity at the mother tube will come into a stagnation point and a higher shear stress will be generated in the inner walls of the daughter tubes. On the other hand, the flows at the daughter tubes will be merged into the mother tube without coming into a stagnation point, and with less shear stress at the walls of the mother tube. Increasing the inertia at the mother tube will result in a higher loss at the stagnation point (bifurcation tip) and higher velocity gradient at the inner walls in the daughter tubes. Therefore, increasing the inertia will lead to higher pressure drops in the backward than the forward flow. The results demonstrate the potential of multifunction capability of the bifurcation structure, where it can mix the flow without a net flow rate in the Reynolds number region of 0.2–5, and it can efficiently rectify the flow with a maximum diodicity at Re = 60. The rectification is, as expected, in the forward direction. Examples of the backward flow fields are given in Figure 2.16 at Reynolds number equal to 0.2 and 60

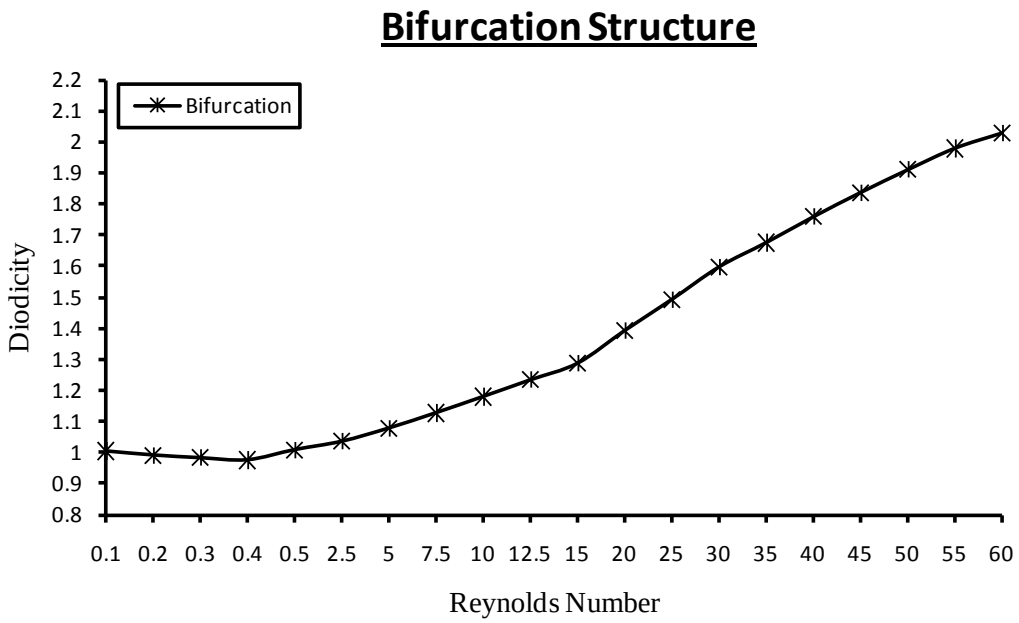

Figure 2.15: The diodicity versus Reynolds number in the case of bifurcation structure

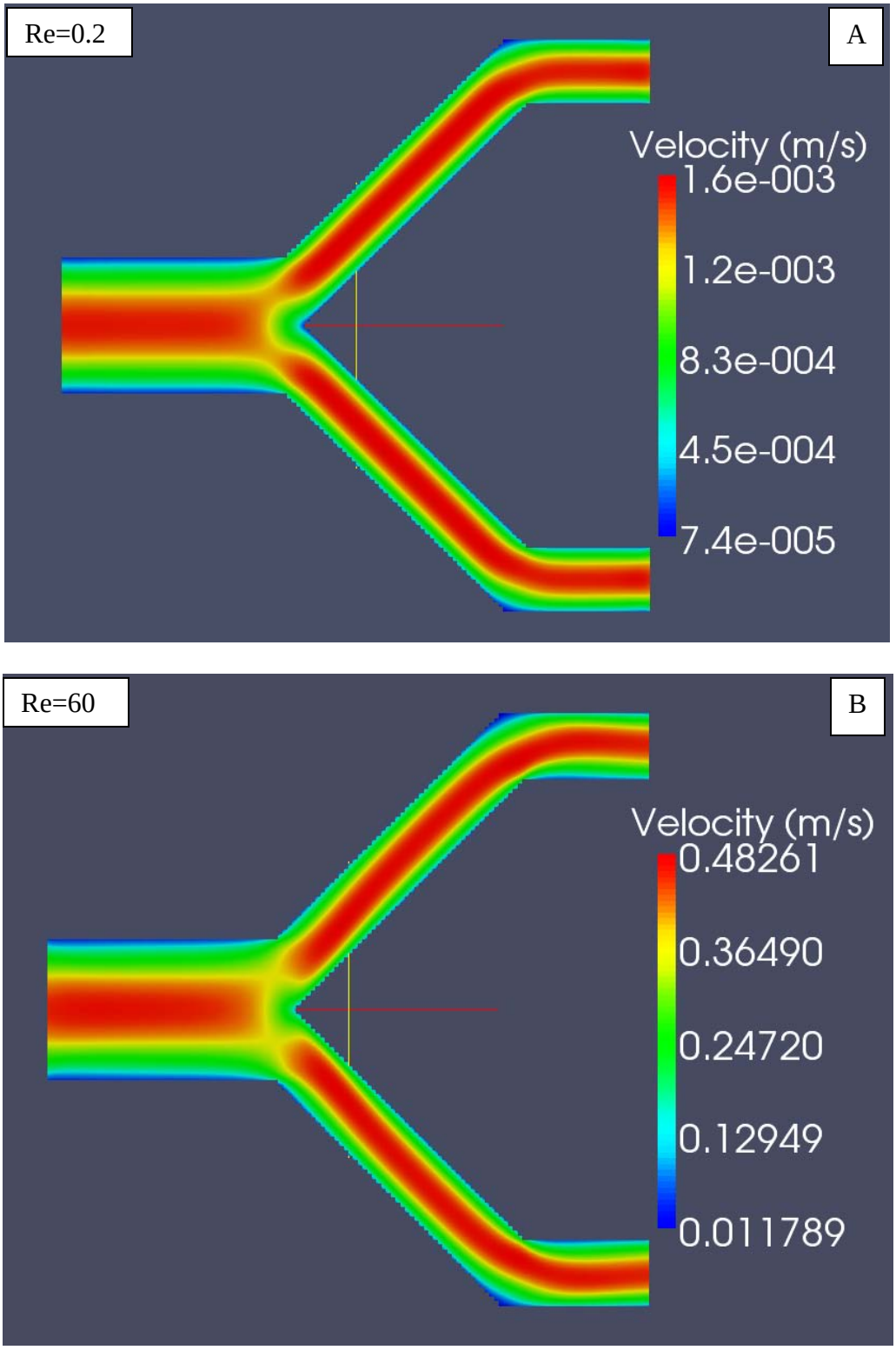

Figure 2.16: The backward flow fields in the case of bifurcation geometry; A: Re=0.2; B: Re=60

2.8 Conclusion

The conclusions of the study can be summarized in the following points:

(1) LBM was successfully adapted for the first time, to numerically evaluate the microfluidic diodicity for several rectifying structures including the conventional structures. The numerical model was validated and the results were in agreement with the published benched mark results.

(2) Unconventional structures can be used to rectify the flow and may potentially be used in the valve-less rectification micropumps. In this study, alternative structures were found to rectify the flow at very low Reynolds numbers. For example, the heart shape, semicircle, half circle, and bifurcation structures were studied, and they can rectify the flow as well as mixing the flow (when D & 1) at very low Reynolds numbers. In contrast, rectification is not achievable in the case of the Tesla and triangle structures.

(3) At very low Reynolds numbers, the nozzle/diffuser and bifurcation structures can efficiently rectify the flow, where the maximum diodicity was reached at Re = 60.

(4) In the nozzle/diffuser structure, the direction of the rectifying flow depends on the divergence angle and the Reynolds number. The results of the present work suggest that at 36.8divergence angle and Re = {25–60} the losses in the diffuser will be larger than those in the nozzle. As a result, the rectifying direction will be backward instead of forward. The ‘‘vena-contracta’’ effects can explain the results as the flow separation was clearly observed in the diffuser element when Re = {25–60}.

(5) In the investigated range of Reynolds numbers, the diodicity values start approximately at one before reaching the maximum at Re = 60. This trend may be beneficial in biological applications to accomplish both mixing and pumping with one microdevice.

(6) In the case of the semicircle and half circle structures, the value of the microfluidic diodicity can be found in three regions: less than one, equal to one, and more than one. The ability to change the value of the microfluidic diodicity, with respect to Reynolds numbers between {0.2–60}, demonstrates the potential to achieve rectification (D = 1), mixing (D = 1), and bidirectional pumping (D<1 and D<1) by changing the Reynolds numbers within the investigated ranges.

CHAPTER 3

3 Valve-less Rectification Micropumps Based on Bifurcation Geometry

“Facts are not science - as the dictionary is not literature.”

Martin H. Fischer

3.1 Abstract

In this chapter, a novel valve-less rectification micropump based on bifurcation geometry was introduced. Three micropumps based on three different bifurcation configurations were designed, fabricated and experimentally investigated. These designs demonstrate the potentials of developing bidirectional micropumps and multifunction microfluidic devices (combined functions of micro pumping and mixing). Polydimethylsiloxane (PDMS) was employed to fabricate the micropumps. Circular piezoelectric transducers (PZT) were used as flow actuators. Detailed fabrication procedures are illustrated. The micropumps were tested against two ranges of actuator frequencies. The first test was conducted in a frequency range between 0 and 100 Hz with small increments of 5 Hz, while the second test was conducted in a frequency range between 0 and 300 Hz with increments of 50 Hz. Ethanol was used as the working fluid in all experiments. A new dimensionless parameter was introduced to better evaluate the efficiency of valve-less rectification micropumps and determine the optimum operational frequency. The flow rate and maximum back pressure were measured. Results of experiments confirmed and demonstrated the feasibility of valve-less rectification micropumps based on bifurcation geometry at a low frequency range. Additionally, results showed the potentials of multifunctional, bidirectional, and self-priming micropumps based on bifurcation geometries.

3.2 Introduction

Many studies on developing, modeling and optimization of micropumps have been published in the past decade (Nguyen, et al., 2002; Laser, et al., 2004; Iverson, et al., 2008; Amirouche, et al., 2009). Micropumps can be categorized with respect to their working principles as mechanical and non-mechanical micropumps. Mechanical micropumps usually use mechanical parts to deliver a constant fluid volume. Examples of mechanical micropumps are rotary, peristaltic, check valves, and valve-less rectification micropumps. The valve-less rectification micropump can be further categorized as a displacement mechanical micropump. On the other hand, non-mechanical micropumps add momentum to the fluid by converting another energy form into kinetic energy. Examples of nonmechanical micropumps are electrokinetic, magnetohydrodynamic, and electrochemical micropumps.

The valve-less rectification micropumps have gained increased research attentions in recent years. The advantages of valve-less rectification micropumps include having no-moving parts, easy to fabricate, cost effective, having the ability to pump particles-laden fluids and live cells, being compatible with a wide range of materials and working fluids, and delivering a favorable flow rates and back pressures ((Stemme, et al., 1993; Olsson, et al., 2000; Yamahata, et al., 2005). Figure 3.1 shows the working principles of the valve-less rectification micropump. In the supply mode, the piezoelectric transducers (PZT) diaphragm moves upward and generates a negative pressure inside the pump chamber. As a result, the fluid flows into the chamber. More fluid enters from the right bifurcation compared to the left one due to the difference in the flow resistance. On the other hand, when the PZT moves downward, in the pump

mode, a positive pressure is generated inside the pump chamber. Therefore, the fluid flows out of the chamber. More fluid exits the left bifurcation compared to the right one during the pump mode. Due to the combined effects of the PZT diaphragm oscillation, a net flow rate is observed from the direction of right to left.

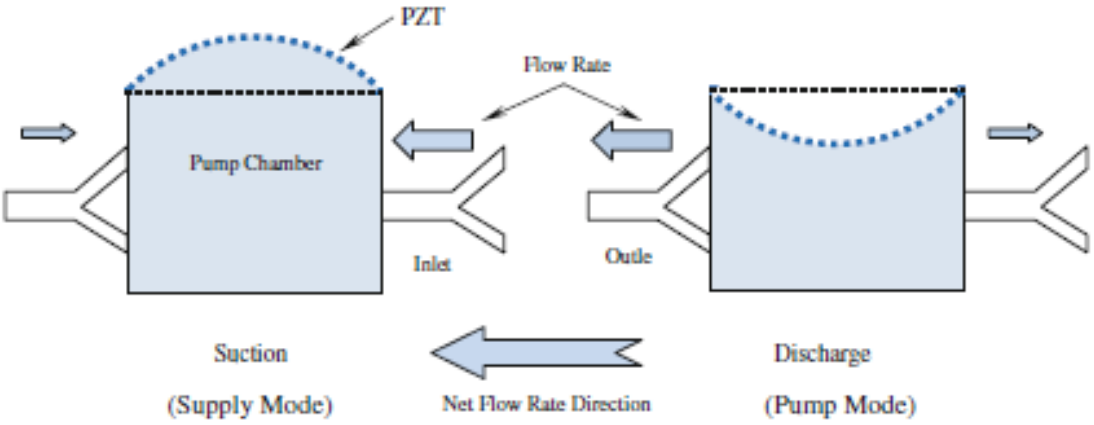

Figure 3.1: The pumping mechanism of the valve-less rectification micropump

The efficiency of the valve-less rectification micropump depends primarily on the microfluidic diodicity (the ratio of the pressure drop of the backward flow to the forward flow). The backward flow is the flow in the direction where the flow faces a higher flow resistance, while the forward flow is the flow in the direction where the flow faces a lower flow resistance. There are two conventional rectifying geometries commonly studied in the literature: nozzle/diffuser and Tesla geometries (Olsson, et al., 1995; Foster, et al., 1995). Fadl, et al., (2007) experimentally measured the microfluidic diodicity for several nonconventional geometries, and the results suggested that flow rectification might be achievable by using nonconventional rectifying geometries. Recently, Fadl, et al., (2009) numerically evaluated the

microfluidic diodicity at low Reynolds numbers for both conventional and nonconventional geometries, and the results suggested that there are nonconventional geometries such as the bifurcation geometry which can effectively rectify the flow at low Reynolds number. The work by Fadl, et al., (2009) showed that the bifurcation geometry has the highest microfluidic diodicity at low Reynolds numbers among other nonconventional rectifying geometries investigated in the study.

Several studies were published in the literature that focused primarily on valve-less rectification micropumps. Most of the studies have used either Tesla or nozzle/diffuser geometries for flow rectification. For example, Stemme, et al., (1993); Olsson, et al., (1995, 1997b); Gerlach, et al., (1995); Gerlach (1997); Jiang, et al., (1998); Büttgenbach, et al., (1999); Singhal, et al., (2004b); Chen, et al., (2008); and Shen, et al., (2008) conducted researches on valve-less rectification micropumps based on nozzle/diffuser geometries. They employed flat walled and pyramid-trunk-shaped nozzle/diffuser geometries. They also tested micropumps with one chamber versus two chambers. In their studies, a PZT diaphragm was utilized to actuate the micropump, and silicon-glass or polydimethylsiloxane (PDMS)-glass were used to fabricate the micropumps. There were many inconclusive results throughout the literature as discussed by Fadl et al. (2009). However, most results showed that the micropump performance has a strong dependence on the flow Reynolds number and nozzle/diffuser angle. The performance of valve-less rectification micropump has been numerically simulated and characterized by many researchers (Olsson, et al., 1997a; Olsson, et al., 2000; Sun, et al., 2006; Cui, et al., 2008). Other studies had also been

conducted to characterize the losses within a nozzle/diffuser geometry (Yang, et al., 2004; Rosa, et al., 2006; Wang, et al., 2009a).

Similar to the nozzle/diffuser-based micropump research, valve-less rectification micropumps based on the valvular conduits (Tesla's geometry) have been reported in the literature as well. Design, fabrication, and testing of the micropumps were conducted by Forster, et al., (1995) and Bardell, et al., (1997). Other studies included the transport of particle-laden fluids using valve-less rectification micropumps (Jang, et al., 2009), the effect of the particle-laden fluids on the performance of the valve-less rectification micropumps (Jang, et al., 2000), optimization (Gamboa, et al., 2005), and a low-order modeling of resonance for valve-less rectification micropumps (Morris, et al., 2003) were also included in the literature.

According to our literature search, the majority of the valve-less rectification micropumps are based on nozzle/diffuser and Tesla structures. Both structures work effectively at high frequency. In fact, Gerlach, et al., (1995); Olsson, et al., (1996); and Koch, et al., (1998) (nozzle diffuser) reported that flow rectification is not achievable in laminar flow. Moreover, Gamboa, et al., (2005) (Tesla structure) showed in his results that flow rectification is not achievable when Re is less than 200. However, most microbiological applications have fluid flows at low Reynolds number (Geschke, et al., 2004). Wang, et al., (2009b) have reported an optimized design for a valve-less rectification micropump based on nozzle/diffuser where they examined the pump performance against low actuator frequencies (0–20 Hz). The maximum reported flow rate was 0.06 µl/min. Moreover, valve-less rectification micropumps based on nozzle/diffuser and Tesla structures are unidirectional when no structural

modifications are introduced. In this study, we introduce a valve-less rectification micropump that is capable of rectifying the flow at low Reynolds number (e.g. low frequency), achieve bidirectional pumping, and multifunctions (pumping and mixing). Additionally, because of the nature of the bifurcation, they can well integrate in microarrays since they can be designed in single and multiple generations. Therefore, the nature design of microarrays by itself can be used to rectify the flow when an oscillatory flow is introduced. As a result, the extra pressure drop introduced by external rectifying geometries can be eliminated.

The first bidirectional valve-less rectification micropump was claimed by van der Wijngaart, et al., (2000) where maximum flows of +30 µl/min and -30 µl/min were measured. However, the operating frequencies were between 0.1 and 80 kHz. Another bidirectional valve-less micropump was reported by Hayamizu, et al., (2003) where the micropump was controlled by driving waveform. The micropump generated maximum flow rates of +393 nl/s and -323 nl/s in the forward and backward directions, respectively. Moreover, an additional bidirectional valve-less rectification micropump was reported by using two oblique channels and two pump chambers with two PZT actuators (Yoon, et al., 2007). The reported flow rate ratio (the ratio between the discharge flow rate and the suction flow rate) was only between 1.01 and 1.03. It is noted that the net flow rate is the difference between the rates of the suction and discharge flows.

Microsystems devices that can combine mixing and pumping work were reported in the literature. Lastochkin, et al., (2004) reported a microfluidic pump and mixer based on AC faradic, Yang, et al., (1998) reported the first micropump with active

micromixer using turbulence to enhance the mixing of liquids, Rife, et al., 2000) miniaturized acousto-fluidic devices to operate a valve-less micropump and produce mixing in low Reynolds number flows, Deshmukh, et al., (2001) reported a continuous micromixer with pulsatile flow micropump using silicon on insulator (SOI) and quartz dies and, finally, Sheen, et al., (2007) studied the flow characteristics and mixing performance in a PZT self-priming micromixer by using microparticle- image velocimetry (micro-VIP).

According to our literature review, the only work which employed the bifurcation geometry to rectify the flow was reported exclusively at the macro scale (Jianhui et al. 2007). In this work, the bifurcation geometry was made of a Y-shaped circular tube (which will be difficult to fabricate at the micro scale). The reported maximum flow rate and the mean pressure were 3 ml/min and 33 Pa, respectively.

In this chapter, we introduce a novel valve-less rectification micropump based on a bifurcation geometry and PDMS micro fabrication techniques. Three different micropumps based on three different bifurcation configurations were designed, fabricated, and experimentally investigated at a low frequency range. Additionally, we introduce a new dimensionless parameter to better evaluate the efficiency of the valve-less rectification micropumps and determine the optimum micropump operational frequency.

3.3 Pumping Mechanism and Characterization

Valve-less rectification micropumps are displacement mechanical micropumps and recognized by being valve-less. Instead of having dynamic valves, the valve-less rectification micropumps have rectifying geometries (passive valves) to rectify the

flow. The rectifying geometries have flow resistances that depend on the flow direction. The ratio of the pressure drop in both directions is called microfluidic diodicity and it is defined as follows (Forster et al. 1995):

$$D_i = \frac{\Delta P_b}{\Delta P_f} \tag{3.1}$$

where D_i , ΔP_b, and ΔP_f are the microfluidic diodicity, pressure drop in the backward direction, and pressure drop in the forward direction, respectively. In order to achieve flow rectification, the value of the microfluidic diodicity must be different than one. The efficiency of the flow rectification depends on the value of the microfluidic diodicity. High rectification efficiency means efficient micropump.

To achieve net flow rates through flow rectification, the following two conditions must be met: first, generation of oscillatory flows; second, flow oscillation in rectifying geometries. Typically, PZT actuators are used to generate oscillatory flows, and the rectifying geometries are used to rectify the flows. Nozzle/diffuser and Tesla structures are typical rectifying geometries in the literature. Regardless of the rectifying geometries type, all valve-less rectification micropumps share the same pumping mechanism and factors that may affect the pumping performance. The parameters that affect the pumping performance are mainly associated with the actuators (PZT) and rectifying geometries. Therefore, the valve-less rectification micropumps can be characterized with respect to the actuator characteristics as well as geometrical characteristics of the rectifying geometries. In general, parameters that have an influence on the oscillatory flow behavior will certainly affect the pumping performance to certain extend.

With respect to the rectifying geometries, the flow resistance coefficients in the forward and backward directions (ξ_f and ξ_b) are employed to characterize the micropumping efficiency (Olsson et al. 1995, 2000; Jiang et al. 1998; Singhal et al. 2004; Yang et al. 2008). In the present design, the backward direction is the direction from the main channel to the secondary channels, while the forward direction is the direction from the secondary channels to the main channel. The forward and backward flow resistance coefficients can be defined as:

$$\xi_f = \frac{\Delta P_f}{\rho V_f^2/2} \tag{3.2}$$

$$\xi_b = \frac{\Delta P_b}{\rho V_b^2/2} \tag{3.3}$$

where ξ_f, ξ_b, V_f, V_b, and ρ are the flow resistance coefficients in the forward direction, flow resistance coefficients in the backward direction, flow velocity in the forward direction (secondary channels), flow velocity in the backward direction (main channel), and the fluid density, respectively. The pressure drop along the rectifying geometry is influenced apparently by the geometrical parameters of the rectifying geometries such as nozzle diffuser angle and nozzle diffuser length in the case of the nozzle/diffuser micropumps (Olsson et al. 1997a, b, 2000; Yang et al. 2004; Gamboa et al. 2005). In our design, the geometrical parameters may include the bifurcation angle, the width ratio between the main and secondary channels, number of generations, and the symmetry of the secondary channels. The flow resistance coefficient and the time dependent chamber volume are utilized to calculate the flow rates and pump pressure, respectively, with different arrangement of pump chambers (Ullmann 1998).

In addition to the friction factor, the flow resistance can be predicted by the geometry effects such as conversion and diversion in the case of nozzle/diffuser (Jiang et al 1998; Olsson et al. 1999). The rectifying-directing capability of the rectifying geometries is defined by the ratio of the resistance coefficient in the backward direction to the resistance coefficient in the forward direction as

$$\eta = \frac{\xi_b}{\xi_f} \tag{3.4}$$

the value of η is larger than one when the net flow rate in the forward direction (as predicted) and smaller than one when a reverse flow in the backward direction may occur. Besides the flow resistance, the flow inductance needs to be considered to investigate the effects of the unsteady flow on the flow behavior in the valve-less rectification micropumps. The conventional expression given in the literature for the flow impedance is given as follows

$$\hat{Z} = \frac{\Delta\hat{P}}{\hat{Q}} = R + i\omega I \tag{3.5}$$

where $\hat{Z}$, $\Delta\hat{P}$, $\hat{Q}$, R, ω and I are the complex form of the flow impedance, complex form of pressure drop, volume of flow rate, flow resistance, radian frequency, and fluid inductance, respectively. It shows that impedance is primarily affected by flow resistance and pressure oscillating frequency (Morris and Forster 2003, 2004). In the case of oscillating flow, the velocity is derived based on the time-dependent pressure gradient. Since the pressure gradient is only a function of time and typically expressed in the form of Fourier series or Euler formula, a phase-lag may exist between the flow velocity and the pressure gradient. The synchronization between the flow velocity and the pressure gradient can be identified qualitatively by using Wormersley number (Wo) where it can compare the transient initial force to the viscous force (Loudon and

Tordesillas 1998)

$$W_O = r\sqrt{\frac{n}{v_f}} \tag{3.6}$$

where r, n, and v_f are characteristic length of channel, radial oscillating frequency, and kinematic viscosity of the fluid, respectively. When Wo<1 no phase-lag can be observed and the flow velocity synchronize well with the time-dependent pressure gradient. However, this is not the case when Wo is larger than one where phase-lag between the flow velocity and the pressure gradient can be observed. Moreover, when Wo = 10 the parabolic-shape velocity profile is no longer exists when the flow oscillates in circular tubes. The maximum velocity is not located at the center; instead, it is shifted toward the channel wall (Uchida 1956; White 1999).

Reynolds number is a critical parameter that is used widely to characterize the valve-less rectification micropumping (Olsson et al. 1995, 2000; Jiang et al. 1998; Yang et al. 2004; Gamboa et al. 2005; Singhal et al. 2004; Chen et al. 2008; Wang et al. 2009a). However, contradictions over flow rectification with respect to Reynolds number were reported in the literature. For example, some studies suggested that flow rectification in a nozzle/diffuser element is not achievable in laminar flow (Gerlach and Wurmus 1995; Olsson et al. 1996; Koch et al. 1998), while Singhal et al. (2004) reported that flow rectification is achievable in a nozzle/diffuser element in laminar flow.

PZT actuators play also an important role in characterizing the valve-less rectification micropumps. The PZT's type, frequency, thickness, excitation signals, driving voltage, and displacement are factors that were reported in the literature to have an apparent influence on the micropumping performance (Stemme and Stemme

1993; Forster et al. 1995; Gerlach and Wurmus 1995; Jang et al. 1999; Morris and Forster 2003; Tracey et al. 2006; Sun and Huang 2006; Cui et al. 2007; Yoon et al. 2007; Cui et al. 2008). Additionally, local and global sharp peaks pumping flows were reported when the PZT actuators reach local and global resonance frequencies, respectively (Park et al. 2002; Feng and Kim 2004).

Additionally, Jianhui et al. (2007) have predicted the flow rate and mean pressure of valve-less rectification pump in the macro scale based on bifurcation geometry. In their work, they showed analytically that the pumping characteristics depend on the characteristics of the rectifying geometry, flow field, and PZT like other pumps in their category. However, their work was in the mini scale and the bifurcation was fabricated in circular tubes.

Finally, air bubbles were reported in the literature to have a negative effect on the micropumping performance of the valve-less rectification micropumps (Richter et al. 1998; Shen and Lu 2008). To summarize, all valves-less rectification micropumps have the same pumping principles, but differ in the type of the rectifying geometries. Many factors have an effect on the pumping performance of the valve-less rectification micropumps, and they are divided into two categories: first, parameters that are related to the rectifying geometry and, secondly, parameters that are related to the pumping actuators. The presence of bubbles is found to have a negative effect on the pumping performance of the valve-less rectification micropumps.

3.4 Bifurcation Based Design

Computer-aided design software (AutoCAD, Autodesk Inc., San Rafael, CA, USA) was used to design the desired bifurcation rectifying configurations. Three different

bifurcation designs were employed: a single bifurcation, double-generation bifurcation, and hybrid bifurcation design (combined micromixer and micropump applications), as shown in Figure 3.2.

The first design, a single bifurcation shown in panel (a) of Figure 3.2 was intended to be used as a benchmark design as well as to prove the feasibility of the valve-less rectification micropump based on the bifurcation rectification geometry. The second design is the double-generation bifurcation shown in panel (b), which was intended to compare its micropumping performance to the micropumping performance of the single generation design (to investigate the effect of the number of generations on the micropump's efficiency). Both designs, single and double-generation configurations have one inlet and one outlet. In contrast, the third design shown in panel (c) of Figure 3.2 was intended to investigate the capacity of a multifunction microfluidic device and to integrate a micromixer and micropump into one single design. The third design has two inlets and one outlet which is one of the advantages of using the bifurcation geometry to rectify the flow in a micropump. Because of the inherent nature of the bifurcation geometry (one main channel and two secondary channels), it was feasible to pump and mix two different fluids using a single microfluidic device.

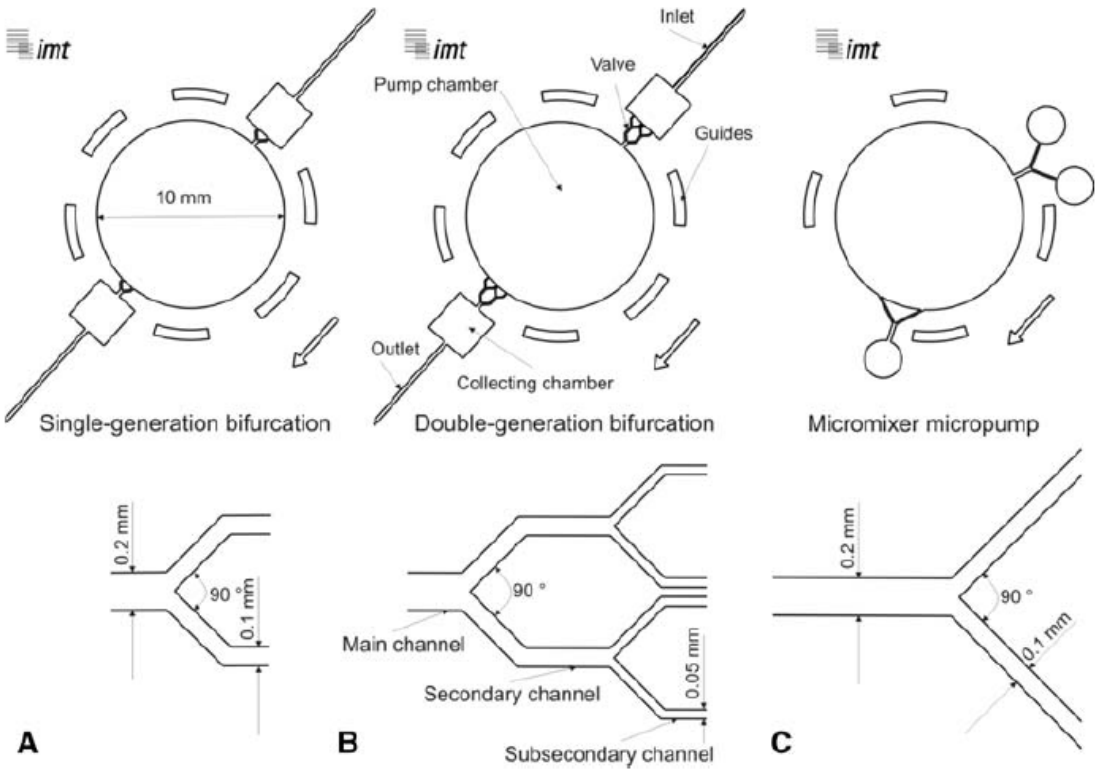

Figure 3.2: Bifurcation designs implemented in the present investigation: a. single bifurcation; b. double-generation bifurcation; c. hybrid bifurcation

The diameters of the micropump chamber and PZT are 10 and 12 mm, respectively. The first design has two secondary channels, while the second design has two secondary and four sub-secondary channels. The height of the channels is 230 µm, and the width ratio of the channels before and after the bifurcating tip is 2. In other words, the width of the main channel is twice the width of the secondary channel. Similarly, the width of the secondary channel is twice the width of the sub-secondary channel, in the case of the double generation design. All the secondary channels have the same width, as do the sub-secondary channels. The width of the main channel is 200 µm and the bifurcation angle is 90º (the angle between the secondary channels as well as the sub-secondary channels). In the case of the first and

second design, the width of the collecting chamber is 2.5 mm (the chamber located between the bifurcation geometry and the inlet/outlet channels). On the other hand, the diameter of the inlet/outlet circle, in the case of the third design, is 2 mm. Guides or aligning structures (the structures that can be seen around the micropump chamber in Figure 3.2) were implemented in the designs to better align the PZT actuators during the fabrication process. The arrows in Figure 3.2 refer to the predicted pumping direction.

3.5 Fabrication Procedure

The bidirectional and multifunction valve-less rectification micropump consists of five components: channels, a pump chamber, a membrane, an actuator, and a sealer. The membrane, the micropump channels, and the pump chamber were fabricated using PDMS Replica Molding (REM). The PZT (Digi-Key Corp., Thief River Falls, MN, USA) was used to actuate the micropump, and soda-lime glass substrates were used to seal the channels and the pump chambers.

The fabrication procedure (see Figure 3.3) starts after the completion of bifurcation configuration design and printing of the glass photo mask (Figure 3.4). The softlithography technique was employed as the main fabrication method. First, a soda-lime glass wafer was automatically cleaned and dried (step 1, Figure 3.3). The glass wafer was then dehydrated on a hot plate at a temperature of 120°C for one hour. Second, a thin layer of chromium (10 nm) was sputtered on the glass wafer to achieve better adhesion between the glass and SU-8 (step 2, Figure 3.3). Now the glass wafer was ready to be used as a base for the master structures (mold). Thirdly, three layers, base and two structure layers, of an epoxy-based negative photoresist (SU-8,

MicroChem Corp., Newton, MA, USA) were spun on using a spinning machine. The first layer was 5 µm thick and acted as an adhesion promoter and a base layer for the second and third SU-8 layers. To create the base layer, 4 ml of SU8-5 was spun on at 500 rpm for 15 seconds and then at 3000 rpm for 30 seconds. The wafer was leveled for 10 min, pre-heated at 95° C for 10 min, flood exposed to UV-light for 100 seconds, and post-heated for 10 min at 95° C, respectively. The second layer was created by spinning 4 ml of SU8-50 at 500 rpm for 15 seconds and then at 1200 rpm for 30 seconds. The wafer was leveled for 30 min and pre-heated at 95°C for two hours. The previous step was repeated, including an additional hour of pre-heating, in order to obtain a total layer thickness of 230 µm (step 3, Figure 3.3). The wafer was then exposed to UV-light for 100 seconds and post-heated for 20 min at 95°C (step 4, Figure 3.3). The first fabrication step ends with developing the master wafer in γ-butyrolactone (GBL) and propylene glycol methyl ether acetate (PGMA, MicroChem Corp., Newton, MA, USA) for 4 min and 20 minutes, respectively (step 5, Figure 3.3). The master wafer was then inspected under the microscope (Figure 3.5) and extra development time was given when needed. The master wafer (Figure 3.6) was then inspected to assure a uniform thickness by using an advanced surface texture measuring system (Dektak8, Veeco Instruments Inc., Tucson, AZ, USA)

The second step included fabricating the channels, pump chamber, membrane, and implementing the actuator (PZT). The PDMS (Sylgard 184 elastomer kit, Dow Corning, Midland, MI, USA) was mixed at a ratio of 10:1 (silicon elastomer base: curing agent). The mix was degassed under vacuum until all trapped air bubbles were released. The double sided molding (Lucas et al. 2008) was used to precisely produce

a 200 μm thick membrane. This is the minimum membrane thickness that can be easily handled during the fabrication steps and to produce a robust membrane. The master wafer was placed inside the double-sided molding and the mix was poured slowly. The double-sided molding was closed and the internal heater (thermo foil) was activated. The heating temperature was kept at 60 °C and the curing time was one hour (step 6, Figure 3.3). After the curing of the PDMS membrane layer, a small droplet of silicon glue (RS Components, Mörfelden-Walldorf, Germany) was placed on the bottom of the PZT and then the PZT was pushed against the membrane (step 7, Figure 3.3). At the same time, a new PDMS mix was prepared and degassed. The new mix was poured on the wafer and placed on the hot plate for one hour at 70 °C (step 8, Figure 3.3). After the PDMS was cured, the PDMS-PZT composite was peeled off carefully and slowly. Each micropump unit was cut and, now, ready for the next step.

The third fabrication step included bonding the PDMS-PZT composite to a lime-soda glass. First, the lime-soda glass was diced to match the micropump size and then cleaned manually using water, acetone, and ethanol, respectively. The glass substrate and the PDMS-PZT composite were placed inside a barrel etcher (Surface Technology Systems, Newport, UK). As a result, an irreversible bond was formed due to the surface treatment in an oxygen plasma environment (step 9, Figure 3.3). Finally, the fabrication procedure ended with fluidic connections of metallic micropipes at the inlets and outlets (Figure 3.7).

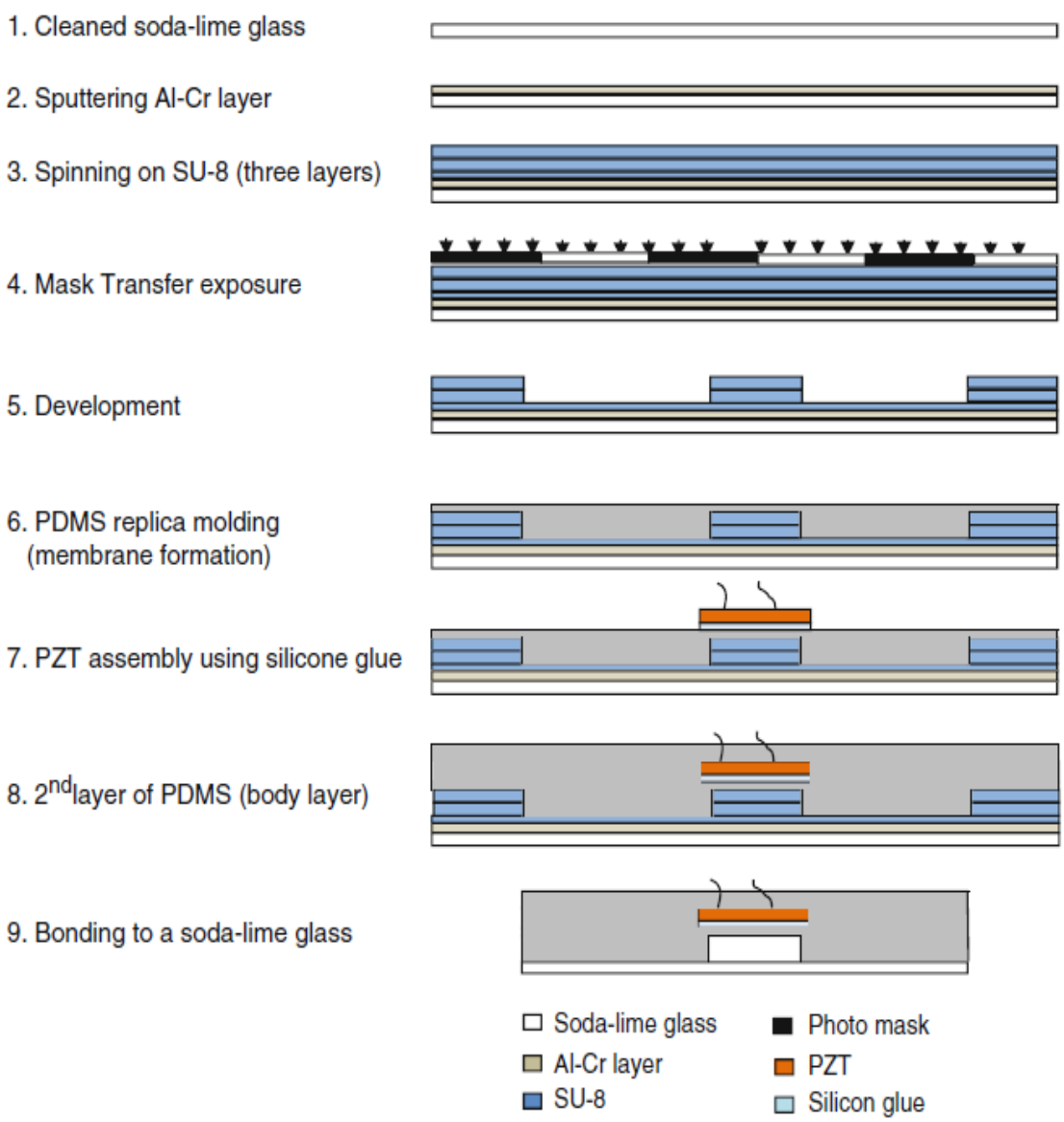

Figure 3.3: The fabrication procedure of the valve-less rectification micropumps based on bifurcation geometry

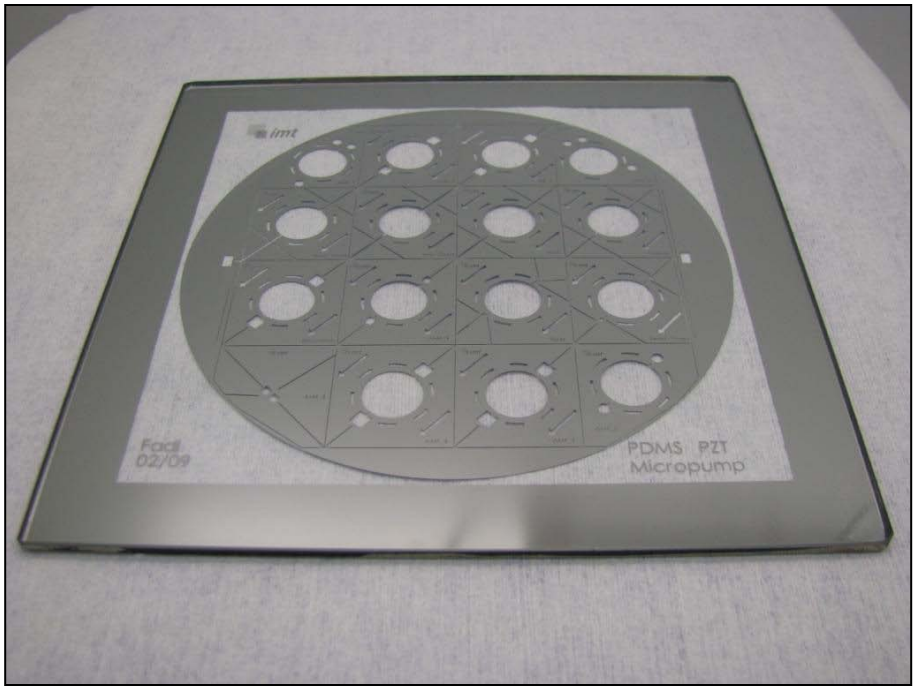

Figure 3.4: The photo mask which contains the current designs and other designs for future work

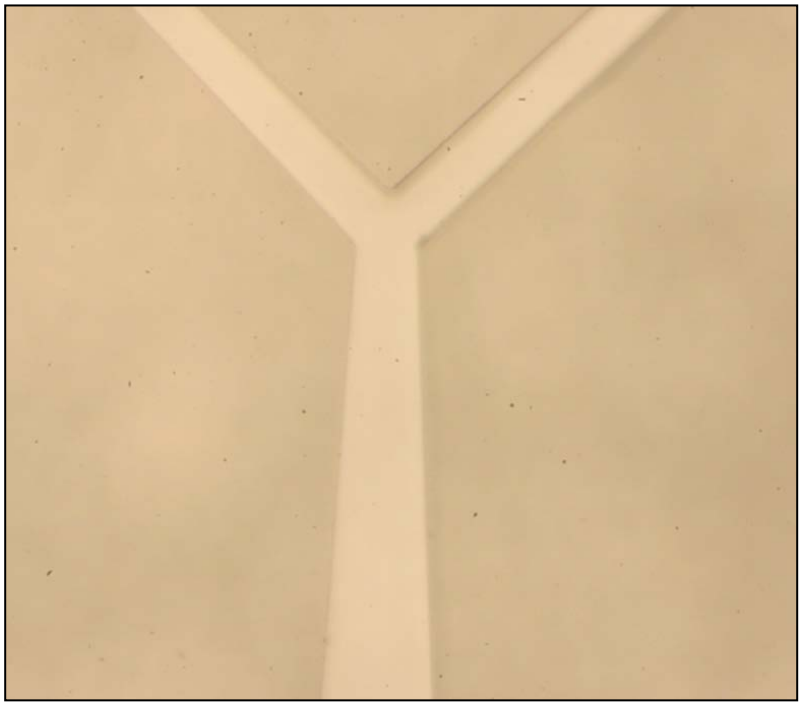

Figure 3.5: The bifurcation structure as it looks under the microscope

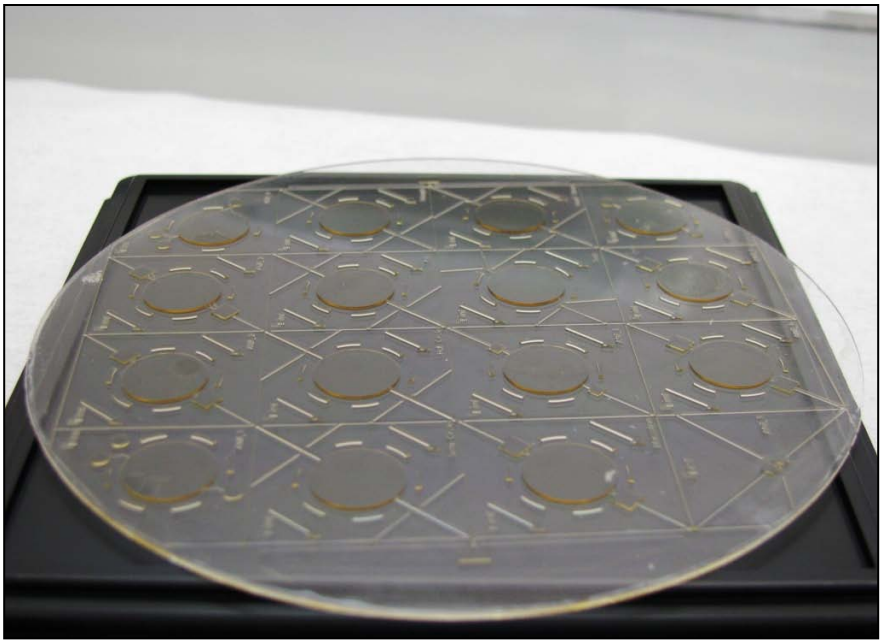

Figure 3.6: The SU-8 master which is used later in the in the replica molding process

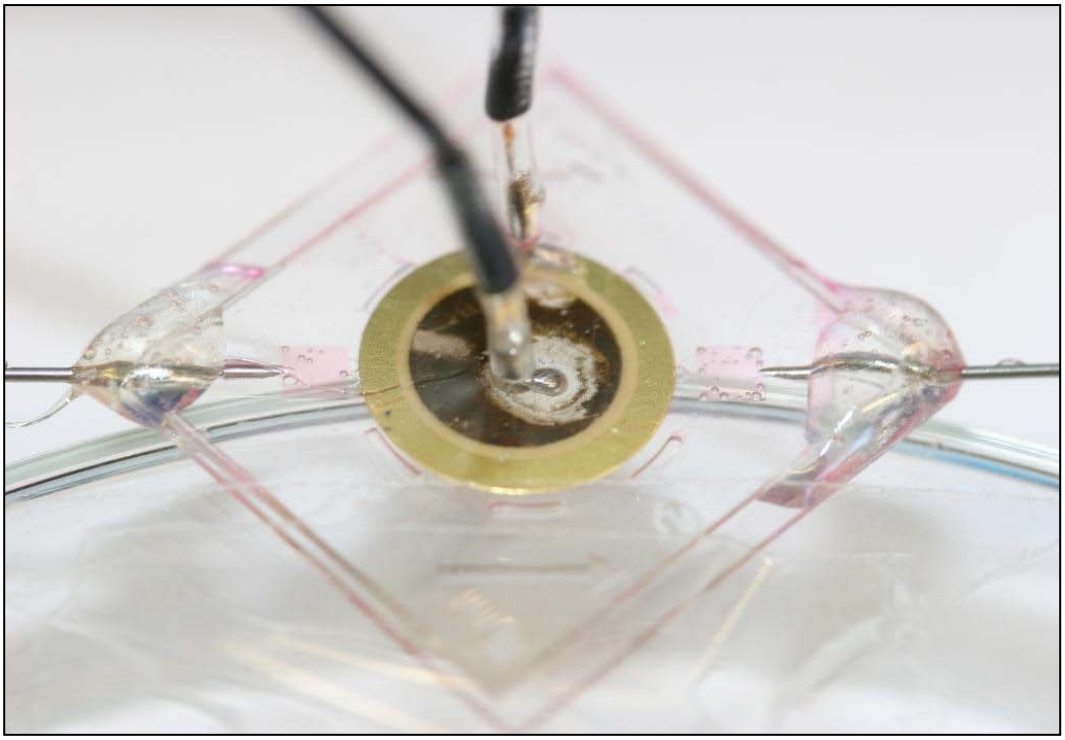

Figure 3.7: The valve-less rectification micropump after applying the fluidic connections

3.6 Experimental Apparatus

Figure 3.8 shows the experimental apparatus which was used in the present investigation. The experimental apparatus consists of an amplifier (E-508.00 HVPZT, PI Physik Instrumente, Karlsruhe, Germany), a frequency generator (Agilent 33220A, Agilent Technologies Deutschland GmbH, Bo¨blingen, Germany), an oscilloscope (Tektronix, Japan), a digital microscopic camera (dnt Gmbh, Dietzenbach, Germany), and a laptop. A square signal and 220 V with a zero offset were used to control the PZT. The choice of the excitation signal was based on the fact that the square signal is the typical exciting signal in microfluidic micropumps (Jang et al. 2009). Indeed, Forster et al. (1995) reported that the output of fixed-valve micropumps was significantly larger for the square signal than the sinusoidal signal. The micropump was investigated against two ranges of actuator frequencies, 0–100 Hz and 0–300 Hz, the first range has small increments (5 Hz) and was chosen to test flow rectification at low frequency and to observe the changes in the flow rectification behavior when small increments were chosen. The second range was chosen to investigate the flow rectification when larger increments (50 Hz) were utilized. The second range is large enough to accommodate the 50 Hz increments and keep the fluid flow in the laminar region (the Reynolds number for the oscillating flow in the main channel is around 2000 when the PZT actuator's frequency is equal to 300 Hz). In general, the choice of the actuator frequencies is arbitrary and it was reported to be between 0.1 and 5000 Hz (Laser and Santiago 2004). Typically, water, methanol, and ethanol were utilized as working fluids in mechanical micropumps (Laser and Santiago 2004). Since PDMS is hydrophobic (exhibit slip boundary condition; Byun et al. 2008) and methanol is toxic,

ethanol was used as a working fluid in all experiments. Flow rate measurements were conducted based on the bubble tracking method (Yoon et al. 2007; Wang et al. 2009b) in the inlet/outlet tube. To evaluate the flow rate measurement errors, the flow rate was measured using two different methods at two different locations, simultaneously. In the inlet tube, an air bubble was trapped and the bubble velocity between two specified marks was measured using a stopwatch. At the same time, the discharged fluid was collected from the outlet tube during the same time when the bubble moved between the two marks. The discharged fluid was weighed on a scale (Scout Pro SPU402, OHAUS Corp., Pine Brook, NJ, USA), and the mass used to calculate the flow rate. The difference in the flow rate values between the two measurement methods was less than 3%. To evaluate the experimental error (precision error), experimental samples were randomly chosen and repeated three times. The statistical error analysis suggested that the experimental error is equal to or less than 10% with a confidence interval of 90%.

A length scale (ruler) was attached to the experimental stand for maximum back pressure measurements (ethanol column height). The digital microscopic camera was fixed under the micropump chamber to monitor the flow in real time during the experiments. The real-time monitoring of the flow behavior during the experiments provided assistance to analyze the experimental data. A blue dye (Pelikan, Hannover, Germany) was used in the experiments to better visualize the flow behavior and clearly track the position of the air bubble inside the inlet/outlet tubes. The frequency and the voltage were monitored during the experiments by using an oscilloscope.

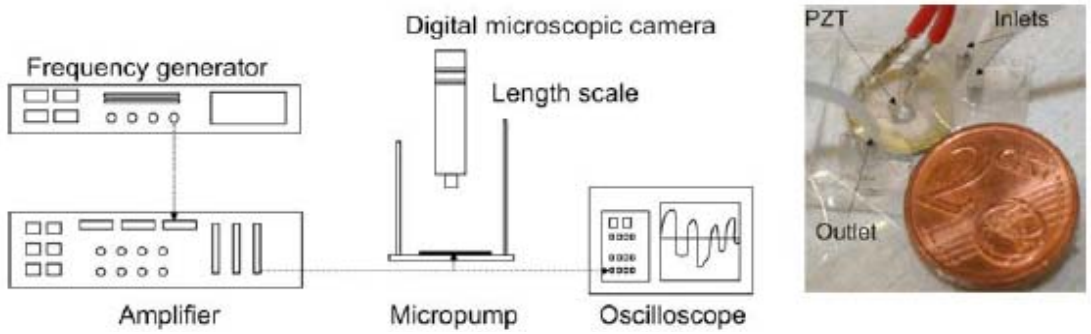

Figure 3.8: The experimental apparatus; the hybrid bifurcation micropump

3.7 Pumping Efficiency

In the micropump literature, researchers have typically characterized the micropump performance by the micropump flow rate and maximum back pressure. Pump flow rate and maximum back pressure are important parameters for pumps of any scale. However, it is noted that the use of the flow rate and maximum back pressure alone to characterize micropumps is not sufficient. For example, power consumption should be a vital parameter to evaluate micropumps. Therefore, the efficiency of the micropumps plays a crucial rule when an evaluation process is considered. Valve-less rectification micropumps were fabricated in different methods (e.g. soft lithography and bulk micromachining); employed different actuators (e.g. pneumatic and PZT actuators), membranes (e.g. PDMS and silicone), and rectification geometries (e.g. Tesla and nozzle/diffuser); tested at different resonance frequencies and voltages; and, not surprisingly, the micropumps delivered different flow rates and maximum back pressures. Valve-less rectification micropumps rectify an oscillating

flow to a one way flow. Therefore, it has two different flow velocities: one is the mean oscillating fluid velocity and the other is the net unidirectional flow velocity. The latter is the velocity difference between the forward and backward flow, which can be observed at the inlet/outlet tube. Thus, only a fraction of the input energy through the actuator can be effectively utilized to generate the net unidirectional flows. The input power $E`E'$ (J/s) utilized to pump the fluid in a channel can be calculated as $E`E'$ = ΔF V, where ΔF is the total force difference across the channel and V is the average fluid velocity. For oscillation flows inside the chamber, the average velocity V_0 can be estimated as $V_o = 2\,h\,f$, where h is the membrane deflection and f is the PZT frequency. Typically, the piezoelectric actuators have relatively small strains on the order of 0.1% (Mulling et al. 2001); therefore, the deflection can be approximated using the following formula:

$$h=0.001*D_{pzt} \tag{3.7}$$

where D_{pzt} is the diameter of the PZT. In other words, the membrane deflection, approximately, is equal to 0.1 % of the PZT diameter. Assuming the difference in ΔF inside the chamber and at the inlet/outlet can be neglected, the ratio of the average fluid velocities in the pump chamber and the inlet/outlet tube can be used as a third parameter to better assess the valve-less rectification micropumps efficiency and locate the optimum operational frequency where the maximum flow rate per each pumping cycle is delivered. It is true that neglecting the force difference is quite arbitrary in the above discussion, a better characterization of the valve-less rectification micropumps efficiency is open for discussions. The following formula was used to evaluate the dimensionless parameter which was employed to evaluate the

efficiency of the valve-less rectification micropumps as well as locating the optimal operational frequency:

$$\text{Efficiency} = \frac{\grave{E}_{out}}{\grave{E_{in}}} \sim \bar{V} = \frac{V_{net}}{V_0} \quad (3.8)$$

where $\grave{E}_{out}$, $\grave{E_{in}}$, $\bar{V}$, V_0, and V_{net} are the output power, input power, dimensionless parameter (the velocity ratio), average velocity inside the micropump chamber, and the average unidirectional velocity inside the inlet/outlet tubes, respectively.

3.8 Results and Discussion

Three bifurcation designs were tested and the results are presented in four different diagrams: flow rate versus frequency (0–100 Hz), flow rate versus frequency (0– 300 Hz), flow Reynolds number versus frequency, and velocity ratio versus frequency.

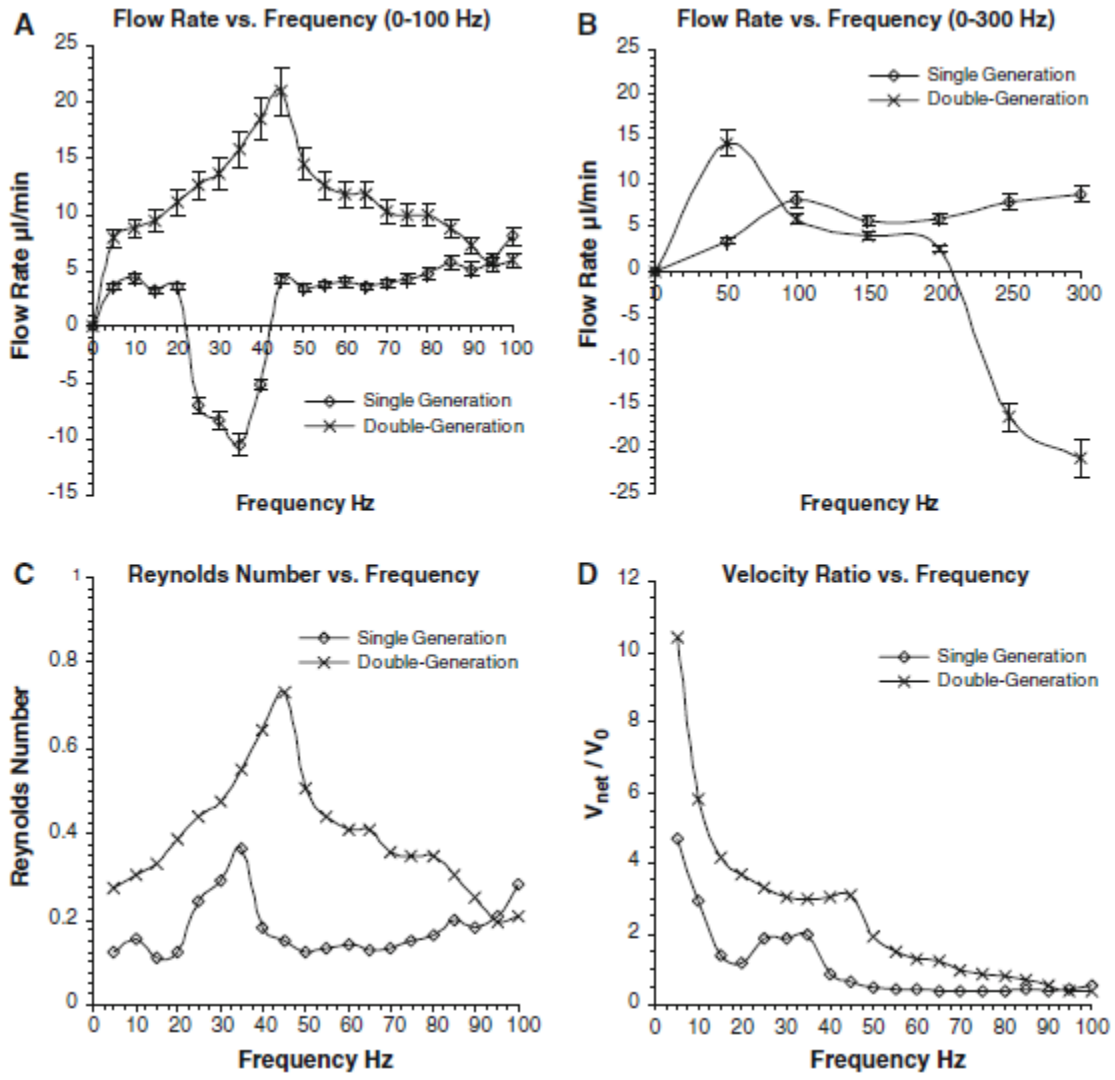

Figure 3.9: The results of the single and double-generation bifurcation designs. a. flow rate versus frequency (0–100 Hz); b. flow rate versus frequency (0–300 Hz); c. Reynolds number versus frequency; d. velocity ratio versus frequency

Figure 3.9 shows a comparison in the results between the single and double-bifurcation micropumps. Panel (a), the flow rate versus frequency diagram in the frequency range of 0–100 Hz, with small increments of 5 Hz, shows that rectification is achievable at all frequencies between 0 and 100 Hz. Additionally, a bidirectional

pumping was observed in this frequency range of the experiments where the flow reverses the direction in the frequency range between 25 and 40 Hz. The maximum positive and negative flow rates are 8 and 10.5 µl/min, respectively. The positive flow is the flow in the predicted direction as shown in Figure 3.2, while the negative flow is the flow in the opposite direction. While the double-generation result shows that flow rectification is achievable at all frequencies. However, the phenomenon of bidirectional pumping was not observed at the frequency range of 25–40 Hz as shown in the single bifurcation micropump design. The maximum positive flow rate is 20.94 µl/min occurring at f = 45 Hz. Panel (b) is the flow rate versus frequency in the oscillation frequency range of 0–300 Hz with increments of 50 Hz. Panel (b) shows that the phenomenon of bidirectional pumping (reversing the flow direction) is not observable when a large increment is employed in the case of the single generation design; and the flow rate increased and reached a local peak at 100 Hz and then decreased and reached a local minimum between the frequency of 150 and 200 Hz. After 200 Hz, the flow rate is increasing monotonically as the frequency increases. The maximum flow rate of 8.7 µl/min was observed at 300 Hz. On the other hand, the double-generation result shows that the phenomenon of bidirectional pumping is observable when the frequency is increased beyond 200 Hz. The flow reverses direction and a negative flow rate was observed at 250 and 300 Hz. The maximum negative flow rate was 20.94 µl/min at 300 Hz, which is the same value as the maximum positive flow rate that occurs at f = 45 Hz as shown in panel (a). Panel (c) displays the Reynolds number versus frequency. In the case of the single generation design, the Reynolds number diagram shows that the Reynolds number in the

inlet/outlet tube ranges between 0.12 and 0.36. Corresponding to panel (a), the flow Reynolds number reaches the maximum at the frequency of 35 Hz. In contrast, Reynolds number in the inlet/outlet tube in the case of the double-generation design is between 0.1 and 0.73, bearing the same patterns displayed in panel (a). The velocity ratio versus the PZT frequency is displayed in panel (d) of Figure 3.9. The pump efficiency can be estimated based on the value of the velocity ratio. Results show that the optimum frequency (maximum velocity ratio) occurs when the frequency is equal to 5 Hz for both designs, single and double generations. At this frequency, the losses in the flow energy were minimized, and the maximum flow rate per each pumping cycle is delivered. The maximum value of the velocity ratio is 4.71 and 10.41 in the case of single generation and double-generation designs, respectively. Furthermore, the maximum back pressure in the case of the single generation design is 0.46 kPa when f = 35 Hz and the flow rate = 0 µl/min; whereas the maximum back pressure in the case of the double-generation design is 1.0 kPa when f = 45 Hz and the flow rate = 0 µl/min.

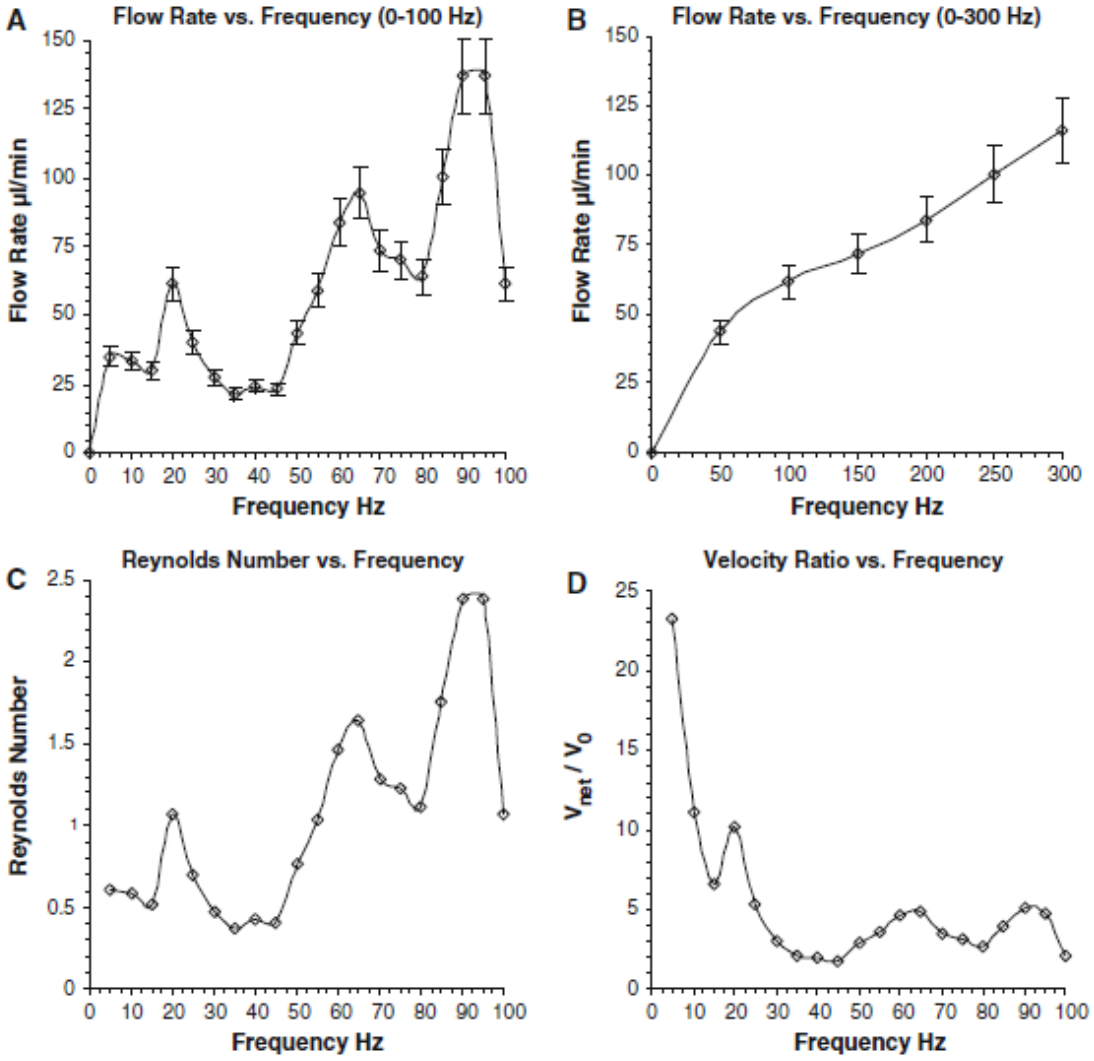

Figure 3.10: The results of the hybrid bifurcation design. a. flow rate versus frequency (0–100 Hz); b. flow rate versus frequency (0–300 Hz); c. Reynolds number versus frequency; d. velocity ratio versus frequency

Figure 3.10 shows the experimental results for the third design of the bifurcation configuration which is intended for the combined micromixing-micropumping applications. Panel (a), the flow rate versus frequency, in the frequency range of 0–100 Hz with small increments of 5 Hz, shows again that rectification is achievable at all frequencies. However, the phenomenon of bidirectional pumping is not observable.

The zigzag flow rate pattern as a function of the frequency has three minimums and three peaks. The three minimums occur at 15, 35, and 80 Hz and the three peaks occur at 20, 65, and 95 Hz, respectively. The measured maximum positive flow rate is 137 µl/min. In panel (b), the flow rate versus frequency between 0 and 300 Hz, with increments of 50 Hz, the results show that the phenomenon of bidirectional pumping is also not observable in the entire range of frequencies under investigation, which is different from the experimental findings with respect to the first and second designs. The flow rate increased monotonically with the actuator frequency. The maximum positive flow rate is observed at f = 300 Hz and equal to 116 µl/min. Panel (c), the Reynolds number versus frequency, shows that the Reynolds number varies between 0.36 and 2.4 in the frequency between 0 and 100 Hz. Panel (d), the velocity ratio versus frequency, shows that the optimum operational frequency (maximum velocity ratio) is f = 5 Hz. At this frequency, the maximum velocity ratio is 23.25 while the maximum back pressure is 2.86 kPa when f = 90 Hz and the flow rate = 0 µl/min.

Experimental results in Fig. 3.9 show that the double generation bifurcation micropump design performed better than the single generation bifurcation design. The double generation design has a higher flow rate as well as maximum back pressure. It is also noted that the capability of bidirectional pumping was observed at different actuator frequencies. The bidirectional pumping phenomenon was observed at a low frequency range for the single bifurcation design, while for the double-generation bifurcation design, it occurs at relatively high frequencies (250 and 300 Hz). Two explanations can be given to justify that the bidirectional pumping phenomenon occurs at two different ranges of actuator frequencies. First, the value of microfluidic

diodicity is not equal for both designs. That means, for a specific frequency each design will confront a different ratio of flow resistance. Second, the single generation design would tolerate larger size air bubbles than the double-generation design (the width of sub-secondary tubes in the double generation design is half the width of the secondary tubes in the single generation design). Thus, the sub-secondary channels in the second design may become blocked by air bubbles that can often pass through the secondary channels, in the first design, due to the difference in channel width between both designs. As a result, an extra deviation in the microfluidic diodicity between both designs would be introduced. Both explanations may suggest that it would be difficult for the bidirectional phenomenon to occur at the same actuator frequency for the two different designs with different values of microfluidic diodicity.

In contradiction to the single-generation and double-generation designs, the hybrid-bifurcation design (for the combined micromixing-micropumping applications) did not exhibit any bidirectional pumping capability. Both the first and second designs have fluid collecting chambers. The existence of these collecting chambers has added additional losses (entrance and exit losses) to the fluid flow. As a result, using the microfluidic diodicity of the bifurcation geometry by itself without taking into consideration the collecting chambers will result in prediction errors. For example, using numerical simulations to predict the experimental results or to determine the rectification efficiency of the micropump based on the microfluidic diodicity of the rectifying geometry alone will not be accurate, since the rectification characteristics of the micropump are entirely dependent on the total microfluidic diodicity which includes the bifurcation geometry as well as the collecting chamber.

Using numerical simulations, Fadl et al. (2009) predicted that the microfluidic diodicity of the bifurcation geometry will increase with the increase of the flow Reynolds number or actuator frequency. As a result, the net flow rate, theoretically, should increase monotonically with the Reynolds number/actuator frequency. However, in practice, many factors affect the characteristics of micropump performance. For example, due to the PDMS permeation of gas, the flow is two-phase instead of a single phase flow (most numerical simulations and theoretical analysis treat the flow as a single phase flow). Additionally, gas permeation through the PDMS walls may lead to a slip boundary condition (Singh et al. 1998; Randall and Doyle 2005; Huang et al. 2006; Tremblay et al. 2006; Sadrzadeh et al. 2009). Air bubbles were clearly visible in the experiments, and they have significant effects on the flow dynamics. It was also observed that the bubbles' size inside the micropump vary with the actuator frequency as shown in Fig. 3.11. Figure 3.11 also shows that the size of air bubbles increases as frequencies increase from f = 10 to f = 80 Hz. This is valid for both designs (single generation and double-generation). Moreover, the way the air bubbles interact with the rectifying geometries has a significant effect on the rectification characteristics. Depending on the bubbles size, the bubbles may pass through the rectifying geometry or stagnate at the entrance of the rectifying geometry. As a result, the value of the microfluidic diodicity would be changed and the outcome would be hard to predict. We believe that the combined effects of extra losses caused by the collecting chamber, permeation properties of the PDMS, dynamics of bubble interactions in the two-phase flow with the rectifying geometries, as well as the possible deformation of the PDMS structures under the oscillatory pressure variations,

have changed the characteristics of the microfluidic diodicity and, as a result, triggered the bidirectional pumping phenomena. Predictions and simulations of these interactions are challenging and are out of the scope of the current investigation.

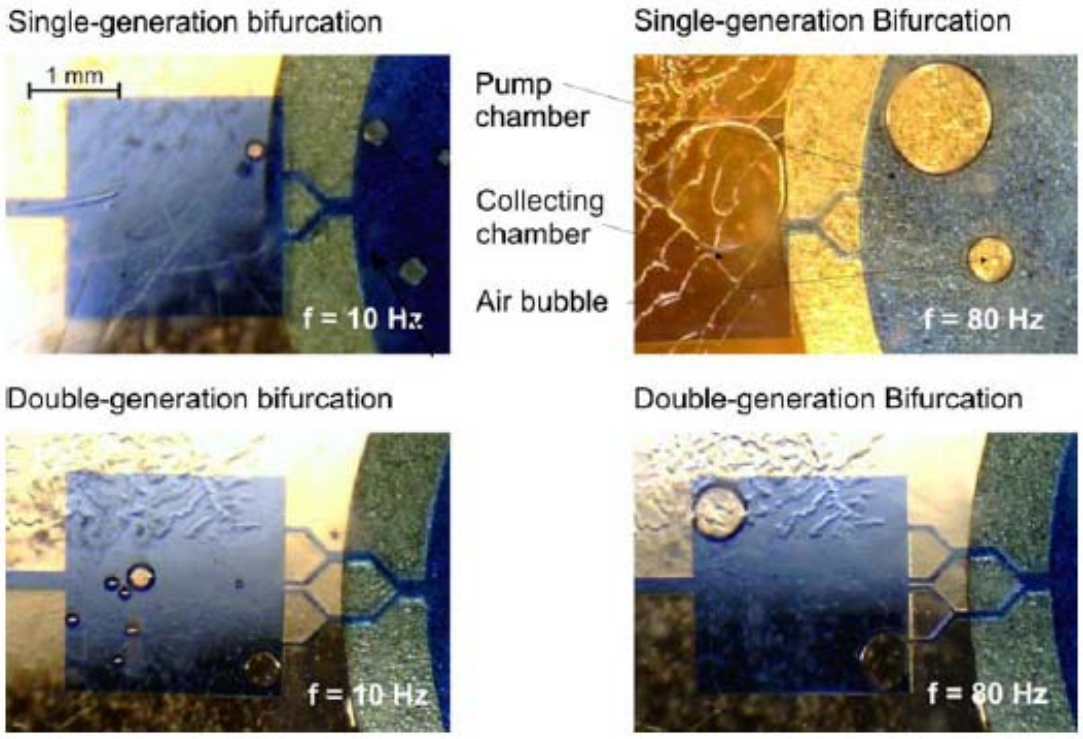

Figure 3.11: Air bubbles inside the pump and collecting chambers in the case of the single generation and double generation designs (notice the difference in the bubble size when the frequency increases from 10 to 80 Hz)

The third design, the hybrid-bifurcation configuration for combined micromixing-micropumping applications, shows some promising results. It has the highest flow rate, maximum back pressure, and velocity ratio among all three designs. It has no collecting chamber as needed in the other two designs. As a result, no extra losses

were introduced and the trend of microfluidic diodicity predicted by computer simulation was not disturbed. The microfluidic diodicity of the bifurcation geometry itself dominates the total diodicity of the micropump. The absence of the collecting chamber has aided the air bubbles to pass through the channels instead of being trapped in the collecting chamber. Additionally, the missing of the introduced losses caused by the collecting chamber has normalized the microfluidic diodicity to be only correlated to the bifurcation geometry. This may explain why the bidirectional pumping phenomenon was not observed in the hybrid design.

The proposed micropump efficiency is related to the flow rates delivered by each pumping cycle (supply mode and pump mode; see Figure 3.1). Therefore, it is feasible to locate the actuator frequency where the flow rate per each pumping cycle is maximized. The results show that the maximum flow rate per each pumping cycle is occurred at 5 Hz for all three designs. However, the maximum total flow rates are delivered at different actuator frequencies for all three designs. For example, the maximum total flow rate for the first design is 10.47 µl/min at 35 Hz which reflects 0.29 µl/min per each pumping cycle. While the flow rate is 3.56 µl/min at 5 Hz which reflects 0.71 µl/min per each pumping cycle. Similarly, the flow rate per each pumping cycle at the maximum total flow rates are 0.46 and 1.4 µl/min, while the flow rates per each pumping cycle are 1.57 and 3.5 at 5 Hz for the second and third designs, respectively. Therefore, the velocity ratio may be used to evaluate the micropump performance beside other conventional parameters (total flow rate and maximum back pressure).

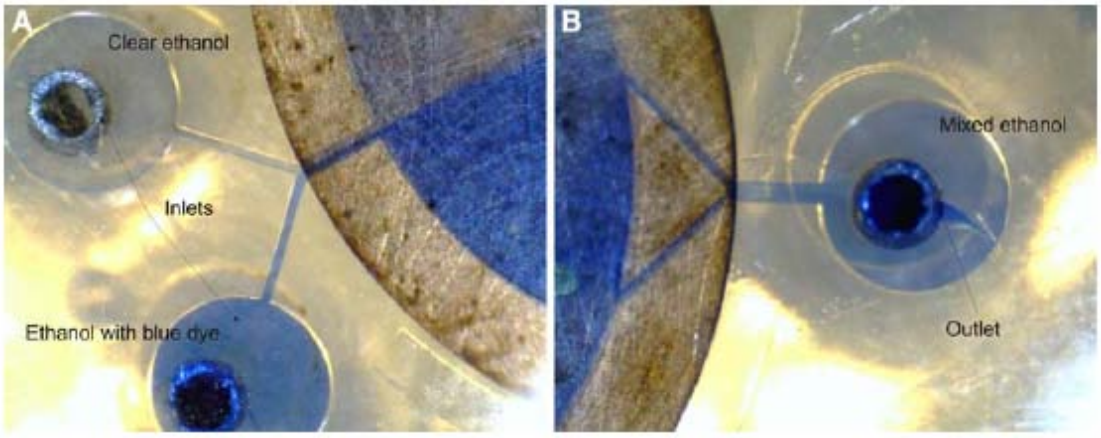

Figure 3.12: The micromixermicropump based microfluidic device. Parallel flow layers are visible at the inlets and a mixing was visually observed at the outlet

The multi-functionality of mixing and pumping was demonstrated in the experiments. The mixing was examined at different frequencies and visually observed at the micropump outlet. However, micromixing in Y-channel was reported by Kim et al. (2003) and Yi and Bau (2003). Panel (a) in Figure 3.12 shows the photo of two streams of ethanol at the inlets. A clear ethanol was introduced to one inlet and an inked ethanol to the second one. Parallel layers were clearly visible at the inlet region and mixing was visually observed at the outlet region as shown in panel (b). The experiment shown in Figure 3.12 was conducted at f = 60 Hz. However, a further investigation is required to quantify the mixing performance of the hybrid design, and it is out of scope of the current work.

Finally, all three bifurcation-based micropump designs are proven to be self-priming. They are capable of pumping liquids and gases. To test the self-priming capability, the micropump was activated when the entire micropump was filled with

air. Subsequently, a liquid flow was established and observed through the micropump and a net flow rate was detected at the outlet tube. When comparing the results with the results reported by Wang et al. (2009b), the valve-less rectification micropup based on the bifurcation geometry has delivered higher flow rate at the same frequency and voltage than the valve-less rectification micropump based on the nozzle/diffuser in the low actuator frequency region. Wang et al. (2009b) have reported 0.06 µl/min at 10 Hz and 200 V, while our third design, hybrid design, delivered 33.5 µl/min at 10 Hz and 220 V. However, this comparison may not be accurate due to differences in the micropump design and experimental parameters such as rectifying geometries, PZT's type, diameter, and excitation signal.

3.9 Conclusions

Three different valve-less rectification micropumps based on bifurcation geometry were designed, fabricated, and tested. All three micropumps are self-priming. The bidirectional pumping capabilities were demonstrated at certain actuator frequencies for the single bifurcation and the double-generation bifurcation micropumps, while the multi-functionality of micromixing-micropumping was demonstrated for the hybrid bifurcation design. While the double-generation bifurcation design shows better results than the single-bifurcation design, the hybrid bifurcation design was associated with the highest flow rate (137 µl/min), maximum back pressure (2.86 kPa), and pump efficiency (23.25). A non-dimensional group was introduced as a third parameter associated with the pump efficiency, in addition to the flow rate and maximum back pressure, to better evaluate the performance and determine the optimum operational frequency of the valve-less rectification micropumps where the maximum flow rate

per each pumping cycle is delivered. Additionally, increasing the actuator frequency with small increments (5 Hz) led to observations of the bidirectional pumping phenomena in the first design. This phenomenon has not been observed when the large increments (50 Hz) were considered. The results also suggest that the highest pumping efficiency occurs at the lowest actuator frequency.

In practice, many factors affect the characteristics of valve-less rectification micropumps and the prediction and simulation of these factors are challenging and need further investigation.

CHAPTER 4

4 Effect of Fabrication Materials on the Efficiency of Valve-less Rectification Micropumps

“The scientist is not a person who gives the right answers, he's one who asks the right questions.”

Claude Lévi-Strauss

4.1 Abstract

Microsystems can be fabricated in different methods and materials. Since different materials have different properties, the material selection may play a role in the performance of microsystems. In this chapter, two valve-less rectification micropumps based on rectification geometry were fabricated using two different materials; Polydimethylsiloxane (PDMS) and SU-8 photoresist. The PDMS is a viscoelastic material that acts like elastic solid at short flow times or after cross linking. On the other side, SU-8 is a viscous photoresist that acts like hard material after thermal treatment. The two micropumps have the same dimensions and actuated by the same type of Piezoelectric Transducers (PZT). The ethanol was used as a working fluid in all experiments. The micropumps were tested and the experimental results were compared in terms of flow rates, maximum back pressures, and velocity ratios.

4.2 Introduction

Micropumps are the heart of many microfluidics devices such as Micro Total Analysis System (μTAS) and Lab-On-a-Chip (LOC). A high efficiency micropump is the key for the realization of more efficient microsystems. Many parameters were reported in the literature to affect the efficiency of valve-less rectification micropumps. Some factors are related to the rectifying geometries such as microfluidic diodicity and geometrical parameters. Others are related to the flow dynamics such as flow Reynolds number and flow phases. Additionally, the actuator characteristics also have also an apparent effect on the micropump efficiency. In the case of the PZT, the characteristic parameters include voltage, frequency, PZT thickness, excitation signal, and PZT deflection (Foster, et al., 1995; Morris, et al.,

2003; Olsson, et al., 1995; Olsson, et al., 1996). Geometrical parameters include the characteristic angle, length of the rectifying geometry, aspect ratio, slenderness, and number of rectifying geometries (Olsson, et al., 1997a;Olsson, et al., 1997b; Olsson, et al., 2000; Nabavi, 2009). Despite the wide range of studied parameters which have effects on the efficiency of velve-less rectification micropumps, the effect of the fabrication materials with different mechanical properties has not yet been reported. In this chapter, PDMS (elastic material in the solid state) and SU-8 (hard material in the solid state) were chosen to fabricate two valve-less rectification micropump based on bifurcation geometry. Both micropumps have the same dimensions, use the same actuator, and experiments were conducted under the same conditions. The results of both micropumps were presented in terms of the flow rates, maximum back pressures, and velocity ratios.

4.3 Micropumps Design

The design of the micropumps is shown in Figure 4.1, which is the hybrid design presented in chapter 3. This design has no collecting chamber and offer two inlet and one outlet to provide mixing and pumping at the same time. The width ratio between the primary and secondary channels is two, and the bifurcation angle is 90 ^{o}. The width of the primary and secondary channels is 200 μm and 100 μm, respectively.

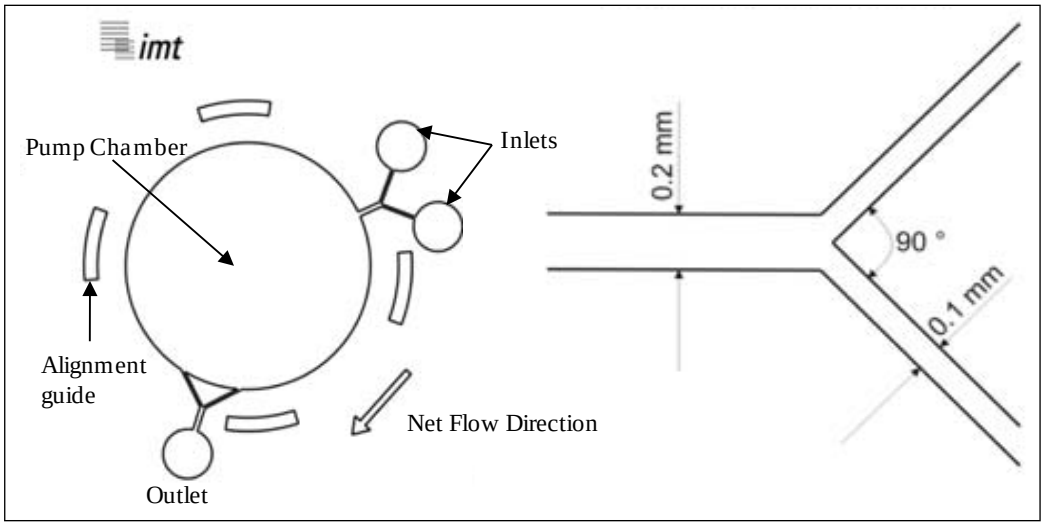

Figure 4.1: Configuration of micropumps used in this chapter

4.4 Fabrication Procedure

Fabrication procedure of the first micropump using PDMS is explained in details in chapter 3. The fabrication procedure of the second micropump using SU-8 has some similarity with the fabrication of the PDMS micropump. In fact, steps 1-5 (Figure 3.3) were repeated in the fabrication's procedure of the SU-8 micropump with one exception. The photo mask that was used with the SU-8 micropumps is different than the one used with the PDMS micropump. The objective of photo mask for the PDMS micropumps is to produce a SU-8 mold to be used later in PDMS replica molding, while the objective of the photo mask for the second micropump is to build the micropump structure inside the SU-8 itself. Therefore, the opaque areas in the first photo mask (PDMS micropump) are transparent in the second photo mask (SU-8 micropump) and vice versa.

After developing the SU-8 layers (Step 5, Figure 3.3), an itched soda lime glass was glued to the SU-8 structure as seen in Figure 4.2 (Step 5). The soda-lime glass

was chemically itched (wet itching) for the inlet and outlets ports as well as a PDMS membrane directly above the pump chamber. The soda-lime glass was glued using silicon glue, and the glue was dispensed under the microscope using micro glue dispenser (Ultimus 2400 Dispenser, GLT Gesellschaft für Löttechnik GmbH, Pforzheim, Germany). A uniform pressure was applied after dispensing the glue and attaching the soda-lime glass on the top of the SU-8 structure to assure uniform distribution of the glue over the surface. The PZT was glued to the top soda-lime glass and mounted on the top of the PDMS membrane (Step 6, Figure 4.2). Finally, rubber tubes were connected to the inlet and outlet ports and securely sealed by silicon glue (Step 7, Figure 4.2). Figure 4.3 shows cross sectional views of both micropumps after being fabricated to illustrate the differences of the fabrication procedures.

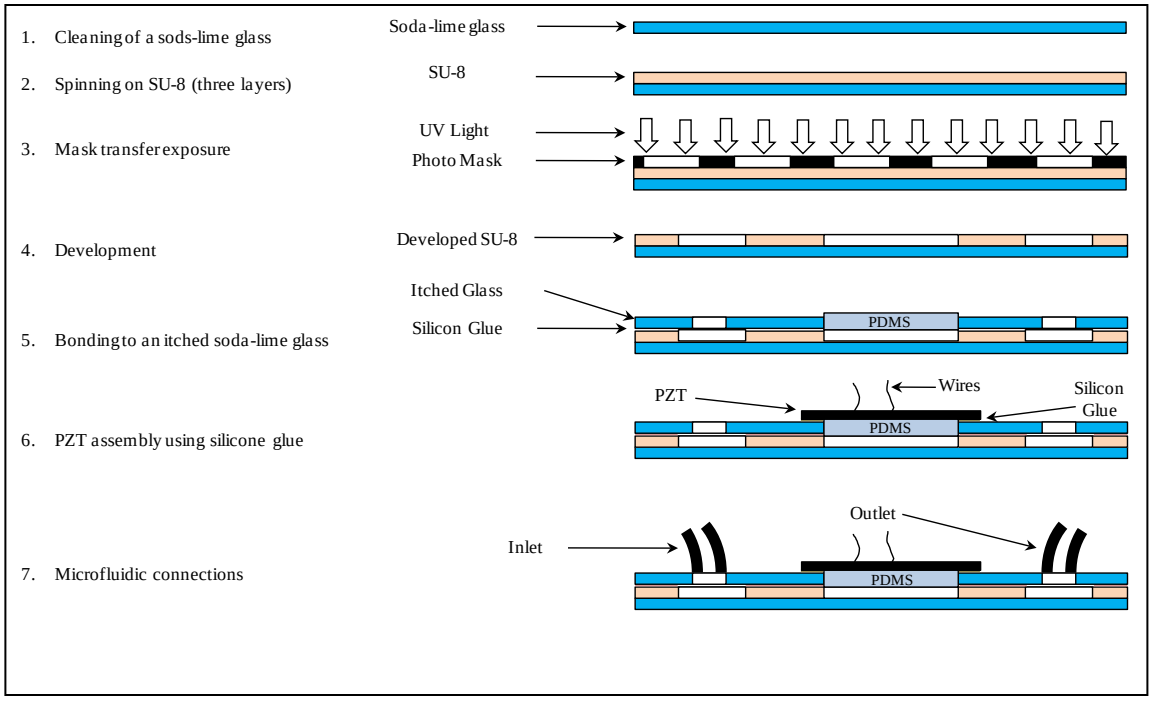

Figure 4.2: The fabrication procedure of the SU-8 valve-less rectification micropump based on rectification geometry

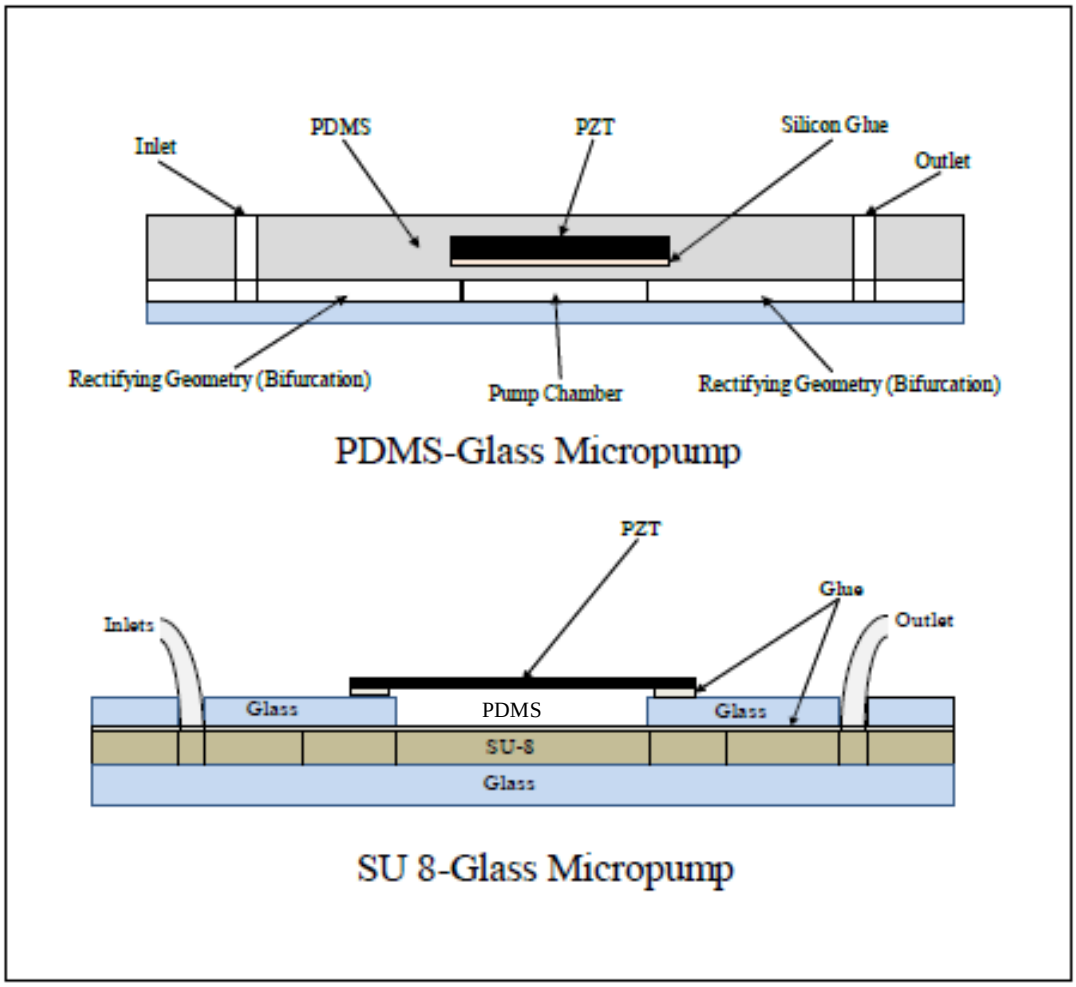

Figure 4.3: Cross sectional views of fabricated micropumps, PDMA and SU-8 valve-less rectification micropumps based on bifurcation geometry

4.5 Experimental Apparatus

The same experimental apparatus used in chapter 3 was used in this study to examine the performance difference between the two micropumps. Please refer to Section 3.6 for more details. To evaluate the flow rate measurement errors, the flow rate was measured using two different methods at two different locations, simultaneously. In the inlet tube, the bubble tracking method (Yoon, et al., 2007) was employed by measuring the velocity of a trapped bubble between two specified marks

using a stopwatch. At the same time, the discharged fluid was collected from the outlet tube during the same time when the bubble moved between the two marks. The discharged fluid was weighed on a scale (Scout Pro SPU402, OHAUS Corp., Pine Brook, NJ, USA), and the mass was used to calculate the flow rate. The difference in the flow rate values between the two measurement methods was less than 4 %. To evaluate the experimental error, experimental samples were randomly chosen and repeated three times. The error analysis suggested that the experimental error is equal to or less than 10% with a confidence interval of 90%.

4.6 Results and Discussion

Experimental results are presented in terms of flow rates, Reynolds numbers, maximum back pressure, and velocity ratio as a function of the PZT actuator frequency. Figure 4.4 shows the flow rates against the actuator frequency for the two micropumps. The frequency range varies between 0 to 300 Hz. The results show that the SU-8 micropump has outperformed the PDMS micropump at all frequencies. The flow rate was monotonically increasing in both micropumps and reached the maximum at 300 Hz. The pace of flow rate increase for SU-8 pump is much faster than that of PDMS micropump: the flow rate were 43.7 µl/min and 78.5 µl/min at 50 Hz, while the maximum flow rates at 300 Hz were 116 µl/min and 472 µl/min in the case of PDMS and SU-8 micropumps, respectively. As it can be seen, the SU-8 flow rates is almost doubled at 50 Hz and four times higher than the PDMS micropump at 300 Hz.

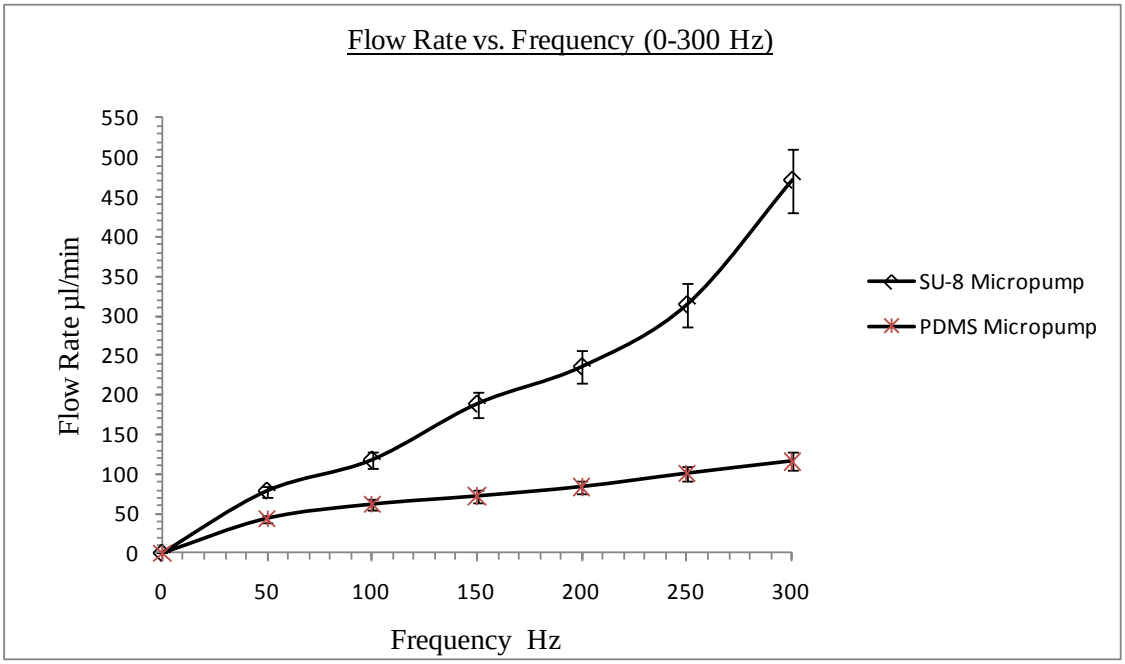

Figure 4.4: Flow rate as a function of the actuator frequency

Figure 4.5 compares the results of Reynolds numbers at the pump outlet as a function of the actuator frequency for the two micropumps. The Reynolds number was higher in the SU-8 micropump, but still in the low Reynolds number region. As expected, the Reynolds number increased monotonically with the actuator frequency and the maximum was observed at 300 Hz.

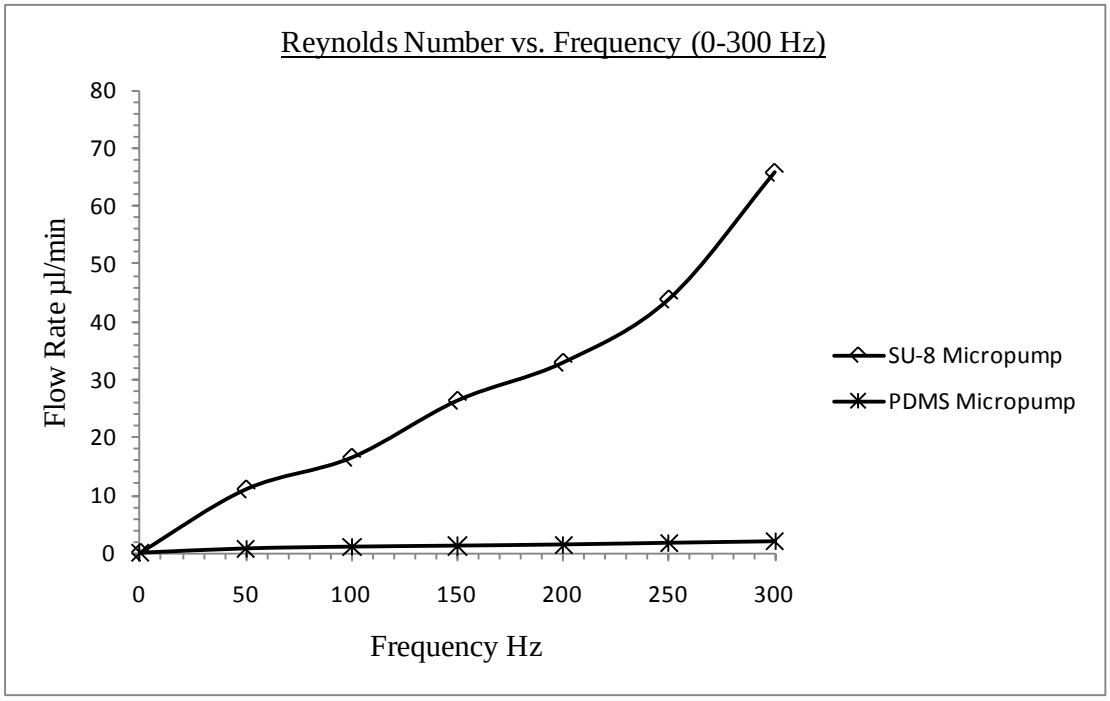

Figure 4.5: Reynolds number at the pump outlet as a function of the actuator frequency

To effectively assess the micropump performance, the parameter of velocity ratio (see the definition in chapter 3) was employed which was first introduced in the literature by our research group. The velocity ratio is an additional parameter, along with the flow rate and maximum back pressure, to better evaluate the efficiency of the micropumps. The velocity ratio is an indicator of the flow rate per each pumping cycle which relates the total net flow rate to the actuator frequency. Higher velocity ratio means higher total net flow rate at lower actuator frequency.

Figure 4.6 shows the velocity ratio at a frequency range between 0 and 300 Hz with 50 Hz increments. In general, the SU-8 micropump has a higher velocity ratio than the PDMS micropump at all frequencies. In the case of the SU-8 micropump, the

maximum velocity ratio occurred at 50 and 300 Hz. This means, the optimum operation in terms of flow rate per each pumping cycle is at 50 or 300 Hz. However, the total flow rate at 300 Hz is four times higher than the flow rate at 50 Hz. The maximum velocity ratios were 16.7 and 2.9 in the case of SU-8 and PDMS micropumps, respectively.

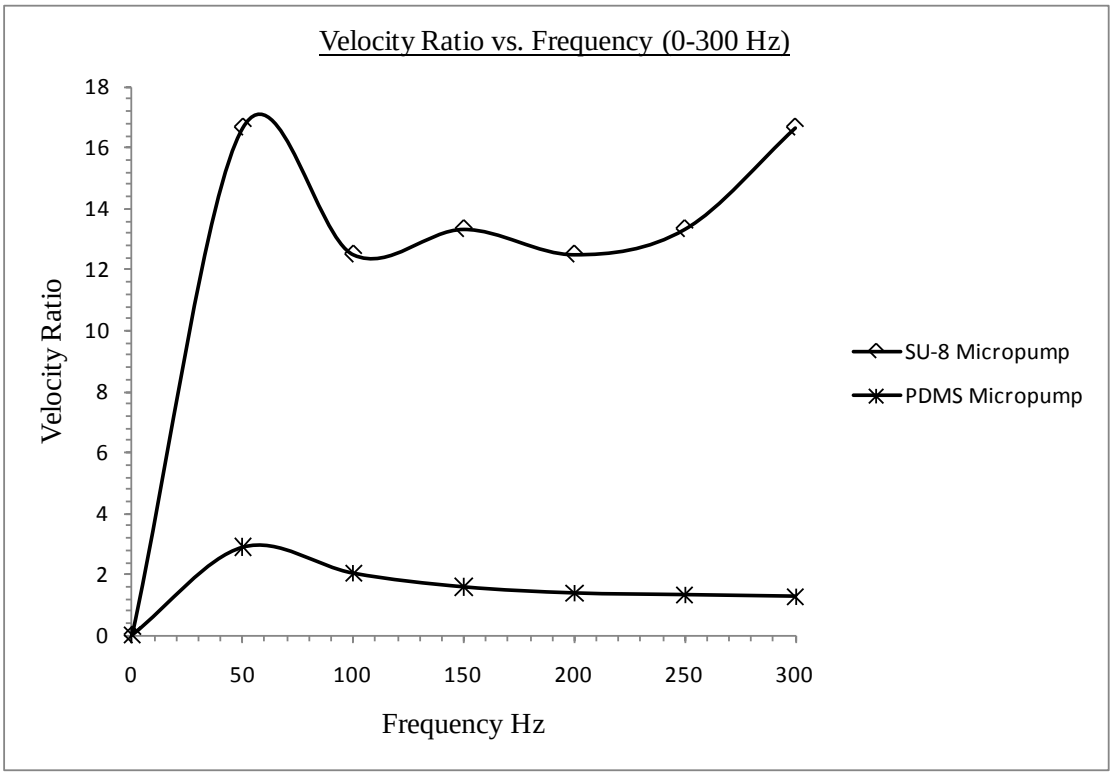

Figure 4.6: Velocity ratio as a function of the actuator frequency (0-300 Hz)

Figure 4.7 shows the velocity ratio in a frequency range between 0 and 100 Hz with 5 Hz increments. Again, the velocity ratio of the SU-8 micropump is higher than the PDMS micropump. The maximum velocity ration occurred at 5 Hz in both micropumps. The maximum velocity ratios were 74.1 and 23.2 in the cases of SU-8 and PDMS micropumps, respectively.

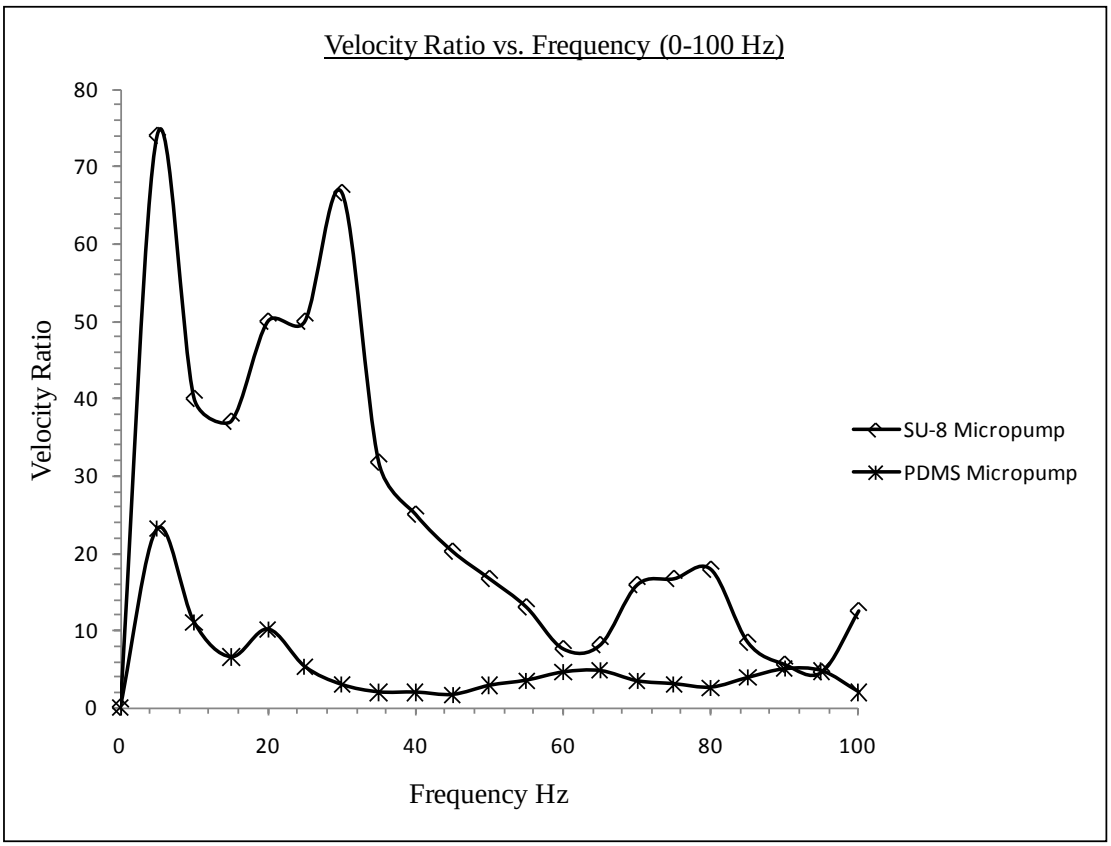

Figure 4.7: Velocity ratio as a function of the actuator frequency (0-100 Hz)

The maximum back pressures were measured at zero maximum flow rates by using a length scale (ruler). The maximum back pressures were 4.5 kPa and 2.86 kPa in the case of SU-8 and PDMS micropumps. It is clear that SU-8 micropump has a higher maximum back pressure in comparison to the PDMS micropump.

The above results show that fabricating the valve-less rectification micropump from hard material such as SU-8 has an apparent positive effect on the micropump efficiency. In other words, using elastic materials may reduce the efficiency for the valve-less rectification micropumps. Elastic materials such as PDMS may absorb the PZT vibration resulting in smaller membrane deflection and pump displacement

volume. Also, the distortions may lead to unexpected fluid dynamics behavior. As a result, the value of the microfluidic diodcity may change in unfavorable way. Additionally, the gas permeation of the PDMS will result in more bubble generations during the micropump operation and may contribute to the poor pumping efficiency in comparison to the SU-8 micropump.

4.7 Conclusions

Two valve-less rectification micropumps fabricated based on the same bifurcation geometry and from two different materials were tested under the same experimental conditions. The results show that he SU-8 micropump outperformed the PDMS in terms of flow rate, maximum back pressure, and velocity ratio. The elasticity of the PDMS as well as gas permeation may have a negative effect on the efficiency of the valve-less rectification micropumps.

CHAPTER 5

5 Valve-less Rectification Micropumps Based on Dynamic Structures

"Physics is mathematical not because we know so much about the physical world, but because we know so little; it is only its mathematical properties that we can discover."

Bertrand Russell

5.1 Abstract

Most valve-less rectification micropumps are based on passive rectifying structures. The rectifying structures are fabricated in pairs and usually placed on both sides of the pump chamber, and they rectify the oscillatory flow generated in the pump chamber by PZT actuator. In this chapter, a valve-less rectification geometry based on dynamic rectifying geometry is introduced. The dynamic geometry used to generate and rectify the oscillatory flows is based on a hollow spherical structure. To change the flow rate direction, two dynamic geometries were employed. Magnetic actuator was used to oscillate the rectifying geometry inside the pump chamber. The new concept was proven and results were presented in terms of flow rate, maximum back pressure, and velocity ratio.

5.2 Introduction

Valve-less rectification micropumps are mechanical displacement micropumps. Their pumping principles are based on rectification geometries with directional flow resistance. Rectification geometries such as the pair of nozzle/diffuser, Tesla (valvular conduit), and bifurcation channels rectify the oscillatory flows resulting in a net flow. Most rectifying geometries are passive, which means oscillatory flows are independently generated inside the pump chambers then pass through rectifying geometries located at the inlet and outlet of the chambers. This Type of valve-less rectification micropumps (Foster, et al., 1995; Gerlach, 1997; Iverson, et al., 2008; Foster, et al., 1995; Nguyen, et al., 2002; Olsson, et al., 1995; Olsson, et al., 1997a; Olsson, et al., 1997b; Olsson, et al., 2000; Singhal, et al., 2004b; Singhal, et al., 2004a) are exclusively studied. While, valve-less rectification micropumps are well

documented in the literature, valve-less rectification micropumps based on dynamic rectification geometry has not yet been reported. In this chapter, the new concept of a dynamic valve-less rectification micropumps is introduced. In the dynamic valve-less rectification micropumps, the dynamic rectifying geometry is directly connected to the actuator to allow flow rectification as well as oscillatory flow generation. The oscillatory motion of the rectifying geometry inside the pump chamber will not only function as an oscillatory flow generator and rectifier, it will also provide the function of fluid dynamic mixing in the case of sequential fluids at a pump inlet. The proving and realizing the concept of dynamics flow rectification will open a new topic in the field of valve-less rectification micropumps research and provide more options for microsystems designers.

5.3 Design

The design of the dynamic micropumps consists of five parts: two plungers, pump chamber, fluidic connectors, and magnetic actuator as shown in Figure 5.1. The plungers have an umbrella shape which can be generated by rotating a half circle 360º, and they were fabricated from Aluminum. In the first Plunger, the driving shaft was connected inside the umbrella, and it called concave plunger. On the other side, the driving shaft in the case of the second plunger was connected outside the umbrella, and it was called convex plunger. Each plunger delivers the flow in a different direction. The concave plunger delivers the flow from the right to left, while the convex plunger delivers the flow rate in the opposite direction.

The pump chamber, pump cover, and actuator support are made of polycarbonate (a transparent polymer that allows flow visualization during experiments) and

fabricated by lathing and milling. The pump chamber has a cylindrical shape to match the plunger design and connected directly to the inlet and outlet. Two ports are placed at the top and bottom of the pump chamber. The top and bottom ports are the fluid entrance and exit in the case of the concave plunger, respectively, while in the case of convex plunger, they are the fluid exit and entrance, respectively. The ports are connected first to metal tubes and then to rubber tubes. The pump cover has a square shape and placed by four screws, and a Teflon gasket was used to prevent leakage during the micropumps operation. Please see figure 5.2 for more details.

An actuator support is placed under the micropump chamber to sustain and control the position of the actuator. A magnetic actuator (Digi-Key Corp., Thief River Falls, MN, USA) shown in Figure 5.3 is employed to oscillate the plunger inside the pump chamber. The actuator holder has two tracks to adjust the starting position of the plunger inside the pump chamber.

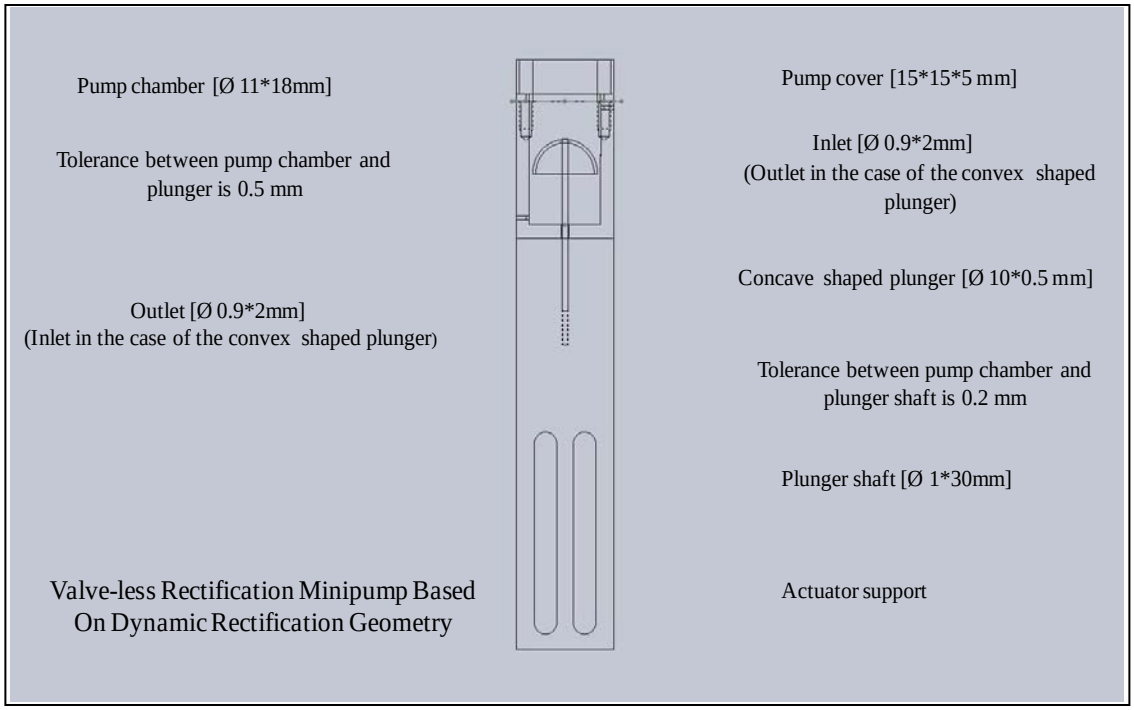

Figure 5.1: The dynamic valve-less rectification micropump with concave plunger

Figure 5.2: A picture of the dynamic valve-less rectification micropump

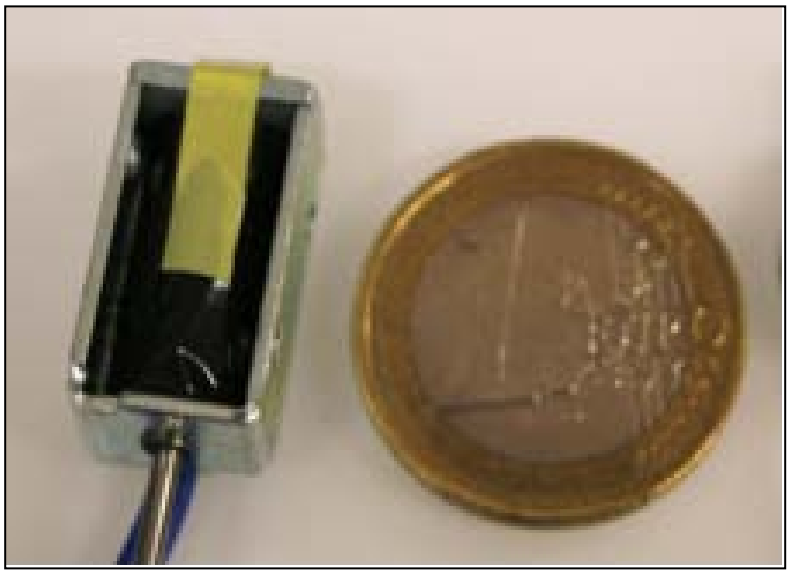

Figure 5.3: The sinusoidal magnetic actuator

5.4 Experimental Apparatus

A frequency generator (Agilent 33220A, Agilent Technologies Deutschland GmbH, Böblingen, Germany) was used to control the sinusoidal magnetic actuator and a 12 Volts square signal was used to drive the magnetic actuator. The micropump was tested within a low frequency range between 0 to 10 Hz. Water was chosen as the working fluid in all experiments, and the flow rate measurements were based on the bubble tracking method (Yoon, et al., 2007). To measure the maximum back pressure, a length scale (ruler) was used to measure the height of the water column when the maximum flow rate goes to zero. The length scale was attached to the experimental apparatus. The experiments were conducted and the flow rate measurements were performed for both plungers. To reduce the leakage between the plunger shaft and its

housing during oscillations, lubrication grease was applied on the shaft to reduce leakage as well as friction with the housing surface.

To evaluate the flow rate measurement errors, the flow rate was measured using two different methods at two different locations, simultaneously. In the inlet tube, the bubble tracking method was employed by measuring the velocity of a trapped bubble between two specified marks using a stopwatch. At the same time, the discharged fluid was collected from the outlet tube during the same time when the bubble moved between the two marks. The discharged fluid was weighed on a scale (Scout Pro SPU402, OHAUS Corp., Pine Brook, NJ, USA), and the mass was used to calculate the flow rate. The difference in the flow rate values between the two measurement methods was less than 1.5 %. To evaluate the experimental error, experimental samples were randomly chosen and repeated three times. The error analysis suggested that the experimental error is equal to or less than 12% with a confidence interval of 90%.

5.5 Results and Discussion

The results were presented in terms of flow rate, maximum back pressure, and velocity ratio as a function of actuator oscillating frequency. The definition of the velocity ratio was discussed in Chapter 3. Figure 5.4 compares results between the mcicropumps using concave and convex plungers. The results show that both pumps bear the same trend, where the flow rates increase monotonically as frequencies increase till they reach the maximum value and reduce monotonically till frequency equal to 10 Hz. The micropump with a concave plunger delivered higher flow rates than that with a convex plunger; the maximum flow rate for concave and convex

plunger micropumps were 100.5 µl/min and 94.3 µl/min, respectively. However, the maximum flow rates occurred at different frequencies. The maximum flow rate of the micropump with concave plunger occurred at 6 Hz, while for the convex plunger, the maximum flow rate occurred at 7 Hz.

Not only the micropump with the concave plunger has higher maximum flow rate than the one with convex plunger, but also it has the higher maximum back pressure as well. The maximum back pressures were 1.4 kPa and 0.2 kPa in the case of concave and convex plunger micropumps, respectively.

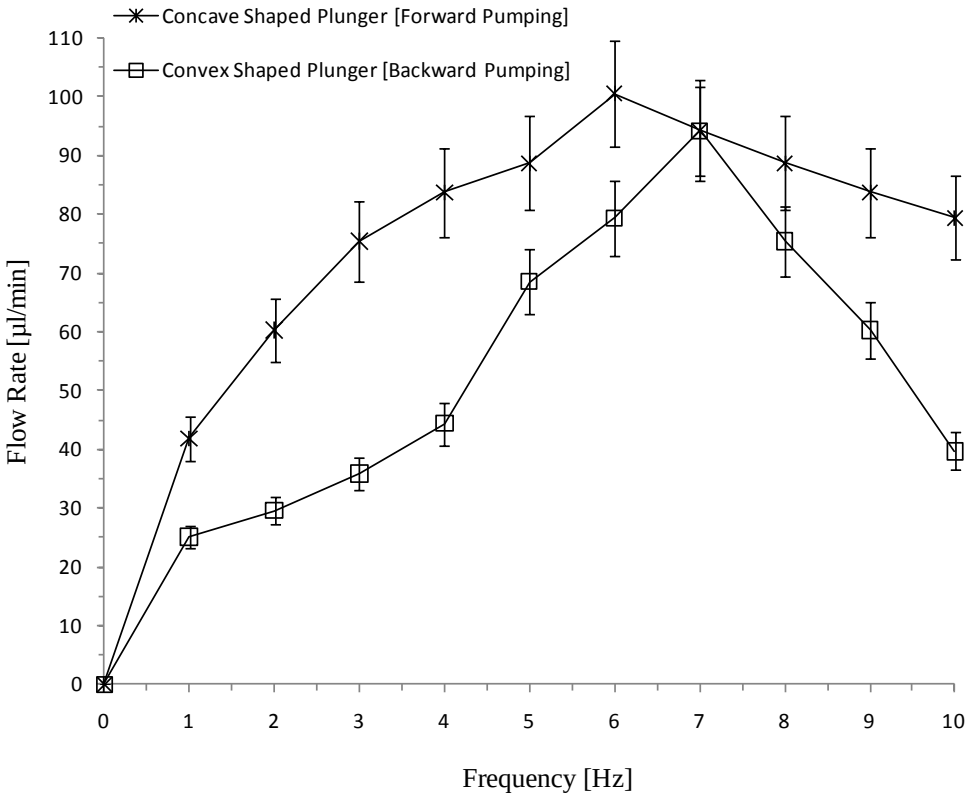

Figure 5.4: The flow rates of the dynamic valve-less rectification micropump as a function of the actuator frequency

Figure 5.5 shows the velocity ratio as a function of the actuator frequency. The velocity ratio is used to better evaluate the valve-less rectification micropumps along with the maximum flow rate and back pressure. The two micropumps have the maximum velocity ratio at 1 Hz which is used along with the flow rate and maximum back pressure to evaluate the micropump efficiency. In other words, the maximum flow rate per each pumping cycle is at actuator frequency equal to 1 Hz. The micropump with the concave plunger has a higher velocity ratio than the one with convex plunger. However, the two micropumps have the same velocity ratio at 7 Hz.

It is also noticed that the micropump with concave plunger has higher flow rates at frequencies with only one exception; the two micropumps have the flow rate at actuator frequency equal to 7 Hz. During the experiments, it was observed that leakage between the plunger shaft and its housing increased monotonically with the actuator frequencies. This observation may explain the monotonically reduction of the flow rate in both micropumps after reaching its maximum flow rate. The leakage needs to be addressed before using this pump at higher frequencies. The direction of the net flow rate in the case of the concave plunger works in the favor of the direction of gravity, while it is against the gravity in the case of the convex plunger micropump. This may played a role in enhancing the efficiency of the micropump with concave plunger and can explain the higher flow rates delivered with the concave plunger.

The bidirectional function of this type of micropumps is realized by using two plungers, where each one will deliver the flow in a different direction. Depending on the application and desired flow direction, switching the pump plunger will change the

direction of the flow rate. The oscillatory motion of the plungers inside the pump chamber can promote dynamic mixing when sequential fluids are introduced at the inlet. However, characterizing the mixing of this pump will be considered in future works and out of scope of present investigation. The tolerance between the plunger and chamber is also another key parameter to be further investigated.

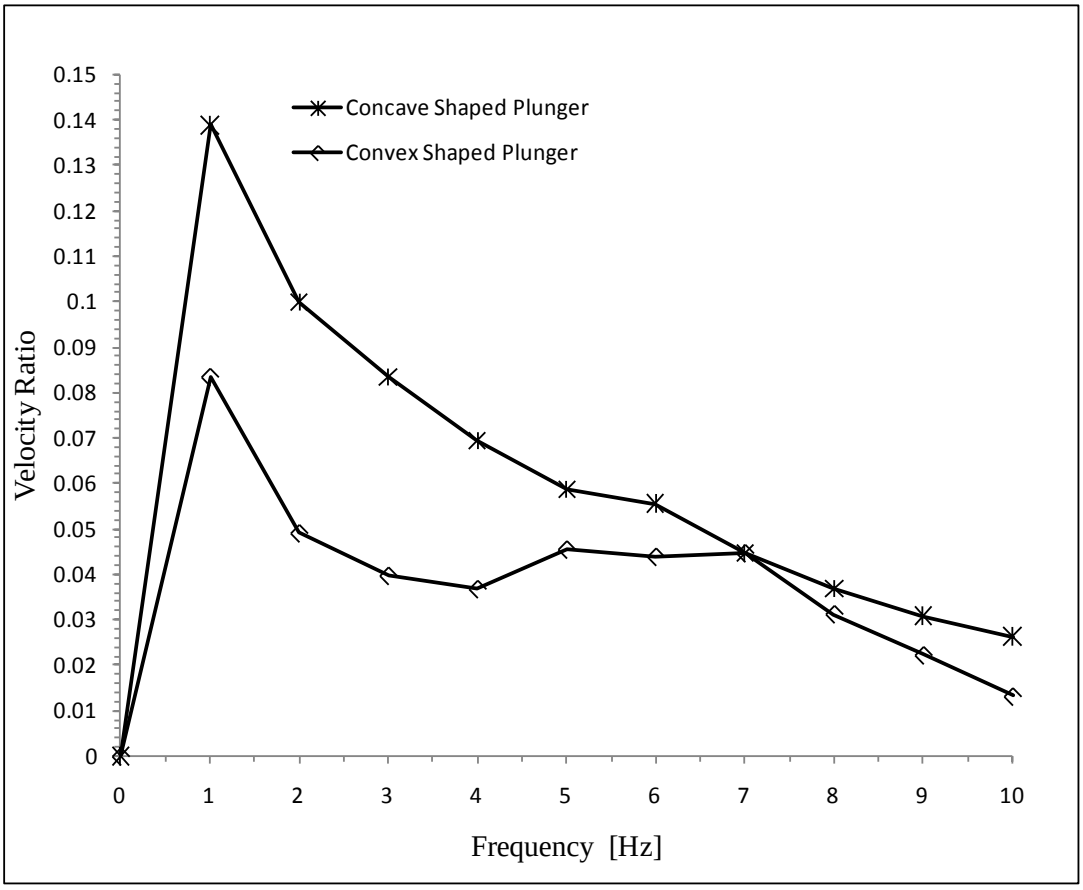

Figure 5.5: Velocity ratio as a function of the actuator frequency (0-10 Hz)

5.6 Conclusions

The concept of the micro pumping using dynamic rectifying geometry was introduced and verified. A valve-less rectification micropump based on dynamic rectifying geometry was designed, fabricated, and tested. Two plungers (dynamic rectifying geometries) were used alternatively to change the flow direction. The micropump with the concave plunger had a higher maximum flow rate, maximum back pressure, and velocity ratio. A leakage was noticed between the plunger shaft and its housing. This problem needs to be addressed before running the micropump at higher frequencies.

Dynamic mixing can be performed inside the pumping chamber when sequential fluids are introduced at the inlet. However, an additional work needs to be conducted to investigate the mixing in valve-less rectification micropumps based on dynamic geometries. Other future works include parametric studies such as the ports and chamber diameters, volume of the pump chamber, displacement volume, and ratio between the diameters of the ports and pump chamber diameters, and tolerance between the plunger shaft and its housing as well as between the plunger and pump chamber. Additionally, the displacement of the plunger inside the pump chamber is another factor that may be considered in future works. This factor is related to the micropump actuator.

6 CONCLUSION

“The whole of science is nothing more than a refinement of everyday thinking.”

Albert Einstein

6.1 Summary

The works described is related to the area of valve-less rectification micropumps and can be divided into four parts. The first part is concerned the numerical simulations of the microfluidic diodicity, a parameter that measures the efficiency of the rectifying geometries. Lattice Boltzmann Method (LBM) is used to investigate the flow diodicity at low Reynolds numbers for both conventional and non-conventional rectifying geometries. Results are presented in Chapter Two. The conclusions drawn from Part 1 are as follows:

- LBM is successfully used to evaluate the microfluidic diodicity for both conventional and non-conventional rectifying geometries at low Reynolds numbers (0.2-60).
- Flow rectification performance at low Reynolds numbers strongly depends on rectifying geometries.
- Tesla and triangle geometries are not capable of achieving flow rectification at low Reynolds numbers.
- The configuration of half circle, semi circle, and heart shape are capable of achieving moderate flow rectifications.
- The configuration of nozzle/diffuser as well as bifurcation geometry can achieve favorable flow rectification. The maximum microfluidic diodicities occurred at Re=60 for both geometries.
- Bifurcation is a non-conventional rectifying geometry that can successfully rectify the flow at low Reynolds number as efficient as the nozzle/diffuser geometry. The bifurcation geometry is known for its capability to generate

streaming flows, and it has a potential for bidirectional and multifunctional micropump design.

The second part of the thesis work involves the development of a bidirectional, multifunctional, and efficient valve-less rectification micropump based on bifurcation geometry. Three different micropumps were designed, fabricated, and tested including single and double generations bifurcation with single inlet and outlet, and the hybrid design which had a single generation with two inlets and one outlet. Soft lithography was used to fabricate the micropumps and ethanol was used in all experiments. PZT was employed to actuate the micropump by generating oscillatory flows. The conclusions from Part 2 (Chapter Three) are as follows:

- Three valve-less rectification micropumps based on bifurcation geometry are designed, fabricated, and tested.
- A new parameter is introduced for evaluation of valve-less rectification micropumps, along with the conventional parameters of flow rate and maximum back pressure.
- The design of collecting chambers has a great impact on the micropump efficiency.
- The double-generation micropump has a higher performance than the single generation micropump.
- The hybrid design has the highest pumping performance among all three designs.
- The occurrence of air bubbles increases with the actuator frequency as has a negative impact on the micropump efficiency.

- Bidirectional pumping was achieved in the single and double-generation micropumps designs.
- Fluid mixing was realized in the hybrid design owning to its unique design of two inlets and one outlet.
- All three micropump designs are self-primed.

The third part, which described in Chapter Four, is an investigation of the effect of the selection of the fabrication material on the pumping efficiency. In this part, two micropumps are fabricated from two different materials, PDMS and SU-8, and the testing results are compared in terms of flow rate, maximum back pressure, and velocity ratio. The following are the conclusions from Part 3:

- The SU-8-glass valve-less rectification micropump performs with a maximum flow rate four times higher than the maximum flow rate delivered by the PDMS-glass valve-less rectification micropump.
- The SU-8-glass micropump has higher flow rates, maximum back pressure, and velocity ratio compared to the PDMS-glass micropump.
- The elasticity of the PDMS may contribute to the lower pumping performance of the PDMS-glass micropump.
- Using hard material to fabricate the valve-less rectification micropumps may have a positive effect on the pumping performance.

The fourth part of the dissertation, which is described in the fifth Chapter, is the introduction of the concept of a new dynamic valve-less rectification micropump. The micropump based on the new concept is designed, fabricated, and tested. Two

plungers with different orientation were used to change the direction of the output flow. The conclusions from Part 4 are as follows:

- A new concept of using dynamic rectifying geometries in micro pumping is introduced and verified.
- A valve-less rectification micropump based on a dynamic rectifying geometry is designed, fabricated, and tested. Results are presented in terms of flow rate, maximum back pressure, and velocity ration.
- Bidirectional pumping is achieved by using two plungers of different orientations.
- The micropump with the concave plunger has higher flow rates, maximum back pressure, and velocity ratios than the micropump with the convex plunger.
- The new micropump has a potential of dynamic mixing when sequential fluids are introduced at the inlet.

6.2 Outlook and Future Work

There are many new and exciting future work can be done as an extension of the current thesis work. The possible new research topics include but not limit to:

- Numerical evaluation of the microfluidic diodicity for unsteady three dimensional flows.
- Numerically search and optimize the rectifying geometry with given flow rate, back pressure and efficiency, in addition to the conventional and non-conventional rectifying geometries discussed in the thesis work.

- Optimize the bifurcation geometry by conducting parametric investigation which includes the bifurcation angle, aspect ratio, bifurcation width ratio, and number of generations (more than two).
- Quantitatively investigate the mixing function of the hybrid design in more details.
- Fabricate the hybrid design using silicon–glass and compare its results with the current results.
- Study the pumping performance of the valve-less rectification micropump based on bifurcation geometry when it is implemented in a real microsystem. In other words, study the effect of the microsystem's flow resistance on the micropump overall microfluidic diodicity and, as a result, efficiency.
- Quantitatively investigate the mixing function of the valve-less rectification micropumps based on the dynamic geometry.

BIBLIOGRAPHY

Ahn, C. H., and M. G. Allen. "Fluid Micropumps Based on Rotary Magnetic Actuators." IEEE 8th Int. Workshop on MEMS (MEMS'95). 1995. 408–412.

Ahn, S. H., and Y. K. Kim. "Fabrication and Experiment of a Planar Micro Ion Drag Pump." (Sensors and Actuators A) 70 (1998): 1-5.

Amirouche, F., Y. Zhou, and T. Johnson. "Current micropump technologies and their biomedical applications." (Journal of Microsystem Technologies) 15 (2009): 647–666.

Bardell, R., R. Sharma, F. K. Forster, M. A. Afromowitz, and R. Penney. "Designing high-performance micro-pumps based on no-moving-parts valves." (In: Lin L, Goodson KE et al (eds) Microelectromechanical systems (MEMS), Proceedings of the ASME IMECE (International Mechanical Engineering Congress and Exposition)) DSC-234/HTD-354 (1997): 47-53.

Bart, S. F., L. S. Tavrow, M. Mehregany, and J. H. Lang. "Microfabricated Electrohydrodynamic Pumps." (Sensors and Actuators A) 21, no. 23 (1990): 193-197.

Benard, W. L., H. Kahn, A. H. Heuer, and M. A. Huff. "Thin Film Shape-Memory Alloy Actuated Micropumps." (Journal of Microelectomechanical Systems) 7, no. 2 (1998): 245-251.

Benzi, R., S. Succi, and M. Verassola. "The lattice Boltzmann equation-theory and application." (Future Generation Computer Systems) 14 (1998): 209-214.

Bhatnagar, P. L., E. P. Gross, and M. Krook. "A model for collision processes in gases, I. Small amplitude processes in charged and neutral one-component system." (Physical Review) 94 (1954): 511-525.

Boehm, S., W. Olthuis, and P. Bergveld. "A Bi-Directional Electrochemically Driven Micro Liquid Dosing System With Integrated Sensor/Actuator Electrodes." IEEE 13th Int. Workshop on MEMS (MEMS'00). 2000. 92-95.

Boehm, S., W. Olthuis, and P. Bergveld. "A Plastic Micropump Constructed With Conventional Techniques and Materials." (Sensors and Actuators A) 77 (1999): 223-228.

Bouzidi, M., M. Firdaouss, and P. Lallemand. "Momentum transfer of a Boltzmann lattice fluid with boundaries." (Physics of Fluids) 13 (2001): 3452-3460.

Briant, J. K., and M. Lippman. "Particle Transport Through a Hollow Canine Airway Cast by High-Frequency Oscillatory Ventilation." (Experimental Lung Research) 18 (1992): 385-407.

Büttgenbach, S., and C. Robohm. "Microflow devices for miniaturized chemical analysis systems." Proceedings of International Society for Optical Engineering. 1999. 51-61.

Cabuz, C., E. I. Cabuz, W. R. Herb, T. Rolfer, and D. Zook. "Measoscopic Sampler Based on 3D Array of Electrostatically Activated Diagphragms." Inter. Conf. on Solid-State Sensors and Actuators (Transducers '99). 1999. 1890–1891.

Chen, Y., S. Kang, L. Wu, and S. Lee. "Fabrication and investigation of PDMS micro-diffuser/nozzle." (Journal of Materials Processing Technology) 198 (2008): 478-484.

Chopard B, Droz M. Cellular automata modeling of physical systems. Cambridge: Cambridge University Press, 1998.

Cui, Q., C. Liu, and X. F. Zha. "Simulation and optimization of a piezoelectric micropump for medical applications." (International Journal of Manufacturing Technology) 36 (2008): 516-524.

Cui, Q., C. Liu, and X. F. Zha. "Study on a piezoelectric micropump for the controlled drug delivery system." (Microfluidics and Nanofluidics) 3 (2007): 377-390.

d'Humieres, D., and I. Ginzburg. "Multiple-relaxation-time lattice Boltzmann models in three dimensions." (Philosophical Transactions of the Royal Society A) 360 (2002): 437–451.

Dario, P., N. Croce, M. C. Carrozza, and G. Varallo. "A Fluid Handling System for a Chemical Microanalyzer." (Journal of Micromechanics and Microengineering) 6 (1996): 95-98.

Deshmukh, A. A., D. Liepmann, A. P. Pisano, and L. P. Lee. "Continuous microfluidic mixing using pulsatile micropumps." Ph.D. dissertation. Berkeley Sensor and Actuator Center, University of California, Berkeley, CA, USA, 2001.

Doepper, J., M. Clemens, W. Ehrfeld, S. Jung, K. P. Kaemper, and H. Lehr. "Micro Gear Pumps for Dosing of Viscous Fluids." (Journal of Micromechanics and Microengineering) 7 (1997): 230–232.

Fadl, A., Z. Zhang, M. Faghri, D. Meyer, and E. Simmon. "Experimental investigation of geometric effect on microfluidic diodicity." Proceeding of the fifth International conference on microchannels and minichannels ICNMM2007-30074. Puebla, Mexico, 2007.

Fadl, A., Z. Zhang, S. Geller, J. Tölke, M. Krafczyk, and D. Meyer. "The effect of the microfluidic diodicity on the efficiency of valve-less rectification micropumps using Lattice Boltzmann Method." (Journal of Microsystem Technologies) 15 (2009): 1379-1387.

Folta, J. A., N. F. Raley, and E. W. Hee. "Design Fabrication and Testing of a Miniature Peristaltic Membrane Pump." Tech. Dig. Solid-State Sensor and Actuator Workshop. Hilton Head, 1992. 186–189.

Foster, F. K., L. Bardell, M. A. Afromowitz, N. R. Sharma, and A. Blanchard. "Design, fabrication and testing of fixed-valve micropumps." Proceeding of the ASME Fluids Engineering Division, ASME. 1995. 39-44.

Freudiger, S. "Entwicklung eines parallelen, adaptiven, komponentenbasierten Stro¨mungskerns fu¨r hierarchische Gitter auf Basis des Lattice-Boltzmann-Verfahrens." Ph. D. dissertation. Technische Universita¨t Braunschweig, Braunschweig, Germany, 2009.

Fuhr, G. "From Micro Field Cages for Living Cells to Brownian Pumps for Submicron Particles." Proc. of IEEE Micro Mechatronics and Human Science 97. 1997. 1-4.

Fuhr, G., R. Hagedom, T. Mueller, W. Benecke, and B. Wagner. "Pumping of Water Solutions in Microfabricated Electrohydrodynamic Systems." IEEE 5th Int. Workshop on MEMS (MEMS'92). 1992. 25-30.

Fuhr, G., R. Hagedorn, T. Mueller, W. Benecke, and B. Wagner. "Microfabricated Electrohydrodynamic ~EHD! Pumps for Liquids of Higher Conductivity." (Journal of Microelectromechanical Systems) 1, no. 3 (1992): 141–145.

Fuhr, G., T. Schnelle, and B Wagner. "Travelling Wave-Driven Microfabricated Electrohydrodynamic Pumps for Liquids." (Journal of Micromechanics and Microengineering) 4 (1994): 217–226.

Furuya, A., F. Shimokawa, T. Matsuura, and R. Sawada. "Fabrication of Fluorinated Polyimide Microgrids Using Magnetically Controlled Reactive Ion Etching (MC-RIE) and Their Applications to an Ion Drag Integrated Micropump." (Journal of Micromechanics and Microengineering) 6 (1996): 310–319.

Gamboa, A. R., C. J. Morris, and F. Forster. "Improvements in fixedvalve micropump performance through shape optimization of valves." (Journal of Fluid Engineering) 127 (2005): 339–346.

Gaver, D., and J. Grotberg. "An Experimental Investigation of Oscillating Flow in a Taped Channel." (Journal of Fluid Mechanics) 172 (1986): 47-61.

Gerlach, T. "Pumping gases by a silicon micro pump with dynamic passive valves. International conference on solid-state sensors and actuators." Chicago: Tranceducers'97, 1997.

Gerlach, T., and H. Wurmus. "Working principles and performance of the dynamic micropump." (Sensors and Actuators A) 50 (1995): 135-140.

Geschke, O., H. Klank, and P. Tellemann. Microsystem engineering of Lab-on-a-Chip devices. Weinheim: Wiley-VCH, 2004.

Goldberg, I., Z. Zhang, and M. Tran. "Steady Streaming of Fluid in the Entrance Region of a Tube during Oscillatory Flow." (Physics of Fluids) 11, no. 10 (1999): 2957-2962.

Gravesen, P., J. Branebjerg, and O. S. Jensen. "Microfluidics: a review." (Journal of Micromechanics and Microengineering) 3 (1993): 168–182.

Grosjean, C., and Y. C. Tai. "A Thermopneumatic Peristaltic Micropump." Inter. Conf. on Solid-State Sensors and Actuators (Transducers '99). 1999. 1776–1779.

Grotberg, J. "Volume Cycled Oscillatory Flow in a Taped Channel." (Journal of Fluid Mechanics) 141 (1984): 249-264.

Gunstensen, A. K, and D Rothmann. "Lattice Boltzmann model of immiscible fluids." (Physical Review A) 43, no. 8 (1991): 4320-4327.

Harrison, D. J., A. Manz, and P. G. Glavina. "Electroosmotic Pumping Within a Chemical Sensor System Integrated on Silicon." Proc. of Inter. Conf. on Solid-State Sensors and Actuators Transducers'91. 1991. 792–795.

Harrison, D. J., K. Seiler, A. Manz, and Z. Fan. "Chemical Analysis and Electrophoresis Systems Integrated on Glass and Silicon Chips." Tech. Dig. Solid-State Sensor and Actuator Workshop, Hilton Head. 1992. 110-113.

Haselton, F. R., and P. W. Scherer. "Flow visualization of steady streaming in oscillatory flow through a bifurcating tube." (Journal of Fluid Mechanics) 123 (1982): 315-333.

Haselton, F. R., and P. W. Scherer. "Flow Visualization of Steady Streaming in Oscillatory Flow through a Bifurcation Tube." (Journal of Fluid Mechanics) 123 (1982): 315-333.

Hayamizu, S., K. Higashino, Y. Fujii, Y. Sando, and K. Yamamoto. "Development of a bi-directional valve-less silicon micro pump controlled by driving waveform." (Sensors and Actuators A) 103, no. 1-2 (2003): 83-87.

Iverson, B., and S. Garimella. "Recent advances in microscale pumping technologies: a review and evaluation." (Microfluidics and Nanofluidics) 5 (2008): 145–174.

Jang, L. S., N. Sharma, and F. Forster. "The effect of particles on performance of fixed-valve micropumps." (Micro Total Analysis System) 2000: 283-286.

Jang, L. S., W. H. Kan, M. K. Chen, and Y. M. Chou. "Parameter extraction from BVD electrical model of PZT actuator of micropumps using time-domain measurement technique." (Microfluidics and Nanofluidics) 7 (2009): 559-568.

Jiang, X. N., Z. Y. Zhou, X. Y. Huang, Y. Li, Y. Yang, and C. Y. Liu. "Micronozzle/diffuser flow and its application in microvalveless pumps." (Sensors and Actuators A) 70 (1998): 81-87.

Jones, A. F., and S. Rosenblat. "The Flow Induced by Torsional Oscillations of Infinite Planes." (Journal of Fluid Mechanics) 37 (1969): 337-347.

Judy, J. W., T. Tamagawa, and D. L., Polla. "Surface-Machined Micromechanical Membrane Pump." IEEE 4th Int. Workshop on MEMS. 1991. 182–186.

Jun, T. K., and C. J. Kim. "Microscale Pumping With Traversing Bubbles in Microchannels." Tech. Dig. Solid-State Sensor and Actuator Workshop. Hilton Head, 1996. 144–147.

Jun, T. K., and C.-J. Kim. "Valveless Pumping Using Traversing Vapor Bubbles in Microchannels." (Journal of Applied Physics) 83, no. 11 (1998): 5658–5664.

Kehrwald, D. *Numerical analysis of Immiscible Lattice BGK.* PhD thesis, Universität Kaiserslautern, 2003.

Koch, T., A. G. R. Evans, and A. Brunschweiler. "The dynamic micropump driven with screen printed PZT actuator." (Journal of Micromechanics and Microengineering) 8 (1998): 119–122.

Kurosawa, M., T. Watanabe, and T. Higuchi. "Surface Acoustic Wave Atomizer With Pumping Effect." IEEE 8th Int. Workshop on MEMS (MEMS'95). 1995. 25-30.

Lammerink, T. S. J., M. Elwenspoek, and J. H. J. Fluitman. "Integrated Micro-Liquid Dosing System." IEEE 6th Int. Workshop on MEM-MEMS'93. 1993. 254–259.

Laser, D. J., and J. D. Santiago. "A review of micropumps." (Journal of Micromechanics and Microengineering) 14 (2004): R35-R64.

Lastochkin, D., R. Zhou, P. Wang, Y. Ben, and H. C. Chang. "Electrokinetic micropump and micromixer design based on ac faradic polarization." (Journal of Applied Physics) 96 (2004): 1730-1733.

Lee, J., and C. J. Kim. "Liquid Micromotor Driven by Continuous Electrowetting." IEEE 11th Int. Workshop on MEMS (MEMS'98). 1998. 538-543.

Lemoff, A. V., A. P. Lee, R. R. Miles, and C. F. McConaghy. "An AC Magnetohydrodynamic Micropump: Tpwards a True Integrated Microfluidic System." Int. Conf. on Solid-State Sensors and Actuators (Transducers '99). 1999. 1126–1129.

Lemoff, A. V., and A. P Lee. "An AC Magnetohydrodynamic Micropump." (Sensors and Actuators A) 63 (2000): 178–185.

Li, H. Q., Roberts, D. C., Steyn, J. L., Turner, K. T., Carretero, J. A., Yaglioglu,O., Y. H. Su, L. Saggere, N. W. Hagood, S. M. Spearing, and M.A. Schmidt. "A High Frequency High Flow Rate Piezoelectrically Driven MEMS Micropump." Proceedings IEEE Solid State Sensors and Actuators Workshop. Hilton Head, 2000.

Linneman, R., P. Woias, C. D. Senfft, and J. A. Ditterich. "A Self-Priming and Bubble Tolerant Piezoelectric Silicon Micropump for Liquids and Gases." IEEE 11th Int. Workshop on MEMS-MEMS'98. 1998. 532-537.

Lyne, W. H. "Unsteady Flow Viscous Flow in a Curved Tube." (Journal of Fluid Mechanics) 45 (1970): 13-31.

Madou, M. J., and et al. "Design and Fabrication of CD-Like Microfluidic Platforms for Diagnostics: Microfluidic Functions." (Journal of Biomedical Microdevices) 3, no. 3 (2001): 245-254.

Matsumoto, H., and J. E. Colgate. "Preliminary Investigation of Micropumping Based on Electrical Control of Interfacial Tension." IEEE 3rd Int. Workshop on MEMS (MEMS'90). 1990. 105-110.

Mei, R., D. Yu, and W. Shyy. Force evaluation in the lattice Boltzmann method involving curved geometry. NASA/CR-2002-211622, ICASE Report No. 2002-22, 2002.

Meng, E., X. Q. Wang, H. Mak, and Y. C Tai. "A Check-Valved Silicone Diaphragm Pump." IEEE 13th International Conference on Micro Electro Mechanical Systems (MEMS'00). 2000. 23-27.

Miyazaki, S., T. Kawai, and M Araragi. A Piezoelectric Pump Driven by a Flexural Progressive Wave. IEEE 4th Int. Workshop on MEMS (MEMS'91), 1991. 283–288.

Mizoguchi, H., M. Ando, T. Mizuno, T. Takagi, and N. Nakajima. "Design and Fabrication of Light Driven Micropump." IEEE 5th Int. Workshop on MEMS (MEMS'92). 1992. 31–36.

Moroney, R. M., R. M. White, and R. T. Howe. "Ultrasonically Induced Microtransport." IEEE 4th Int. Workshop on MEMS (MEMS'91). 1991. 277–282.

Morris, C. J., and F. K. Forster. "Low-order modeling of resonance for fixed-valve micropumps based on first principles." (Journal of Microelectromechanical Systems) 12 (2003): 325-334.

Nabavi, Majid. "Steady and unsteady flow analysis in microdiffusers and micropumps: a critical review." (Microfluidics and Nanofluidics) 7 (2009): 599-619.

Nguyen, N. T., A. H. Meng, J. Black, and R. M. White. "Integrated Flow Sensor for In Situ Measurement and Control of Acoustic Streaming in Flexural Plate Wave Micro Pumps." (Sensors and Actuators A) 79 (2000): 115–121.

Nguyen, Nam-Trung, and Steven T. Wereley. Fundamentals and Applications of Microfluidics. Norwood, MA: ARTECH HOUSE, INC, 2006.

Nguyen, Nam-Trung, Xiaoyang Huang, and Toh Kok Chuan. "MEMES-Micropumps: A Review." Transaction of the ASME 124 (JUNE 2002): 384-392.

Nyborg, W. L. "Acoustic Streaming due to Attenuated Plane." (Journal of American Society of Accostic) 25 (1953): 68-75.

Olsson, A., G. Stemme, and E. Stemme. "A valve-less planar fluid pump with two pump chambers." (Sensors and Actuators A) 46, no. 47 (1995): 549–556.

Olsson, A., G. Stemme, and E. Stemme. "Diffuser-element design investigation for valve-less pumps." (Sensors and Actuators A) 57 (1996): 137-143.

Olsson, A., G. Stemme, and E. Stemme. "Numerical and experimental studies of flat-walled diffuser elements for valve-less micropumps." (Sensors and Actuators A) 84 (2000): 165–175.

Olsson, A., G. Stemme, and E. Stemme. "Simulation studies of diffuser and nozzle elements for valve-less micropumps." Transducers 97. June 16–19, Chicago, USA, 1997a.

Olsson, A., P. Enoksson, G. Stemme, and E. Stemme. "Micromachined flat-walled valve-less diffuser pumps." (Journal Microelectromechanical Systems) 6, no. 2 (1997b): 161-166.

Ozaki, K. "Pumping Mechanism Using Periodic Phase Changes of a Fluid." IEEE 8th Int. Workshop on MEMS (MEMS'95). 1995. 31-36.

Pingen, G. "Topology and shape optimization of fluid-structure interaction problems." Thesis proposal. Department of Aerospace Engineering Sciences, University of Colorado, 2005.

Qian, Y. H., D. d'Humieres, and P. Lallemand. "Lattice BGK models for Navier Stokes fluid flow." (Europhysics Letters) 17 (1992): 479-484.

Rapp, R., W. K. Schomburg, D. Maas, J. Schulz, and W. Stark. "LIGA Micropump for Gases and Liquids." (Sensors and Actuators A) 40 (1994): 57–61.

Richter, A., A. Plettner, K. A. Hofmann, and H. Sandmaier. "A Micromachined Electrohydrodynamic (EHD) Pump." (Sensors and Actuators A) 29 (1991): 159–168.

Richter, A., and H Sandmaier. "An Electrohydrodynamic Micropump." IEEE 3rd Int. Workshop on MEMS (MEMS'90). 1990. 99-104.

Richter, M., R. Linnemann, and P. Woias. "Robust Design of Gas and Liquid Micropumps." (Sensors and Actuators A) 68 (1998): 480–486.

Rife, J. C., M. I. Bell, J. S. Horwitz, M. N. Kabler, R. C. Y. Auyeung, and W. J. Kim. "Miniature valveless ultrasonic pumps and mixers." (Sensors and Actuators A) 86 (2000): 135–140.

Riley, N. "Oscillating Viscous Flows." (Mathematika) 12 (1965): 161-170.

Riley, N. "Oscillating Viscous Flows, Review and Extension." (Journal of the Institute of Mathematics and Its Applications) 3 (1967): 419-434.

Rosa, S., and F. T. Pinho. "Pressure drop coefficient of laminar Newtonian flow in axisymmetric diffusers." (International Journal of Heat Fluid Flow) 27 (2006): 319–328.

Rosenblat, S. "Flow between Torsional oscillating disks." (Journal of Fluid Mechanics) 8 (1960): 388-399.

Rosenblat, S. "Torsional oscillation of a plane in viscous fluids." (Journal of Fluid Mechanics) 6 (1959): 206 – 220.

Runstadler, P. W., F. X. Dolan, and R. C. Dean. Diffuser data book. New Hampshire: Creare, 1975.

Schäfer, M., and S. Turek. "Benchmark computations of laminar flow around a cylinder." (Notes in Numerical Fluid Mechanics) 52 (1996): 547–566.

Schomburg, W. K., J. Fahrenberg, D. Maas, and R. Rapp. "Active Valves and Pumps for Microfluidics." (Journal of Micromechanics and Microengineering) 3 (1993): 216-218.

Sheen, H. J., C. J. Hsu, T. H. Wu, H. C. Chu, C. C. Chang, and U. Lei. "Experimental study of flow characteristics and mixing performance in a PZT self-pumping micromixer." (Sensors and Actuators A) 139 (2007): 237–244.

Shen, C.-Y., and H.-K. Liu. "Fabrication and drive test of piezoelectric PDMS valveless micro pump." (Journal of the Chinese Institute of Engineering) 31, no. 4 (2008): 615-623.

Shinohara, J., M. Suda, K. Furuta, and T. Sakuhara. "A High Pressure Resistance Micropump Using Active and Normally Closed Valves." IEEE 13th Int. Workshop on MEMS (MEMS'00). 2000. 86–91.

Shoji, S., S. Nakafawa, and M. Esashi. "Micropump and Sample Injector for Integrated Chemical Analyzing Systems." (Sensors and Actuators A) 21, no. 23 (1990): 189–192.

Simon, B., G. Weinmann, and W. Mitzner. "Significance of Mean Airway Pressure During High Frequency Ventilation." (The Physiologist) 25 (1982): 282-293.

Singhal, V., S. V. Garimella, and A. Raman. "Microscale pumping technologies for microchannel cooling systems." (Applied Mechanics Reviews) 57, no. 3 (2004a): 191–221.

Singhal, V., S. V. Garimella, and J. Murthy. "Low Reynolds number flow through nozzle-diffuser elements in valveless micropumps." (Sensors and Actuators A) 113 (2004b): 226-235.

Smits, J. G. "Piezoelectric Micropump With Three Valves Working Peristaltically." (Sensors and Actuators A) 15 (1988): 153–167.

Stemme, E., and G. Stemme. "A valve-less diffuser/nozzle based fluid pump." (Sensors and Actuators A) 39 (1993): 159–167.

Succi, S. The lattice Boltzmann equation for fluid dynamics and beyond. Oxford: Oxford University Press, 2001.

Sun, C. L., and K. Huang. "Numerical characterization of the flow rectification of dynamic microdiffusers." (Journal of Micromechanics and Microengineering) 16 (2006): 1331-1339.

Takagi, H., R. Maeda, K. Ozaki, M. Parameswaran, and M. Mehta. "Phase Transformation Type Micropump." Proceedings of Micro Mechatronics and Human Sciences. 1994. 199–202.

Tarbell, J. M., J. S. Ultman, and L. Durlofsky. "Oscillatory Convection Dispersion in a branching Network." (Journal of Biomechanical Engineering) 104 (1982): 338 – 342.

Tölke, J. Gitter-Boltzmann-Verfahren zur Simulation von Zweiphasenströmunge. PhD thesis, TU München, 2001.

Tölke, J., B. Ahrenholz, J. Hegewald, and M. Krafczyk. "Parallel Free-Surface and Multi-Phase Simulations in Complex Geometries using Lattice Boltzmann Methods." Third Joint HLRB and KONWIHR Result and Reviewing Workshop. Fakultät für Informatik, Technische Universität München, 2007.

Van de Pol, F C M. "Apumpbased onmicro-engineering techniques." (Thesis, University of Twente, Enschede, The Netherlands) 1989.

van den Pol, F. C. M., H. T. G. van Lintel, M. Elwonspoek, and J.H. J. Fluitman. "A Thermopneumatic Micropump Based on Micro-Engineering Techniques." (Sensors and Actuators A) 21-23 (1990): 198-202.

van der Wijngaart, W., H. Andersson, P. Enoksson, K. Noren, and G. Stemme. "The first self-priming and bi-directional valve-less diffuser micropump for both liquid and gas." Miyazaki, Japan: MEMS 2000, 2000. 674-679.

van Lintel, H. T. G., F. C. M. van den Pol, and S. Bouwstra. "A Piezoelectric Micropump Based on Micromachining in Silicon." (Sensors and Actuators A) 15 (1988): 153-167.

Wang, C. T., T. S. Leu, and J. M. Sun. "Optimal design and operation for a No-Moving-Parts-Valve (NMPV) micro pump with a diffuser width of 500 μm" (Sensors) 9 (2009b): 3666-3678.

Wang, Y., J. Hsu, P. Kuo, and Y. Lee. "Loss characterization and flow rectification property of diffuser valves for micropumps application." (International Journal of Heat and Mass Transfer) 52 (2009a): 328–336.

Webster, J. R., D. K. Jones, and C. H. Mastrangelo. "Monolithic Capillary Gel Electrophoresis Stage With On-Chip Detector." IEEE 9th Int. Workshop on MEMS (MEMS'96). 1996. 491–496.

Webster, J. R., M. A. Burns, D. T. Burke, and C. H. Mastrangelo. "Electrophoresis System With Integrated On-Chip Fluorescence Detection." IEEE 13th Int. Workshop on MEMS (MEMS'00). 2000. 306–310.

White, F. M. Fluid mechanics. Singapore: WCB/McGraw-Hill, 1999.

Yamahata, C., et al. "Pumping of mammalian cells with a nozzle-diffuser micropump." (Lap on a Chip) 15 (2005): 1083–1088.

Yang, K., I. Chen, B. Shew, and C. Wang. "Investigation of the flow characteristics within a micronozzle/diffuser." (Journal of Micromechanics and Microengineering) 14 (2004): 26–31.

Yang, Z., H. Goto, M. Matsumoto, and T. Yada. "Micromixer incorporated with piezoelectrically driven valveless micropump,." Micro Total Analysis Systems '98. Dordrecht: Kluwer Academic Publishers, 1998. 177–180.

Yoon, J., J. Choi, H. Lee, and M. Kim. "A valveless micropump for bidirectional applications." (Sensors and Actuators A) 135 (2007): 833-838.

Zengerle, R., A. Richter, and H. Sandmaier. "A Micromembrane Pump With Electrostatic Actuation." IEEE 5th Int. Workshop on MEMS-MEMS'92. 1992. 31-36.

Zengerle, R., S. Kluge, M. Richter, and A. Richter. "A Bi-Directional Silicon Micropump." IEEE 8th Int. Workshop on MEMS-MEMS'95. 1995. 19-24.

Zhang, Z., A. Fadl, C. Liu, and D. Meyer. "A Streaming Flow Based Lab-on-Chip Platform Technology." The 1st ASME Micro/Nanoscale Heat Transfer International Conference (MNHT08). Tainan, Taiwan: ASME, 2008